NGU Report 2007.035

Barents Sea Aeromagnetic Survey BAS-06
Acquisition - processing report and preliminary interpretation.

NGU
Norges geologiske undersøkelse
Geological Survey of Norway

Geological Survey of Norway
N-7441 Trondheim, Norway
Tel.: 47 73 90 40 00
Telefax 47 73 92 16 20

REPORT

Report no: 2007.035 | ISSN 0800-3416 | Grading: Confidential to December 2008

Title:

Barents Sea Aeromagnetic Survey BAS-06 - Acquisition - processing report and preliminary interpretation.

Authors:
Laurent Gernigon, Laura Marello, John Olav. Moogaard, Stephanie C. Werner and Jan Reidar Skilbrei

Clients:
Chevron, Eni Norge, Norwegian Petroleum Directorate, RWE-Dea Norge, Statoil

County:

Commune:

Map-sheet name (M=1:250.000)

Map-sheet no. and -name (M=1:50.000)

Deposit name and grid-reference:

Number of pages. 144 Price (NOK).
Map enclosures. X

Fieldwork carried out:	Date of report:	Project no.:	Person responsible:
11.06.06 –09.09.06	23.04.2007	314800	Odleiv Olesen

Summary:

A high sensitivity aeromagnetic survey, BAS-06, was carried out in an area of 46530 km^2 from the Finnmark Platform to the Bjarmeland Platform in the Barents Sea. Data processing comprised spike removal and data editing, systematic (IGRF and lag) corrections, statistical, median and micro levelling. Several potential field maps were produced along the survey area. Examples of various filters applied to the magnetic field have been illustrated. Trend enhancement and a preliminary interpretation of the survey have been carried out.

The new BAS-06 dataset particularly highlighted the salt tectonics in the Nordkapp Basin. One of the major results of this survey was a demonstration that modern, high-resolution aeromagnetic data can provide an efficient geophysical tool for mapping (shallow) salt features and structures within mini-basins. Salt diapirs often coincide with negative magnetic anomalies when the salt domes reach the near surface. Consequently, it can significantly add to the qualitative mapping, on both a regional and prospect scale. Interesting onshore-offshore relationships have been observed north of the Varanger Peninsula. New N70° trends appears on the new dataset and fit with fault zones, anticline and syncline structural features on the mainland.

Keywords. Geofysikk	Berggrunnsgeologi	Magnetometri
Kontinentalsokkel		

CONTENTS

1 INTRODUCTION

Laurent Gernigon

Like several countries (e.g. Australia, Canada, Finland, Sweden, U.S), Norway was one of the first to support a vigorous government program to develop a countrywide, modern, high-resolution aeromagnetic database, which include continuous data acquisition, merging and re-processing of data from individual surveys. In this context, the Geological Survey of Norway (NGU) plays a crucial role in maintaining and continuously updating this national database. NGU's most recent aeromagnetic acquisitions proved the requisite for modern data in order to valid the first order geophysical and geologic features of the Norwegian continental shelf and contiguous oceanic domain. Comparing some of the old aeromagnetic surveys is like comparing 2D seismic lines from the 70ies with the most advanced 3D survey and everybody usually agree that modern data provide much more details and significantly improve our geological knowledge. Consequently, NGU has launched a set of re-mapping projects of the Norwegian continental shelf and adjacent oceanic basins with funding from the petroleum industry and governmental institutions. The need for new high-quality data becomes now a reality for both academy and industry.

NGU initiated the BAS-06 survey in 2006 to acquire, process and interpret a new airborne magnetic dataset covering the eastern part of the undisputed Norwegian Barents Sea. Figures 1.1 and 1.2 underline the location of the new survey area and illustrate the outline of the previous magnetic acquisition in the West Barents Sea area. Except for the NGU HRAMS 97-98 survey, most of the magnetic profiles along the Barents Sea remain old (70ies –80ies). In the meantime, modern and more accurate magnetometers, navigation systems and recent advances in processing techniques allow us to seriously improve the quality of aeromagnetic mapping. Modern magnetometers, as used for the BAS-06 survey, provide new total field measurements of high sensitivity, with virtually no drift and for all intents and purposes can be regarded as giving a reliable reading with a typical noice envelopes of ±0.1 nT. The same cannot be said about the old magnetometers from the vintage surveys across the West Barents Sea. They were not absolute and had to be manually calibrated and were sensitive only to about ±1 nT.

Advances in data acquisition techniques (more sensitive magnetometers, modern Global Positioning Systems, pre-planned drape surveys, etc.), as well as data processing and displaying procedures (such as micro-levelling and advanced gridding techniques), have also significantly improved data quality and resolution, providing levels of detail that are compatible to those derived from seismic, well, and surface geological data. Being aware of such major geophysical improvements, the primary objective of the BAS-06 project was multiple:

1) To provide a better and more reliable magnetic coverage of the study area.
2) To interpret the basement structure, tectonic framework and lithology from the aeromagnetic

geophysical results.
3) To correlate and combine these results with the known geology of the study area to aid identification of new structural features.

The interpretation initiative involves the application of improved processing techniques and cultural source removal from the total magnetic field. In order to enhance the signatures of the basement structures and lithological units, as well as local volcanics lying above the older basement, a number of processed images and interpretations have been produced.

The next chapters of this report describe acquisition, processing, levelling and map production of the BAS-06. Filtering techniques and data enhancement methods were described leading subsequently to an integrated study of the survey and described the most interesting features revealed by this new dataset. Geophysical and geological interpretation based on the magnetic field, including also gravity and available and released seismic lines kindly provided by the Norwegian Petroleum Directory (NPD) led to a preliminary interpretation of the survey area and open discussions on onshore-offshore relationships and salt structures particularly underlined by this new aeromagnetic dataset.

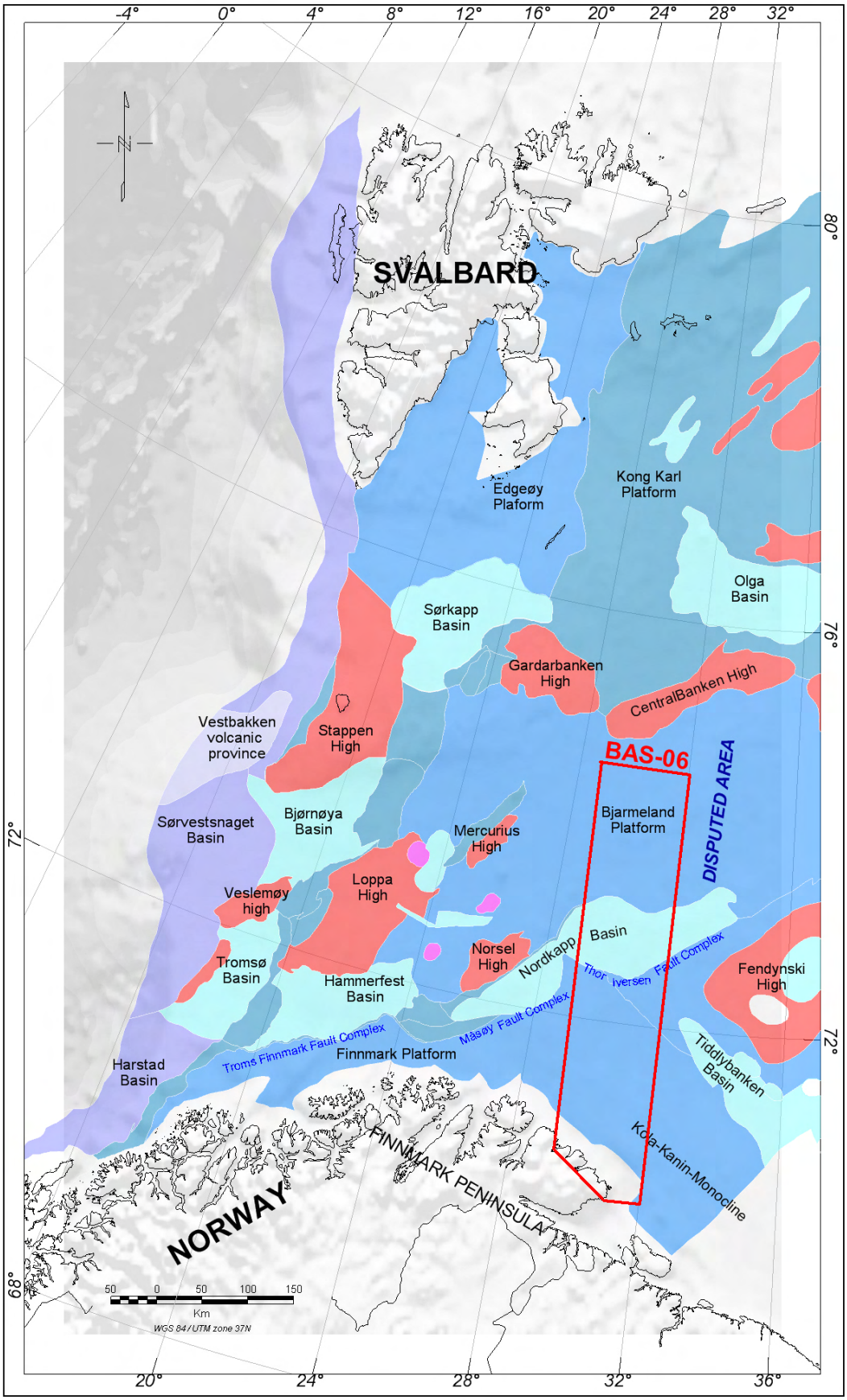

Figure 1.1 Location of the BAS-06 survey area and outline of the main structural elements of the western Barents Sea. Main structural elements from NPD (Gabrielsen et al. 1990).

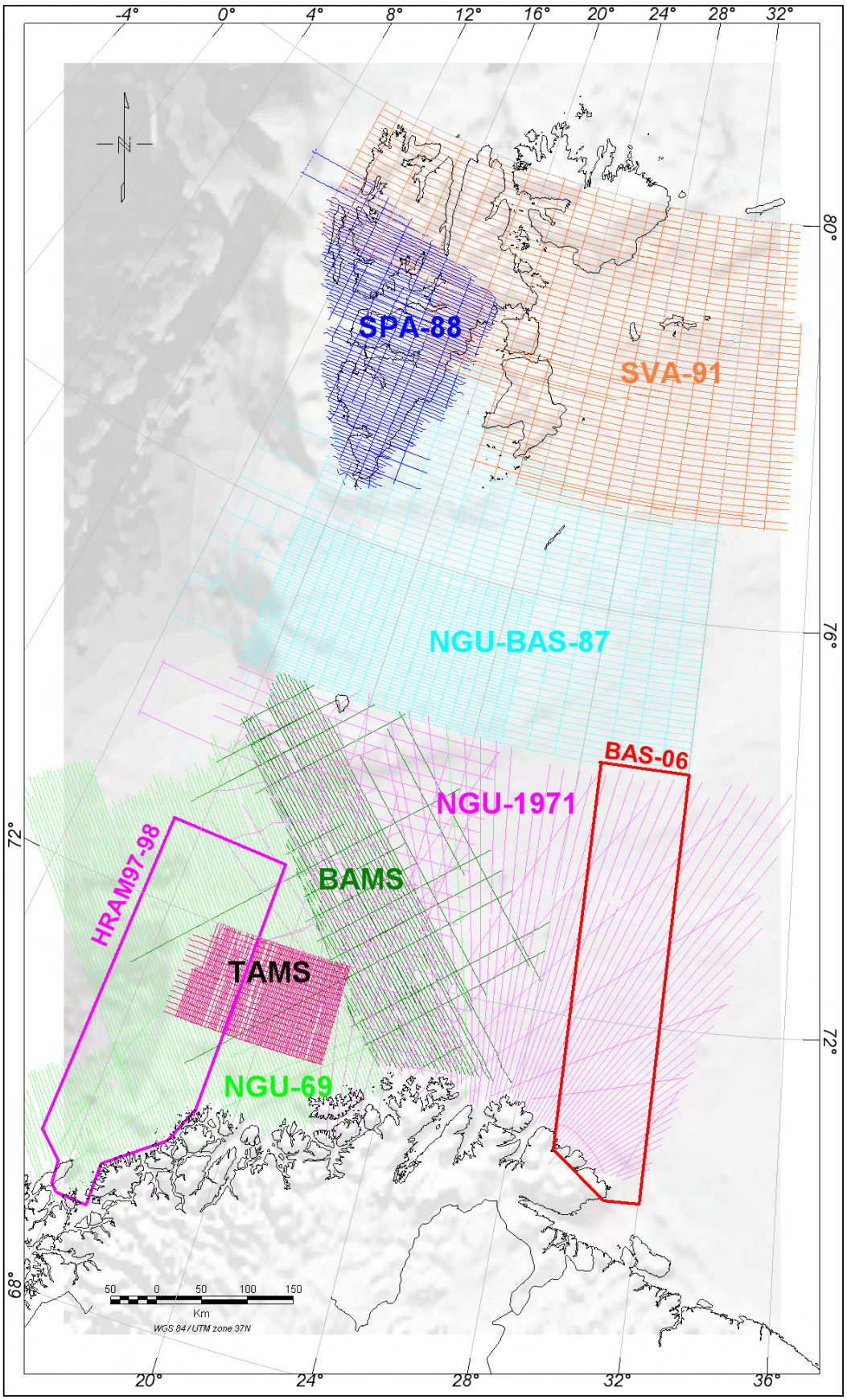

Figure 1.2 Location of the BAS-06 survey area and outline of the previous aeromagnetic surveys in the western Barents Sea area (Skilbrei et al. 1990, Skilbrei 1992, Olesen et al. 2006).

2 SURVEY CHARACTERISTICS and ACQUISITION

Jan Olav Mogaard and Laurent Gernigon

2.1 Survey area and equipment

The BAS-06 is the most recent high-resolution aeromagnetic survey acquired in the Barents Sea. As part of the NGU mapping program, the BAS-06 acquisition was carried out during the two periods 11.06.2006 to 18.07.2006 and 19.08.2006 to 09.09.2006. The area is approximately 470 km long by 99 km wide and runs from the Varanger Peninsula onto the Bjarneland Platform (Figs. 1.1 and 2.1). The survey lies in a “strategic position” since it is close to the Norwegian boundary with the disputed area between Russia and Norway (Fig. 1.1). Magnetic surveying at NGU is carried out using aeroplanes, with a cesium magnetometer, so-called " bird", towed at a sufficient distance from the plane to make the plane's magnetic effects negligible (70 m) (Fig. 2.2). The airborne magnetic surveys were conducted with constant flight-line orientations, usually perpendicular to the regional geological strike, and with a constant line spacing of 2 km (Fig. 2.1). The following coordinates define the survey area.

Corners	Latitude	Longitude	X UTM 36	Y UTM 36
1	74.30.38.52	28.42.10.62	372009.09	8273642.58
2	74.30.47.13	32.01.17.77	470839.89	8269521.60
3	70.15.38.35	32.01.48.09	463438.99	7795232.07
4	70.15.20.30	30.58.35.83	423724.01	7795649.43
5	70.41.17.22	29.18.26.47	363778.25	7846757.43
6	74.30.30.33	28.45.34.83	373677.91	8273268.16
7	74.30.30.33	28.45.34.83	373677.91	8273268.16

The following summary details the essence of the survey program:

Base of operation	Kirkenes
Traverse line spacing and trend	2 km, north – south
Tie line spacing and trend	6 km, east – west
Flying height /sensor altitude	300m/230 m.
Speed	225 km/h
Total line kilometres (planned)	30500
Total line kilometres (acquired)	30800
Data recorded	Total field magnetic intensity, radar altitude and GPS positioning data

2.2 Personel on board

From NGU participated:

Senior engineer. John Olav Mogaard (leader of field operations)
Senior engineer: Janusz Koziel
Engineer: Rolf Lynum

From Fly Taxi Nord participated:
Captain: Ronny Thorbjørnsen
Captain: Ole Thorbjørnsen
Copilot: Karen Anne Hassel
Copilot: Gard Pettersen
Copilot: Kjetil Henriksen

2.3 Equipment and technical specification

The following equipment was used in the survey:

Aircraft: Piper Chieftain PA31 (registration. LN-ABZ) with long range fuel tanks from FlyTaxi Nord in Tromsø (Fig. 2.2).

Magnetometer: A Scintrex Cesium Vapour MEP 410 high sensitivity magnetometer with a CS-2 sensor was applied in the data acquisition. The noise envelope of the onboard magnetometer was 0.1 nT. Most of the data fell within the limits of ±0.04 nT.

Base Magnetometer: A Scintrex MP-3 and an EnviMag proton magnetometer was used for recording diurnals at the base station which was located at Kirkenes airport (Høybuktmoen). Data from the base magnetometer were used in planning of flights and to decide on which lines eventually to refly.

Data logging: A DAS8 datalogger, GR33 chart recorder and a HDR150 tape station from RMS Instruments were used to record the different data from the survey.

Navigation: An Ashtech G12, 12 channel GPS receiver combined with a Trimble Navbeacon DGPS correctional receiver (SATREF) with flight guidance system from Seatex ASA was used for real time differential navigation. The navigation accuracy was better than ±5 m throughout the survey.

Altimeter: A KING KRA 405 radar altimeter is an integrated instrument of the aircraft and the data were both recorded and shown on the pilot's display. Accuracy of 0.25% with a resolution of 1 foot (0.3058 m).

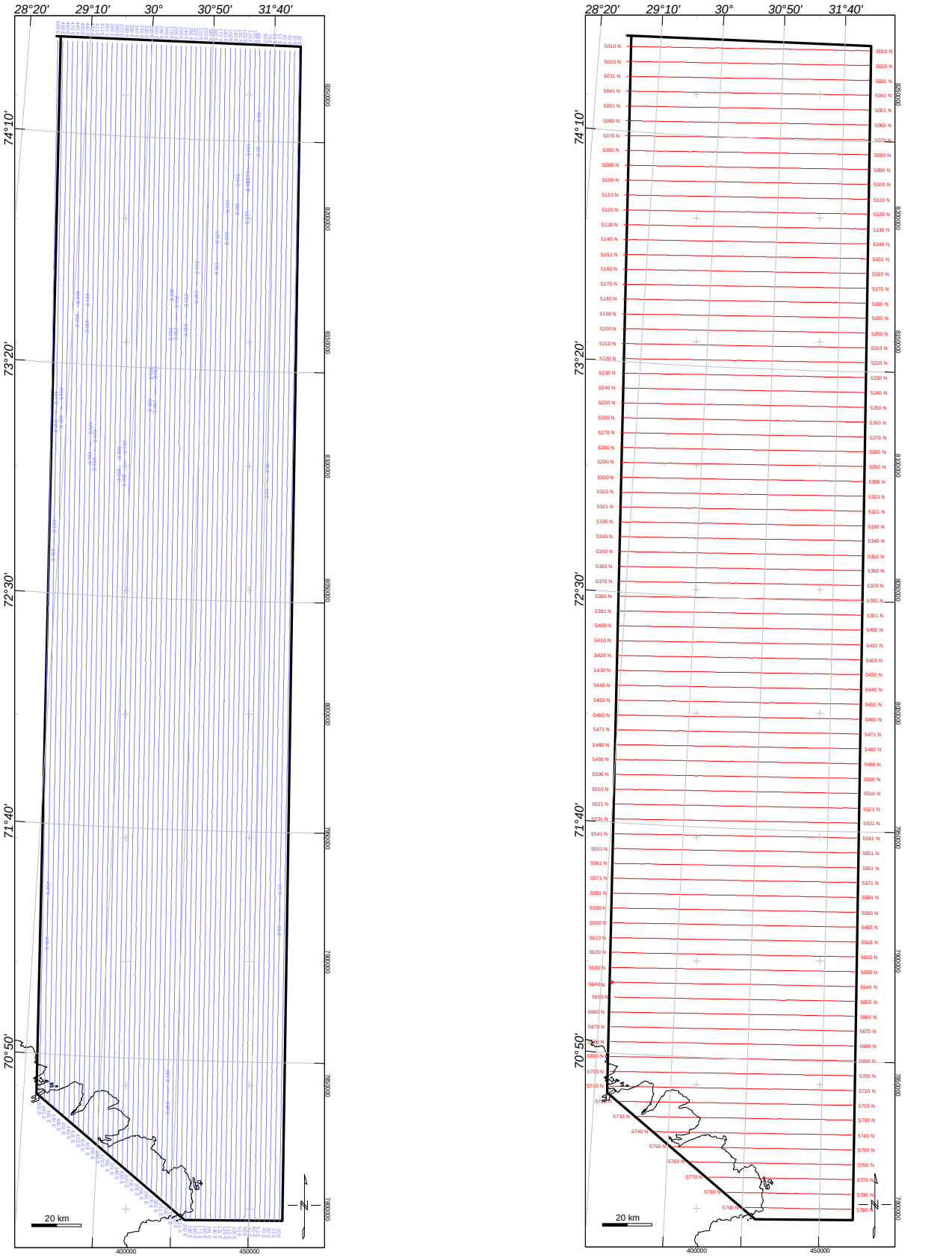

Figure 2.1 Flight pattern (blue lines and red tie-lines) of the BAS-06 survey.

Figure 2.2 Piper Chieftain from Fly Taxi Nord with the docking cradle for the bird containing a Scintrex Cesium Vapour MEP 410 high-sensitivity magnetometer.

2.4 Acquisition

The acquisition period was initially planned for approximately 8 weeks but due to poor weather conditions and some shorter periods with magnetic disturbances, the acquisition has been seriously delayed with regards to the initial schedule. Figure 2.3 shows, however, that the magnetic conditions for aeromagnetic surveying were relatively good during the period of June to September 2006. A total of app. 30.800 line km was produced. The plan was to produce 30.500-profile km but app. 300 km was added later over the Mjølnir crater as infill lines for NGU research purpose (producing 1 km line spacing within this area). The whole area was covered with both tie-lines and traverse lines (Fig. 2. 1). The total survey area constituted c. 45200 km^2 and consisted of 23250 km traverse lines and 7550 tie-lines. The aircraft altitude was 300 m (1000 feet). The magnetic sensor was towed approximately 70 m below and behind the aircraft, giving a sensor altitude of app. 230±5 m. The flying speed was 225 km/h and magnetic data were sampled at a rate of 5 Hz, giving a spatial sampling interval of 12-14 m along the lines.

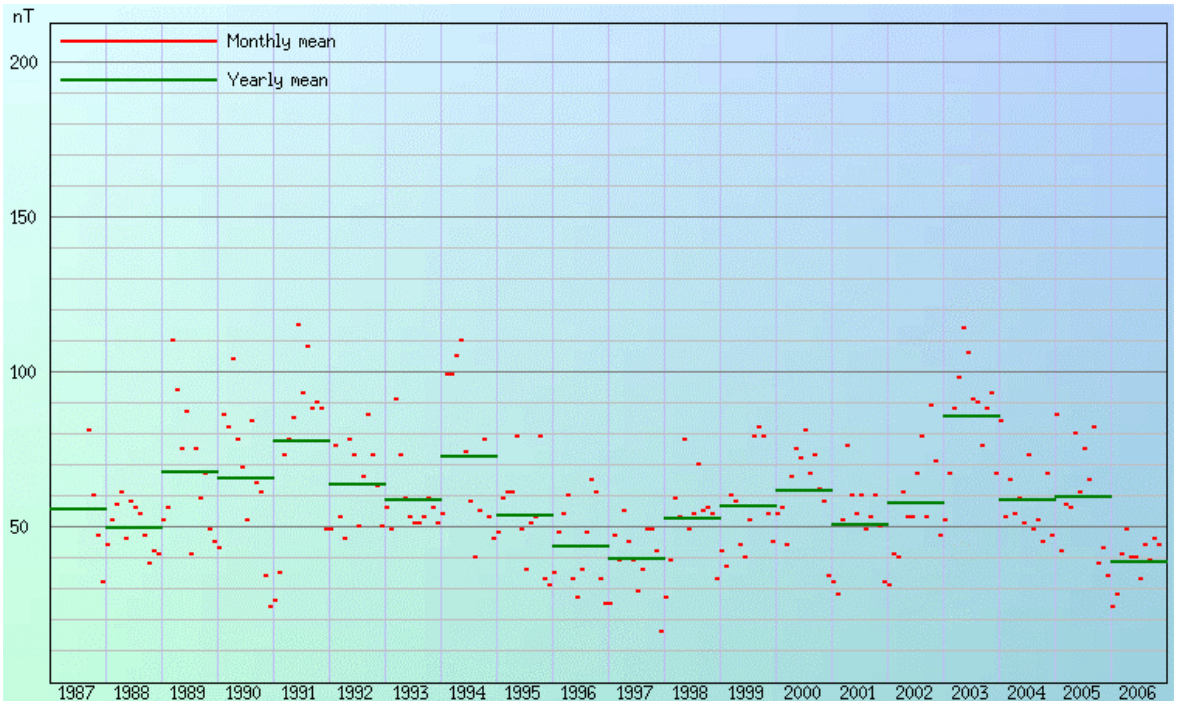

Figure 2.3 Diagram from the Tromsø Geophysical Observatory (http://www.tgo.uit.no/aix) showing relatively good magnetic conditions for aeromagnetic surveying during the two periods in June-July and August-September 2006.

The magnetic signature of the airplane includes 1) its permanent magnetisation induced by its motion through the Earth's magnetic field and 2) a component due to the flow of electric current within the plane. The permanent magnetisation of the plane varies as the plane change its orientation leading to heading error. A magnetic heading test (clover-leaf test) for the BAS-06 survey was carried on the 7th of October 2006 over a small island near Hammerfest at an altitude above 1000 meters (Fig. 2.4). The variation in the four different directions was small (0.6 nT) and consequently no corrections were applied to the magnetic dataset.

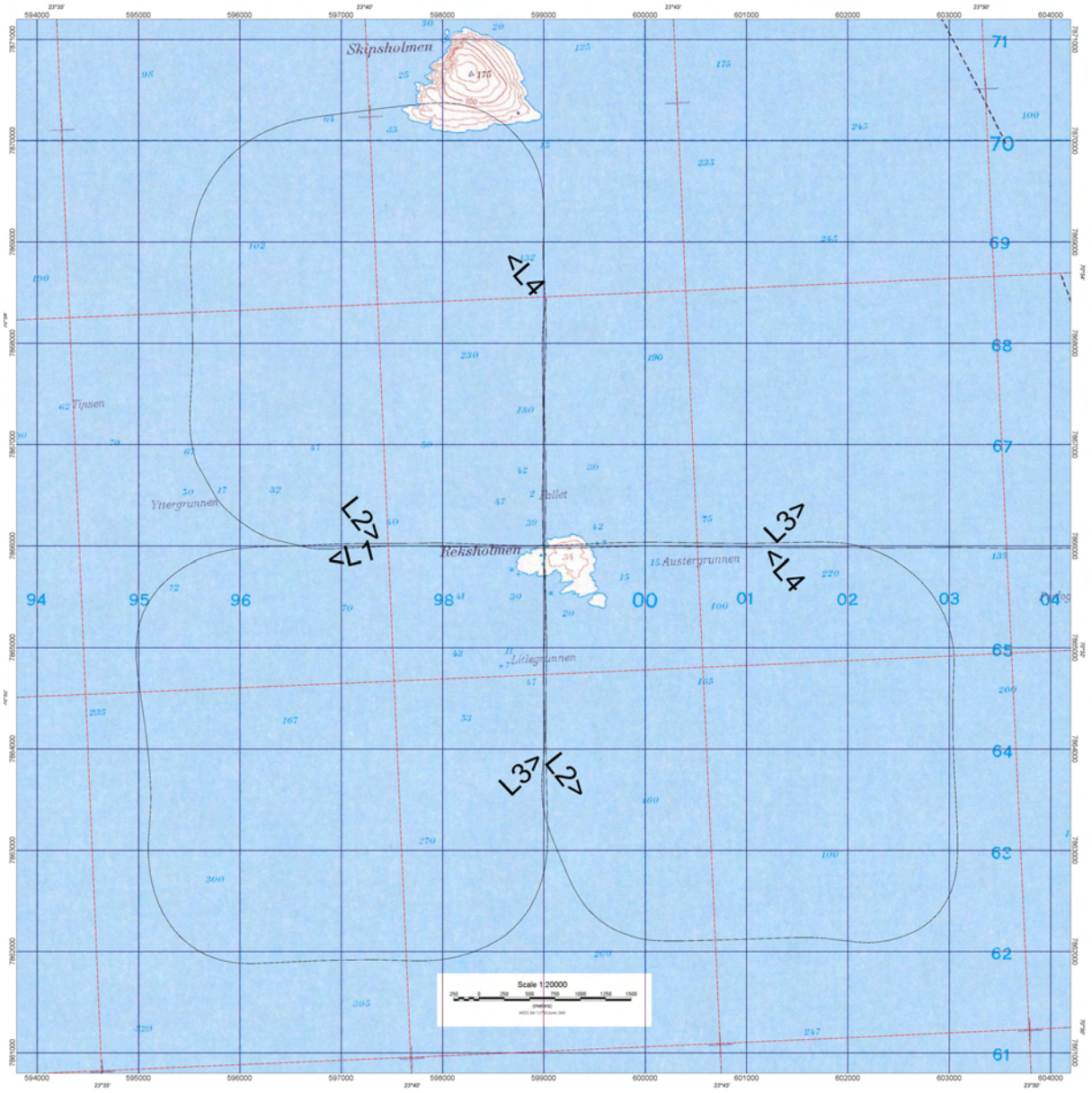

Figure 2.4 Flight path of clover-leaf test flown on the 7th of October 2006 for the BAS-06 survey. The lines are therefore oriented N-S and E-W.

The intensities of the total magnetic field (TMI) for the crossing point are shown below:

Line	TMI	Direction
1	53462.1	EW
2	53461.9	NS
3	53462.5	WE
4	53461.3	SN

The diurnals for all flights are displayed in the BAS06bmag.doc file delivered on the BAS-06 archive DVD. The data from the base magnetometer (EnviMag) located at Kirkenes airport were transferred to a laptop and plotted out flight by flight. The start and termination of each profile (traverse and tie) are indicated by red vertical lines (with annotated profile numbers) on the diurnal

plots. The curve is coloured red for profiles and blue elsewhere. These plots ease the quality control of the acquired profiles The data were classified into two quality groups according to magnetic diurnals:

Class	Criteria	Profile length
1	< 10 nT/10 min. linear	27.242 km
2	10 – 30 nT/10 min. linear	2.558 km
Total		30.800 km

A total of 2558 line km of low quality profiles, affected by diurnal effects was reflown. The lines are shown in the file BAS06bmag.doc and the reflying was done during the four last flights.

3 DATA PROCESSING and PROFILE LEVELLING

Laurent Gernigon

The raw magnetic profiles (Fig. 3.1) cannot be used directly and required a number of processing steps before production of the final aeromagnetic grid used for interpretation. Noise filtering and statistical levelling processing were carried out using the professional OASIS Montaj software (Geosoft 2004, Geosoft 2005a). Micro levelling was performed using both the MAGMAP FFT package from OASIS Montaj of Geosoft (2005b), and the median filtering software developed at NGU (Mauring and Kihle 2006). The various processing steps and standard procedures are outlined below.

3.1 Preliminary noise filtering and basic corrections

3.1.1 Noise filtering

High-frequency noise is usually created as the aeroplane is manoeuvring. After acquisition, initial raw data were imported directly into an Oasis Montaj database and first interpolated to a regular grid of 500x500 m cells, to check the quality of lines and tie lines. Spikes due to minor noise and artefacts were first removed by non-linear (Naudy) filtering and subsequently smoothed with a light low-pass filter (10 fiducials=500 m) in order to keep the signal intact.

3.1.2 Systematic lag corrections

Original magnetic profiles were lag-corrected, utilizing the Oasis Montaj processing package (Geosoft 2005a) with 5 fiducials (=250 m). As part of the processing sequence, lag correction was applied to the BAS-06 data but did not change the data significantly due to minor variations in values as a function of survey direction.

3.1.3 International Geomagnetic Reference Field (IGRF correction)

As part of the processing, the total magnetic field is computed from the recorded magnetic field after subtraction of the International Geomagnetic Reference Field (IGRF) model (Fig. 3.2). The IGRF is a mathematical representation of the undisturbed Earth's geomagnetic main field. The International Geomagnetic Reference Field for 2006 (IGRF-2006) was calculated using the Oasis Montaj IGRF tool (Geosoft 2005a). The result of this subtraction isolates the component of the magnetic total field, which is dominated by the magnetic effects from the underlying crustal rocks.

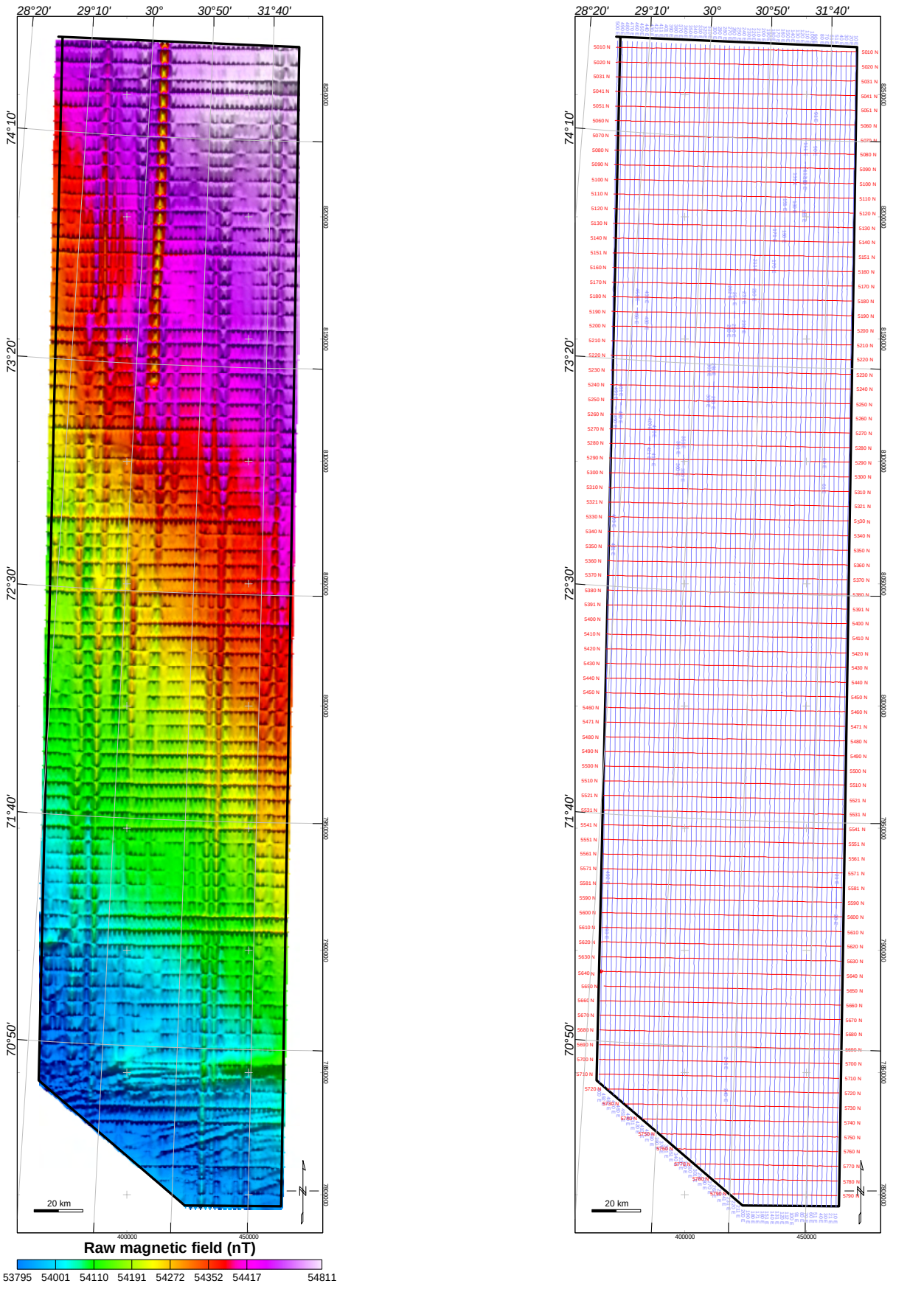

Figure 3.1 Raw magnetic profiles gridded using the minimum curvature algorithm (grid cell at 500 m) (left) and location of the lines (N-S) and tie-lines(E-W) profiles along the BAS-06 survey area (right). Projection UTM 36, WGS 84.

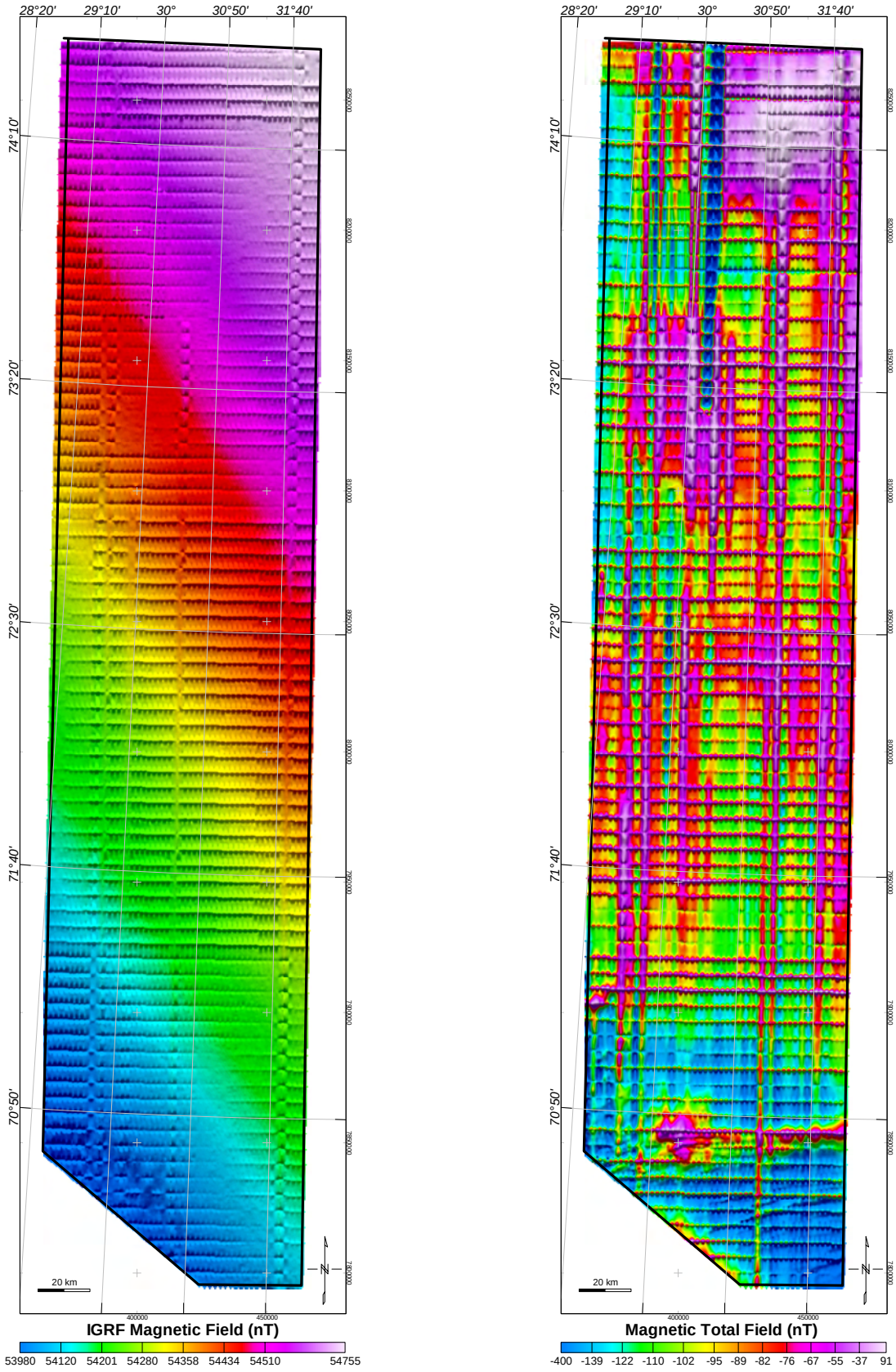

Figure 3.2 The IGRF-2006 model along the BAS-06 survey (left). The map on the right represents the magnetic total field after lag, heading and IGRF corrections (before levelling). Errors at the crossover points are mostly due to altitude and ground clearance variations, wave noise and diurnal effects.

3.2 Levelling and microlevelling of the magnetic profiles

3.2.1 Diurnal variation use of base magnetometer readings

A variety of external, time varying field factors usually influences and causes errors during aeromagnetic acquisition. This includes time variation in the magnetic field, ground clearance variation, altitude variation, magnetic effects of seawater waves and diurnal effects. This usually explains the errors at crossover points between line and tie-lines. The most complex and significant problem is probably the diurnal variation of the Earth's magnetic field influenced by solar wind (Fig. 3.3). In polar latitudes, the most famous and spectacular expression of these diurnal effects are the aurora borealis, known to be caused by the collision of charged particles (e.g. electrons), in the magnetosphere with atoms in the Earth's upper atmosphere. Diurnal variation in the magnetic field can cause tie line and regular survey lines to have different readings at the same geographical point. Even if they are small these long-wavelength effects can be visually distracting particularly on image-enhanced displays. Such misfits can produce artefacts during interpolation and consequently erroneous interpretation if no suitable corrections have been applied.

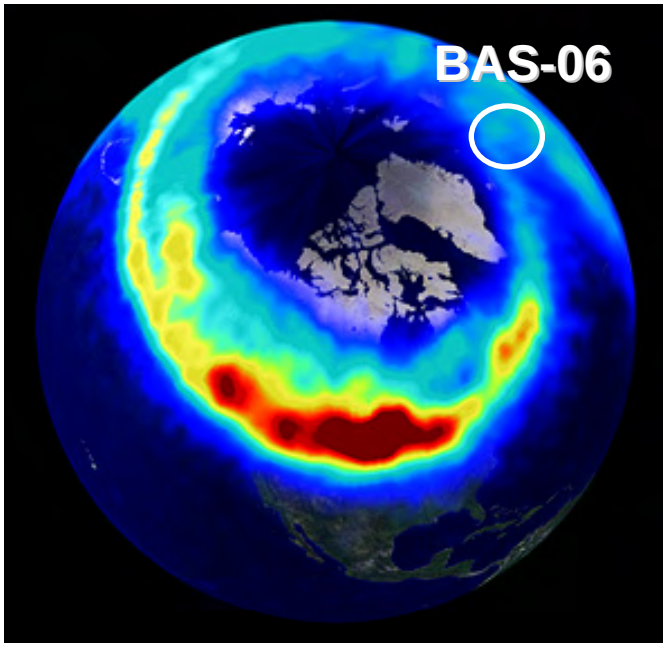

Figure 3.3 Distribution of the magnetic disturbances produced due to solar storms around the magnetic north pole and the polar circle (NASA)

The most important reason for this is the time shift in the Earth's magnetic field variations between the large survey area and the onshore base station (Hammerfest). There is normally a spatial difference in amplitude and frequency of these diurnals. Data from the base magnetometer have therefore only been used to assess the quality of individual lines and to make decisions on which lines eventually to re-fly.

3.2.2 Statistical levelling

Diurnal variations in the magnetic field usually cause tie line and regular survey lines to have different readings at the same geographical point. Even if they are small, these long-wavelength discrepancies are visually distracting particularly on image-enhanced displays. Such misfits can produce artefacts during interpolation and consequently erroneous interpretation if no suitable corrections have been applied.

The purpose of levelling "science" is to minimize these residual differences in a coherent way by proportioning them between lines and tie lines (Fig. 3.4). Proper levelling or microlevelling algorithms usually require close and proper line spacing and the quality of the final result is most of the time a function of this crucial parameter. Usually, large line spacing does not allow proper micro-levelling and interpolation of raw data often produces erroneous or factitious anomalies. It is still the case for the old magnetic surveys.

Levelling was undertaken at NGU using the standard (Geosoft 2005a) statistical levelling method of the tie-lines followed by a statistical levelling of the profiles utilising the levelled tie-lines. We used first a first-order (linear) trend removal in the levelling of the tie-lines but a second order trend was definitively adopted for the tie line levelling after several preliminary tests. Before running the trend-levelling algorithm, 'suspicious' mis-tie values (outliers) were removed manually before levelling of the tie-lines. The linearly detrended tie lines surface was finally used similarly for the final full levelling of the survey lines. Due to small amplitude of the magnetic signal along the BAS-06, automatic statistical levelling could not provide any reasonable solution. Due to the risk of removing or smoothing the magnetic signal to much, no filtering has been applied to the data during the levelling. It was particularly crucial to keep intact the low magnetic variation (<3 nT) observed around the salt features. For each outlier removal, gridding has been systematically realised to check the validity of each trial, until we got a reasonable grid. Instead of smoothing, we re-ran several times the full levelling of the lines to further improve the levelling correction. Extreme mis-tie values (outliers) were checked and removed again manually before calculating the next full levelling correction, until convergence was achieved.
We also tried to apply different spline algorithms during the conventional levelling to remove the

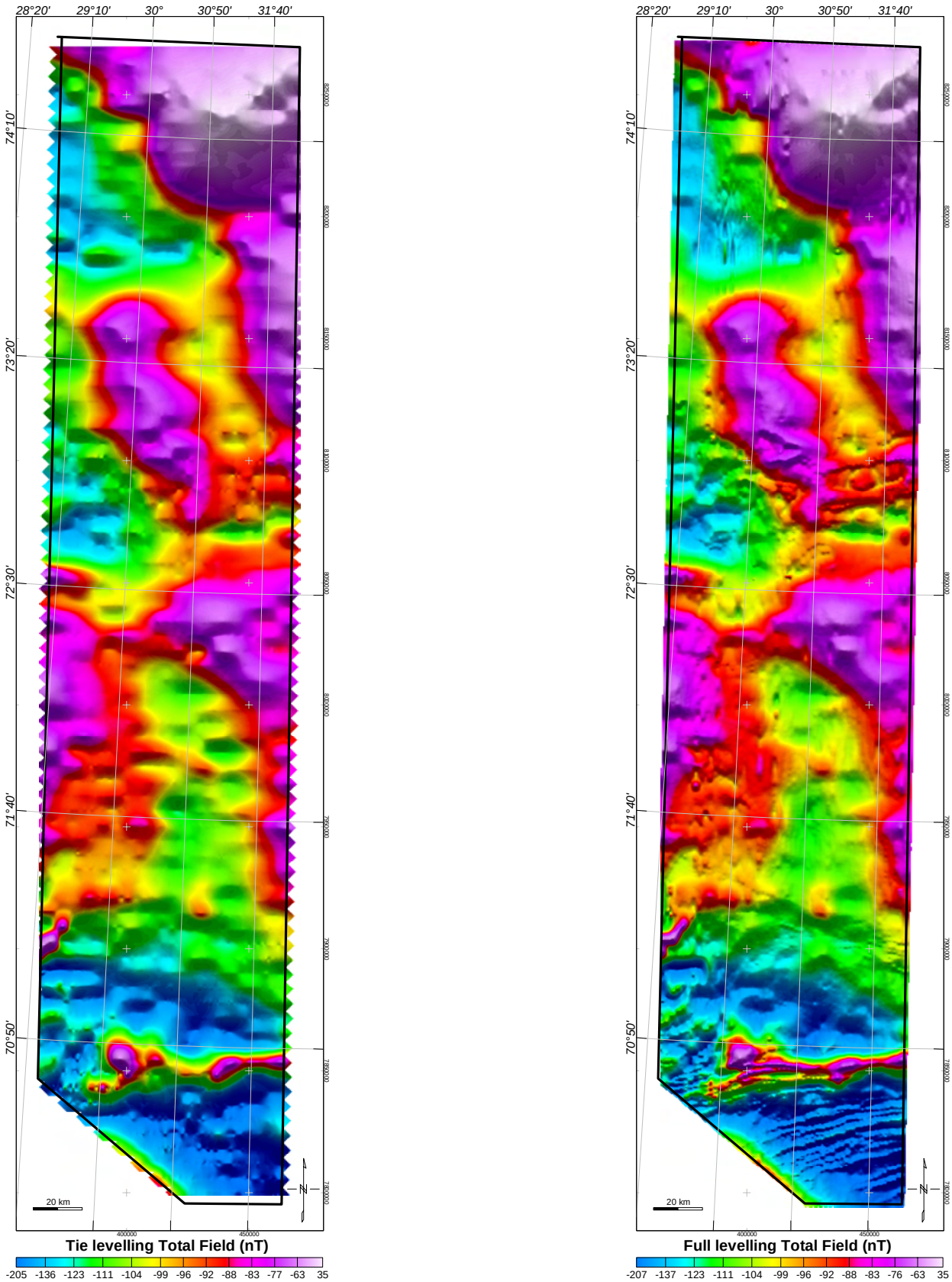

Figure 3.4 Statistical tie lines (left) and full levelling (right) of the magnetic profiles, lag corrected and referred to IGRF-2006. Gridding using the minimum curvature algorithm (x500 m).

residual noise, but there were no observable improvements in the resulting grids. Spline and akima algorithms smoothed the data too much and removed some interesting trends and features, with often small nT variation. The final results were the best compromise between the removal of levelling errors and anomaly preservation.

3.2.3 Micro-levelling

To remove minor levelling errors still remaining along parts of some profiles after the statistical levelling, we performed micro levelling techniques. For these techniques to be used successfully, the regional field must first be removed from the magnetic data. This can be obtained by using the residual from high-pass filtering of the magnetic total field. To get the best results, some tuning of filter parameters for both of these techniques was required. The optimal filter parameters for the BAS-06 data were chosen after several testing. We applied separately two micro-levelling techniques (Fig. 3.5): 1) the Geosoft micro-levelling approach using FFT decorrugation (Geosoft 2005b) and 2) the moving median filtering method developed at NGU (Mauring et al. 2002, Mauring and Kihle 2006).

The Geosoft micro levelling has been realized using the MAGMAP FFT processing package (Geosoft 2005b). MAGMAP applies a decorrugation process in the Fourier domain to isolate the levelling corrections before applying them to the original data. The BAS-06 data have been decorrugated to reduce line-to-line levelling errors, which are visible as linear magnetic features parallel to the flight lines. Decorrugation is simply a frequency domain procedure based on a directional cosine filter. This filter retains anomalies, from gridded data, in the flight line direction only. First, a Butterworth high-pass filter is set to four times the line spacing to pass wavelengths on the order of two to four line separations. Such process results from a line-to-line levelling error. In a second step, a directional cosine filter is set to pass wavelengths only in the direction of the lines. The last result is subtracted from the original data to produce the levelling errors dataset. We apply afterwards a line-based filter to separate the high frequency geological signal from the longer wavelength levelling error. A filter length 10 times the line spacing data was applied to clean the levelling error channel. The micro-levelling result was obtained by subtraction of the cleaned levelling from the original dataset.

The moving median levelling method is described in details in Mauring and Kihle (2006). A floating median filter was applied to each line. For a given line, the 1D median was determined at each station based on data values within a given distance of the station. We can in the same way find a 2-D median value for a circular area around the station. The difference between the 2D and 1D median value was taken to be the micro-levelling error and was added to the magnetic value at that station after smoothing. After different tests, the best result has been obtained using 2000 meters for the distance of the 1D median and 6000 m for the radius of the 2D medium values.

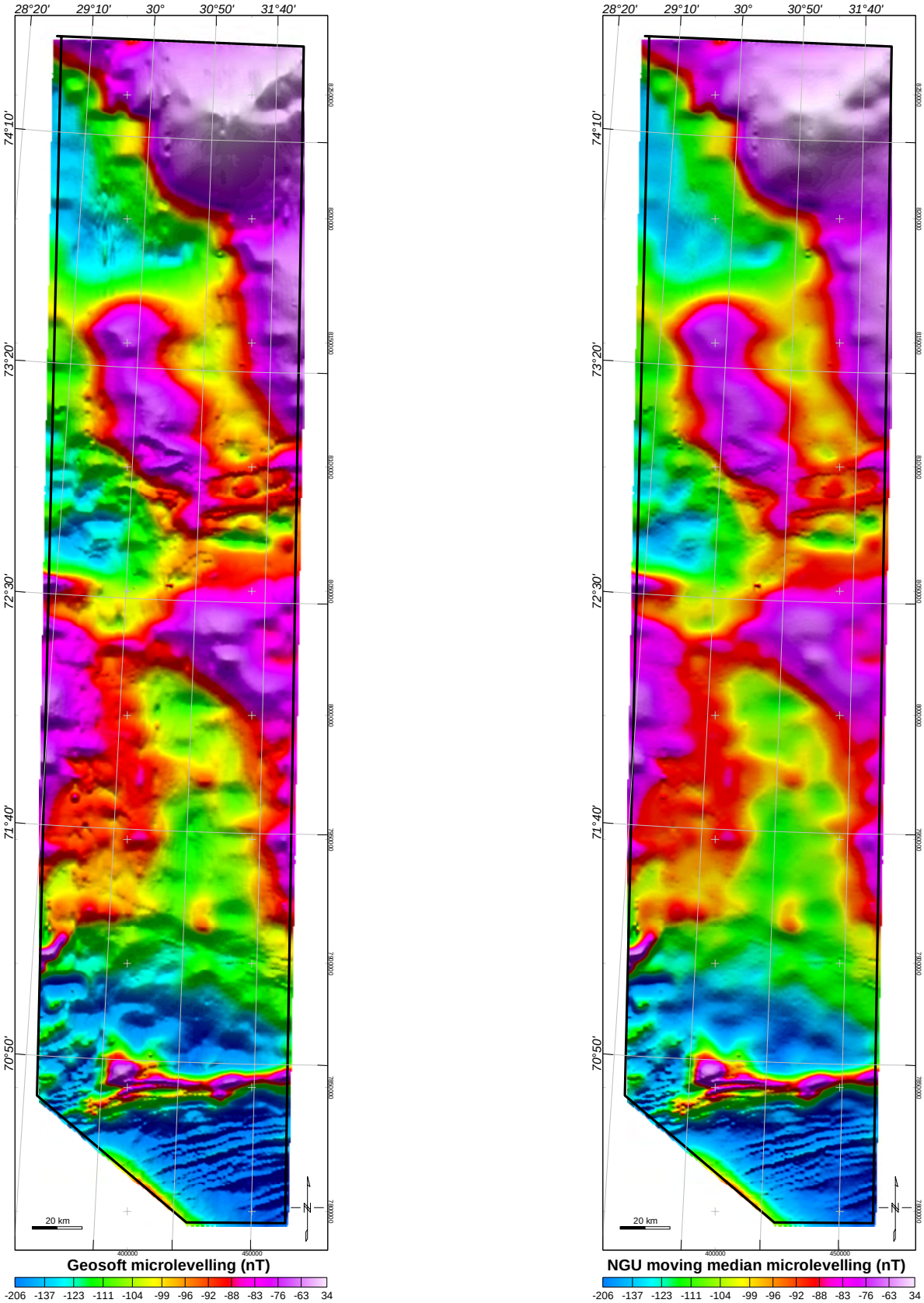

Figure 3.5 Total magnetic field after microlevelling. Results using the FFT decorrugation technique of Geosoft (left) and the median levelling method of Mauring and Kihle (2006) (right).

Compared to the Geosoft decorrugation technique, the median levelling removed partly the levelling errors of the conventionally levelled data without involving a huge smoothing of the aeromagnetic signal. Only small levelling errors still remained, but more filtering will have a negative effect on the grid since most of the amplitudes are especially low. The NGU median filter technique also provides a better display at the end.
The magnetic total field grid, using the median levelling method with 2000 meters for the distance of the 1-D median filter and 6000 m for the radius of the 2-D filter were selected for the final interpretation.

3.2.4 Reduction to the pole (RTP)

The magnetic data were reduced to the pole to properly register and locate the magnetic anomalies spatially above the magnetic bodies within the crust. The correction was derived from inclination and declination from the IGRF-2006 (Fig. 3.6). Even if only minor changes can be observed along the BAS-06 at Barents Sea latitude, the process is usually recommended for the application of magnetic data, and makes magnetic maps more reliable for geological mapping by removing some of the complexity involved in interpreting the anomalies (Blakely 1995). The RTP is a process involving a phase transformation of the magnetic anomaly, within the Fourier domain. The measured total field anomaly is transformed into the vertical component of the field (Blakely 1995).

The assumption following this transformation is that the magnetic anomalies had been magnetised vertically at the pole and that the anomalies are observed from the pole. Key assumptions are that the magnetisation of the source is entirely due to induced magnetisation. Therefore the phase of the anomaly is transformed into simpler symmetrical shapes that are assumed to lie directly over the magnetic sources (Blakely 1995). We will see later that this implication can provide more constraints about the shape of salt features at depth. This assumption is essential for future mapping and analysis of the magnetic anomalies because it is assumed when applying edge enhancement, that the causative field is vertical. Moreover, it is assumed that both the magnetic field and the magnetization of the crust have constant directions within the study area (Arkani-Hamed 1988).

3.3 Grid and map production

3.3.1 Gridding of the BAS-06 dataset

The OASIS Montaj software (Geosoft 2004) was intensively used for the map production. Geosoft format is standard for grav-mag processing and database and grids in Geosoft format are provided on the archive DVD. The grids are presented with a shaded relief technique (illumination from the northeast). Presentation of the maps with the shaded relief technique enhances lineaments that trend

oblique to the illumination direction. Colour scale and colour distribution for the datasets have been computed using a histogram equalisation technique. The grids have a cell size of 500x500m. The grid cell size represents a quarter of the line spacing. Gridding prepared with a lower resolution could provide a better special resolution but can also show high frequency and noise aliasing errors. We used the Geosoft minimum curvature algorithm for all the grids displayed in this report. All the grids have a grid cell size of 500x500m.

The interpolated surface generated by minimum curvature is analogous to a thin, linearly elastic plate passing through each of the data values with a minimum amount of bending. Minimum curvature generates the smoothest possible surface while attempting to honor the data as closely as possible (Press et al. 2002). Minimum curvature produces a grid by repeatedly applying an equation over the grid in an attempt to smooth the grid. Each pass over the grid is counted as one iteration. The grid node values are recalculated until successive changes in the values are less than the maximum residuals value, or the maximum number of iterations is reached (maximum iteration field). The minimum curvature gridding technique is efficient, fast and widely used in the Earth sciences. However, the minimum curvature is not an exact interpolator and this means that the data are not always honored exactly. Sensitivity study with other gridding techniques was not realised in the present study but the processed profiles values still allow to regrid the data using other gridding techniques and favorite software. Gridding techniques like the Kriging technique can be more relevant for specific parts of the survey area. The Kriging algorithm, for example, can be either an exact or a smoothing interpolator depending on the user-specified parameters. It can incorporate anisotropy and underlying trends in an efficient and natural manner and could be used locally to refine better linear magnetic features along the BAS-06. However, the gridding differences are likely lower than the magnetic total field uncertainties (<0.05 nT in average). Therefore, it should not significantly change the interpretation.

We use the UTM projection with datum WGS84 for most of the maps provided in this report. The database provided in the archive DVD also provides geographic and UTM36 coordinates with ED50 projection coordinates. The profile data are archived on the enclosed DVD in ascii and Geosoft formats. The contents of the DVD are described in the Appendix (p. 136). NGU can provide specific filtered grids to the BAS-06 partners on request.

3.3.2 Merge of the BAS-06 grid with the former regional grid

The BAS-06 grid has been merged with the pre-existing NGU magnetic compilation of the Western Barents Sea (Olesen et al. 2006) (Fig. 3.7). The Oasis montaj GridKnit module was used to merge the two geophysical grids with different cell size, projection or grid type. The blending method merged the grids via standard smoothing functions. Trend removal operations were performed with respect to the regional grid. The maximum trend order have been specified, or adjusted

automatically based on a fitting tolerance. However, this technique locally “forces” the magnetic trend envelope of the BAS-06 to be adjusted with the surrounding dataset. Since the surrounding magnetic dataset is old (NGU-1971 survey), has low resolution and is less reliable the merge process could wrongly influence the initial quality of the BAS-06. For local interpretation and modelling, we consequently recommend to use the original BAS-06 grid. The final grid can only be provided to partners, which also purchased the regional NGU magnetic dataset.

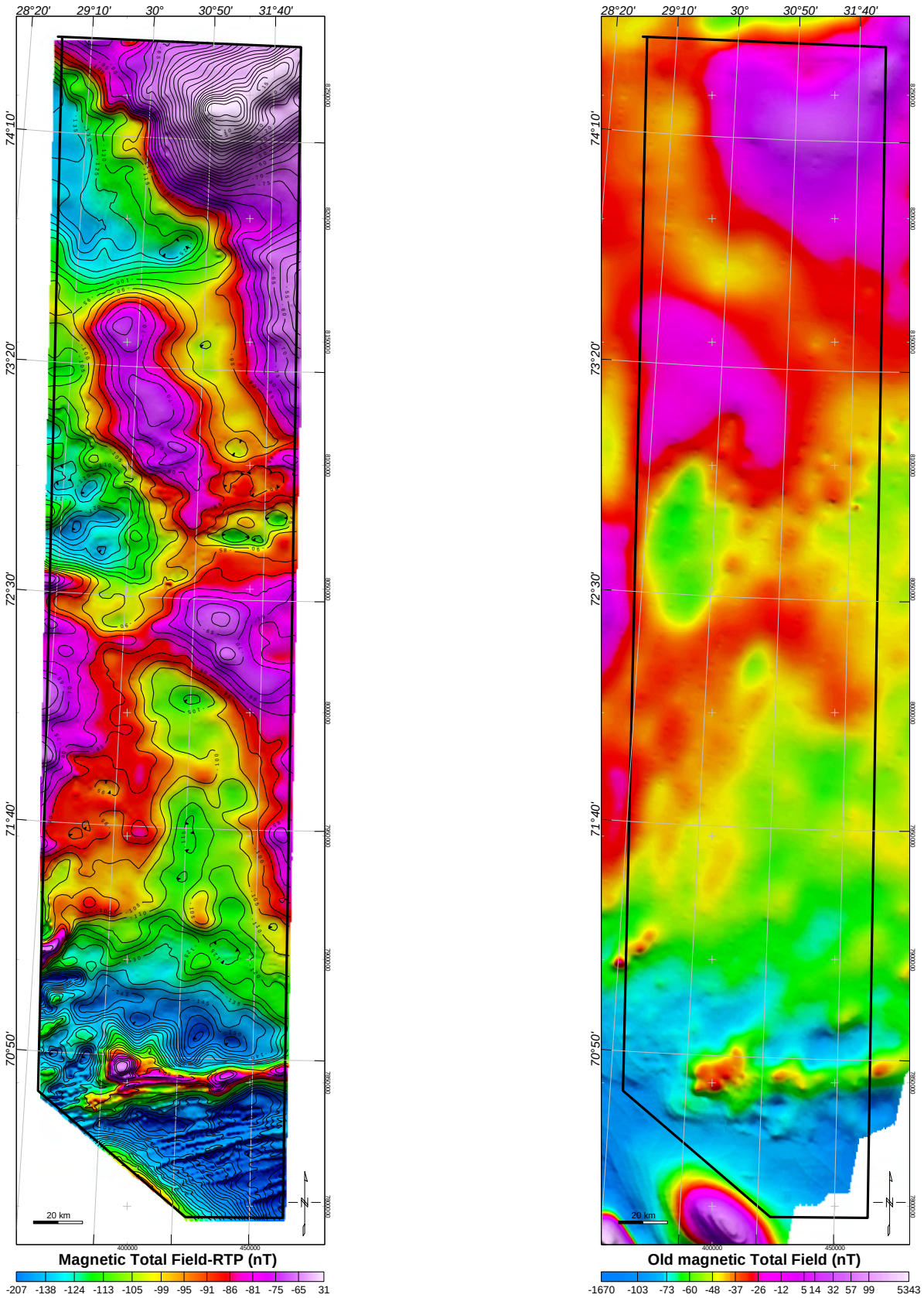

Figure 3.6 Total magnetic field grid and superimposed magnetic contours after reduction to the pole. The final result can be compared with the previous magnetic compilation (Right). Better resolution and higher frequency anomalies are observed on the new survey.

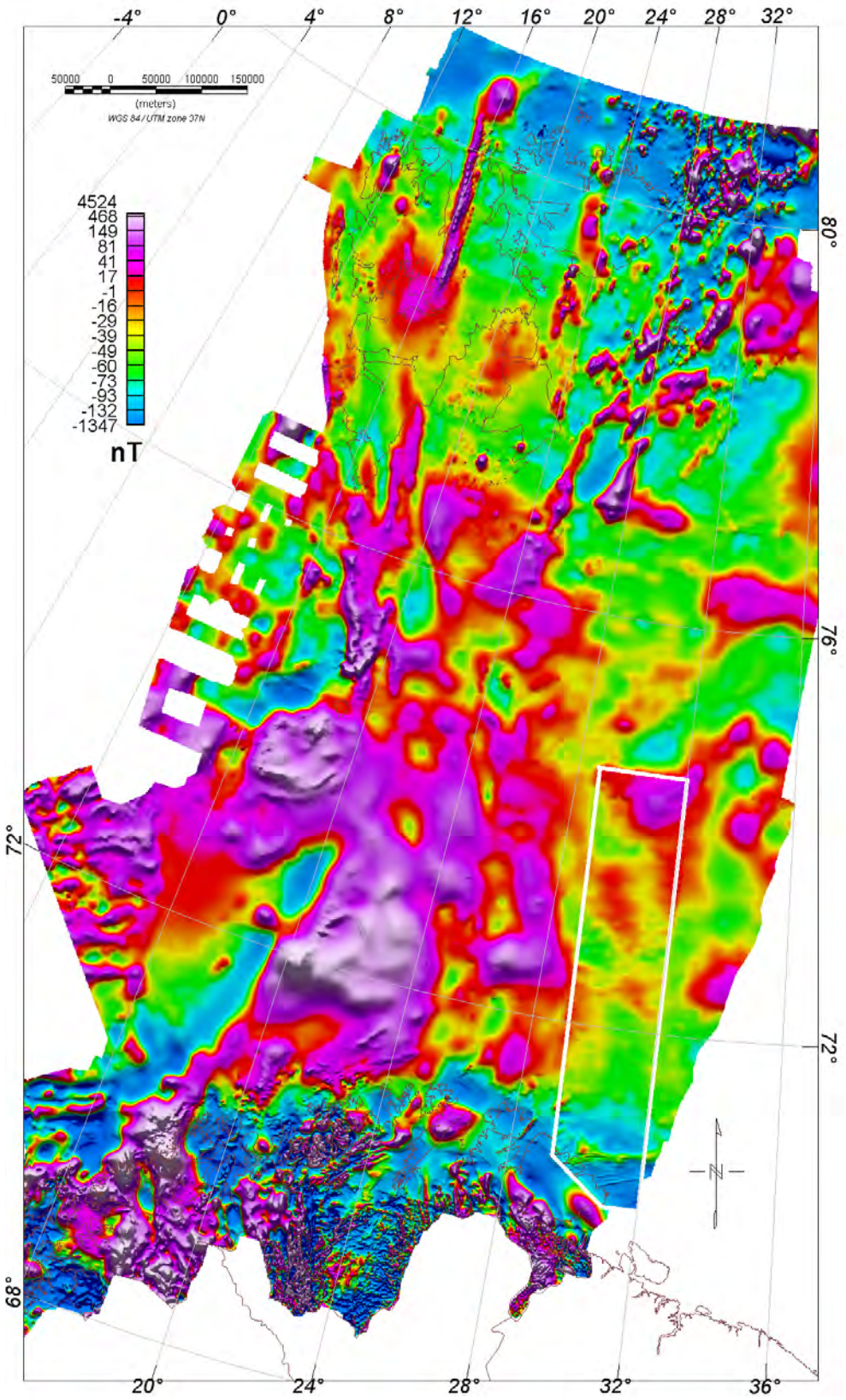

Figure 3.7 Merge of the BAS-06 with the previous regional NGU magnetic grid (Åm 1975, Skilbrei, 1991, 1992, 1993 ,Skilbrei et al. 1990, Olesen et al. 2006).

3.4 Other geophysical datasets

3.4.1 Bathymetry-topography

The bathymetric grid used in this study is a NGU compilation and gridding of several ship-track bathymetric profiles available along the study area (Fig 3.8). All the profiles have been levelled using the moving median filtering method (Mauring et al. 2002, Mauring and Kihle 2006).
A topographic grid at 25x25 m cells from the Varanger Peninusula is also included in the archive CDROM.

3.4.2 Gravity, Free Air and Bouguer

The gravity grid was compiled from gravity stations on mainland Norway in addition to marine gravity data from the Geological Survey of Norway, the Norwegian Mapping Authority, the Norwegian Petroleum Directorate and Norwegian and foreign universities and commercial companies (Skilbrei et al., 2000) (Fig 3.8). The compiled free-air dataset has been interpolated to a square grid of 2 km x 2 km using the minimum curvature method (Geosoft 2005). The simple Bouguer correction at sea (Mathisen 1976) was carried out using the bathymetry data in Fig. 3.8 and a density of 2200 kg/m^3. The International Standardization Net 1971 (I.G.S.N. 71) and the Gravity Formula 1980 for normal gravity have been used to level the surveys.

Since all the partners of this survey do not get access to the Dragon high-resolution gravity dataset, only the NGU gravity grid along the survey area will be presented in the present report.

3.4.3 Seismics

Available 2D seismic lines kindly provided by the Norwegian Petroleum Directory (NPD) led to a preliminary interpretation and modelling of the survey area (Fig 3.8). It should be noted that the seismic data were only available in two-way traveltimes. EasyDepth^{TM} from Beicip Franlab was used for the depth conversion of the lines and allows us to produce a segy file converted to depth. These depth models were used for potential field modelling and directly imported into the GM-SYS package. Interpretation of 3 transects and depth conversion have been realised during this work. We used key horizons presented in the previously published papers and used well information provided by NPD to constrain the geologic model. We note, however, that the final interpretation suffers from the lack of high quality lines and a sparse seismic dataset, which could not allow us to fully constrain the meaning of all anomalies.

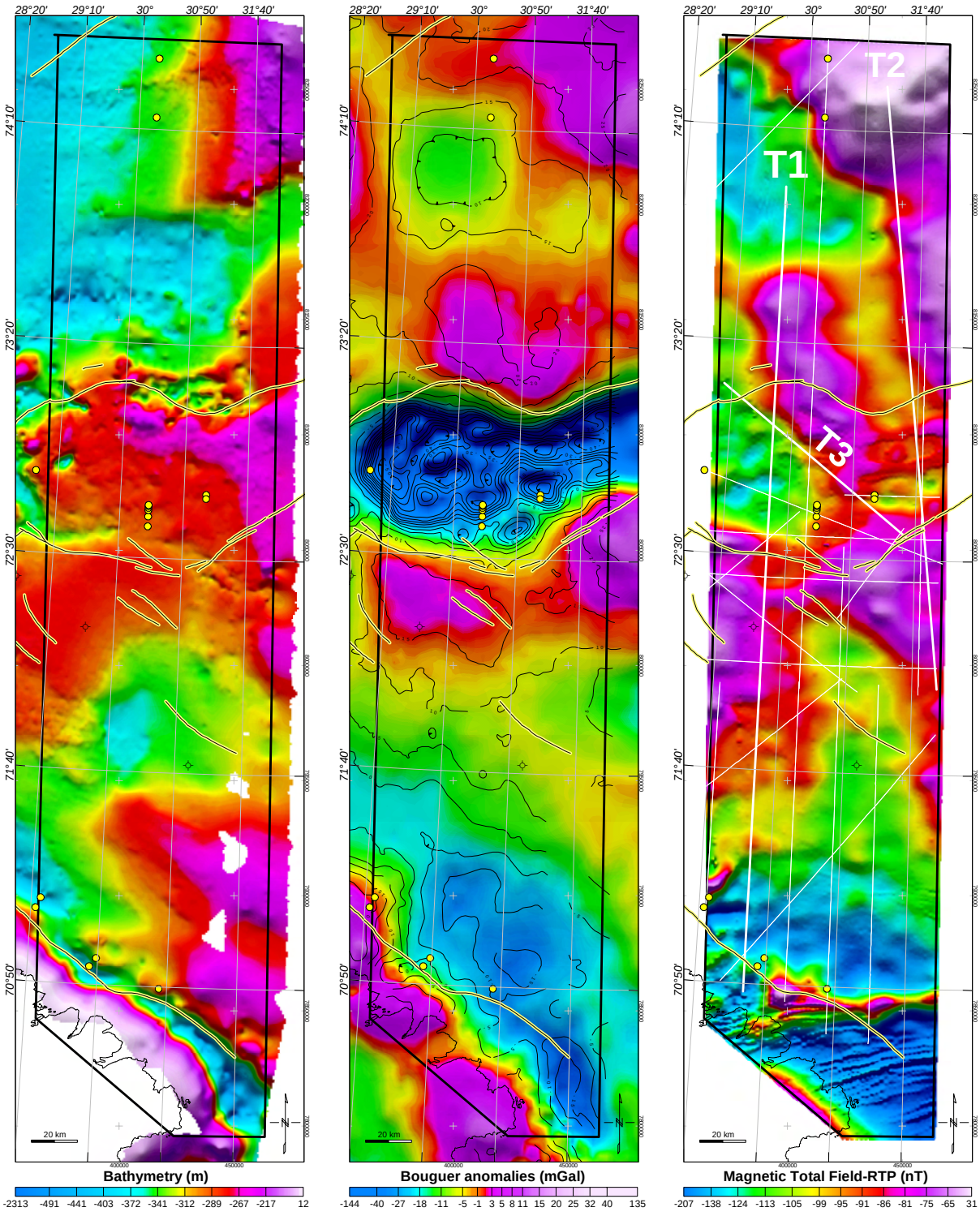

Figure 3.8 Other datasets available for the BAS-06 study. NGU bathymetric compilation (left), NGU Bouguer gravity compilation (centre) and 2D seismic lines provided by the Norwegian Petroleum Directorate draped above the BAS-06 magnetic total field, reduced to the pole (right). Yellow circles represent the IKU shallow well location, Black symbols represent exploration wells. The fault pattern (Gabrielsen et al. 1990) and cultural information have been downloaded from the NPD web site. T1, T2 and T3 represent the three transects modelled in the present study (cf. Chapter 7).

4 FILTERING AND DATA ENHANCEMENT

Laurent Gernigon

4.1 Potential field and integrated study

Potential field methods have an important place among the wide variety of methods in applied geophysics. Affirmed development of the interpretation theory is usually connected with many case studies of successful application of seismic methods combined with gravity and magnetic data in solving problems in exploration and structural geophysics. During this work, potential field techniques have been used intensively as irremediable and complementary tools for the interpretation of our sparse 2D seismic line. It was also a good way to test the validity of other geophysical models. Relevant filtering has been carried out in order to enhance the main structural changes and magmatic features observed along the BAS-06. The purposes of this chapter are 1) to show the applicability of the magnetic data in a structural geological study (lineaments and magnetic foliation) in the Barents Sea; 2) to evaluate the images produced by several enhancement techniques for lineaments mapping; 3) to prepare structural and depth to magnetic basement estimation maps (lineament) based on magnetic and gravity data interpretation. Some newly discovered lineaments and features might be subsequently used as a reference for future geological mapping, interpretation or re-interpretation.
The aim of this section is to briefly discuss the different processing techniques used to enhance and model the gravity and magnetic data across the BAS-06 survey. Specific and preliminary interpretation based on these grids will be presented in the next part of this report.

4.2 Enhancement of trends and structured analysis

During the BAS-06, a number of transformation methods have been used after data levelling in order to enhance the main structural and magnetic features, discussed and interpreted later in this report.

4.2.1 Wavelength filtering

Gravity and magnetic anomalies whose wavelengths are long relative to the dimensions of the geologic objectives of a particular investigation are called regional anomalies. Because shallow geologic features can have large lateral dimensions, one has to be careful, but regional anomalies are usually thought to reflect the effects of relatively deep features. Anomalies whose wavelengths are similar to the dimensions of the geological objectives of a particular investigation are called local anomalies. In the processing of gravity data, it is usually preferable to attempt to separate the

regional and local anomalies prior to interpretation. The regional anomalies can be estimated employing a variety of analytical techniques.

Magnetic and gravity anomalies observed along the BAS-06 survey characterise an amalgamation of sources reflecting the regional field, noise and lateral density and magnetic variations within the crust and upper mantle (e.g. Blakely 1995). Measured gravity anomalies, therefore, represent the combination of wavelengths associated with the spatially distributed sources. To successfully delineate the upper crustal structures it is necessary to distinguish the short wavelength (noise) and long (regional) wavelengths due to deeper sources in order to isolate the wavelengths derived from upper crustal structures.

The techniques used to separate regional and local gravity anomalies take many forms and can all be considered as filtering in a general sense (e.g. Blakely 1995). Many of these techniques are the same as those employed in enhancing traditional remote sensing imagery or processing of digital elevation data.

Filters have been applied to the BAS-06 gridded anomalies which enable us to isolate, interpret or/and enhance the wavelengths of greatest interest, therefore facilitating geological interpretations (e.g. Blakely 1995). The magnetic (and/or gravity) gridded datasets can be transformed from the space domain into the spectral domain and vice-versa using the Fast Fourier Transform. Transformation of the gridded data into the frequency domain is completed by application of a discrete 2D Fourier transform [FFT] (Bhattacharyya 1966, Blakely 1995).

In that context, the NGU gravity anomalies (Skilbrei et al. 2000) were also used to determine the presence of basins and basement highs. The magnetic data were most useful to determine the presence, trends and depth of intrusions, metamorphic terranes, faults and salt structures. High-pass filtering of the data at 50-30 km has been used to highlight sources typically at depths greater than 10-15 km whereas 20-15 km high pass filtering, will be used for source depths greater than 5 km (Fig. 4.1). For spectral analysis we use the Geosoft MAGMAP FFT algorithms, which apply the method of Bhattacharyya (1966).

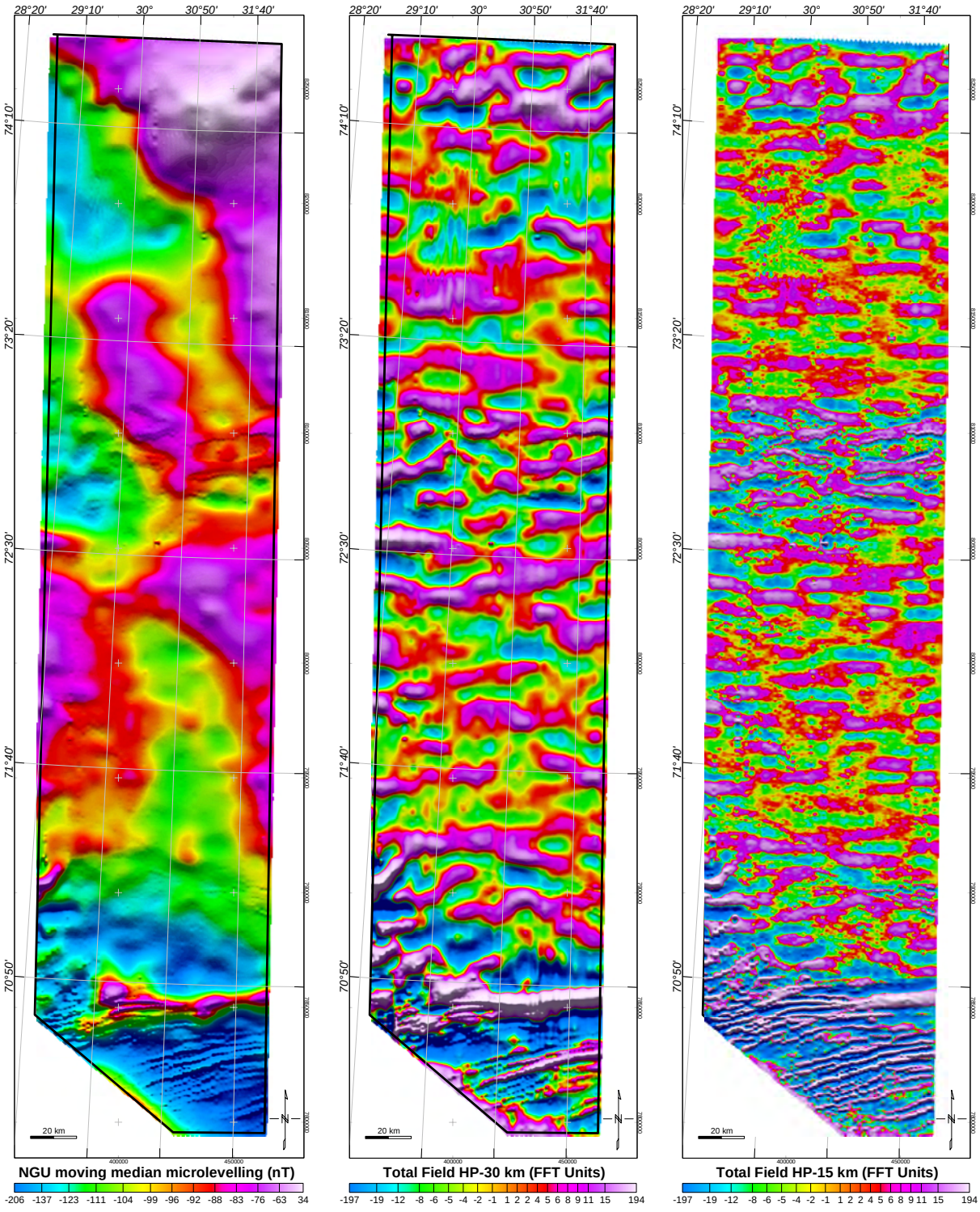

Figure 4.1 Magnetic total field of the BAS-06 (left) and 30km and 15km of high-pass filtering of this grid respectively (right). Medium to high frequency anomalies are mostly observed around the Nordkapp Basin and in the southern part of the Finnmark Platform, south of 71°40´. Along the Nordkapp Basin, E-W to NW-SE elongated anomalies and round-shaped magnetic pattern are observed. High-pass filtering with 15 km cut off wavelength highlights better N70° to N80° high frequency linear features in the southern part of the survey area. They progressively disappear to the north on the Finnmark Platform.

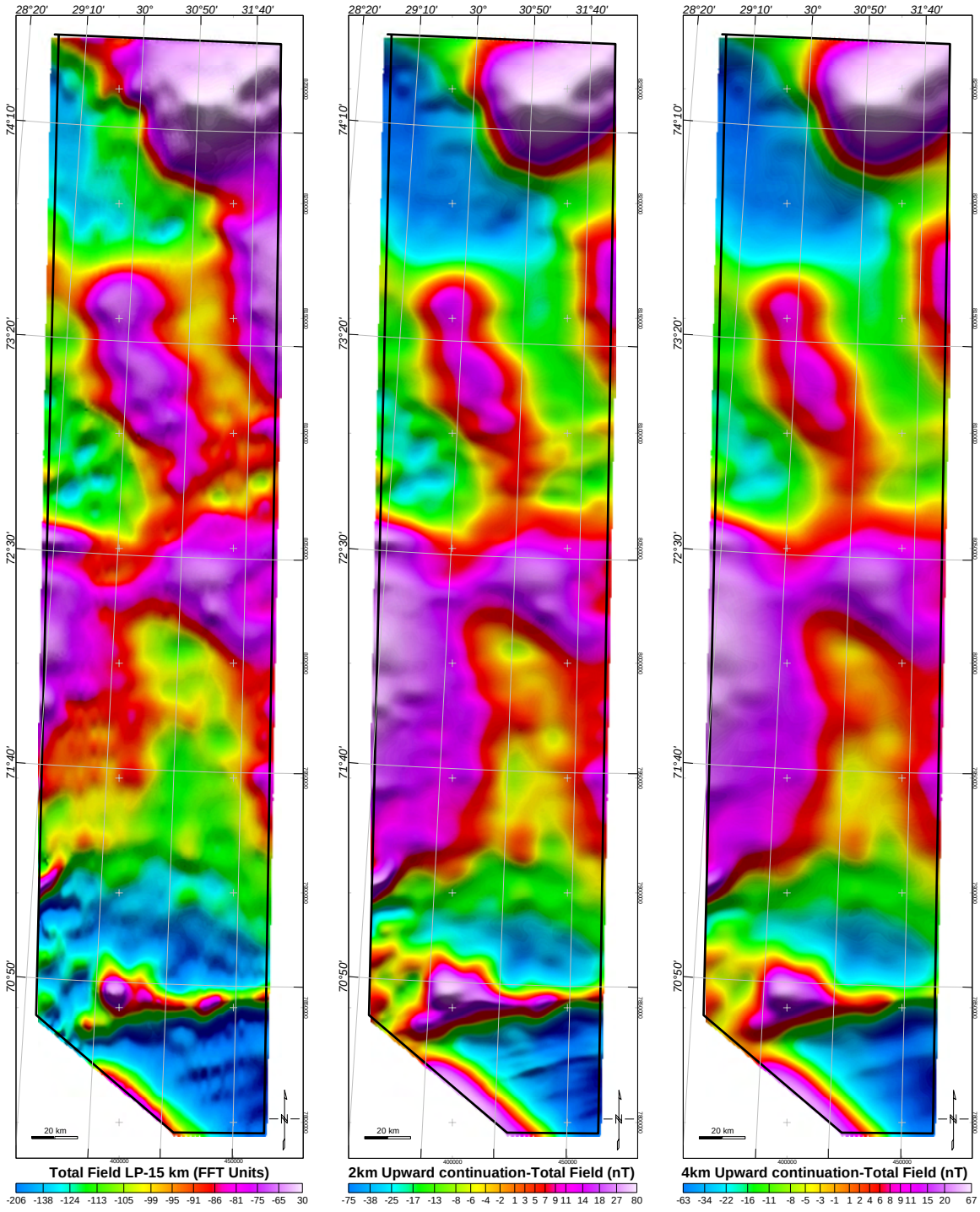

Figure 4.2 15 km low pass filtering of the magnetic total field and upward continuation of the total field to 2 and 4 km. These filters smooth the magnetic signal and underline the distribution of the main magnetic units. A prominent N°70 oriented anomaly divides the regional magnetic low observed in the southern part of the survey. Broad and high amplitude anomalies are mostly observed in the northeastern part of the Bjarmeland Platform and south of the Nordkapp Basin, where a prominent arc-shaped positive magnetic unit is observed west of 30°25'. A distinct N135° to N140°- trending elongated anomaly is continuous from the central part of the Nordkapp Basin to the southern part of the Bjarmeland Platform. It seems to be linked with a similar N130° bending anomaly south of the saliferous basin.

4.2.2 Upward continuation

Upward continuation is a low-pass filtering process by which a map simulating the result as if the survey had been conducted at a higher elevation is constructed (Fig. 4.2). This process is based on the physical fact that the further the observation is from the body causing the anomaly, the broader the anomaly. Upward continuations to 2 and 4 km have been used for the BAS-06 survey to give indications about the main magnetic and tectonic units in the area (Fig. 4.2). Upward continuation underlines crustal block or deep sedimentary units of markedly different magnetic composition.

4.2.3 Derivative filters

Directional derivatives of the magnetic total field and its analytic signal have been computed within this study to enhance short wavelength features along the BAS-06 (Fig. 4.3, 4.4). Computation of the three orthogonal derivatives, (x, y, z) within potential field modelling is considered a universally applicable and basic processing step (Thurston and Brown 1994, Blakely 1995). The horizontal derivatives were used to predict the locations of major basement or sedimentary structures, igneous bodies and changes in basement grain (e.g. Pilkington et al. 2000).
Vertical derivatives were used to enhance localized near-surface sources and trends, and to improve source resolution, assuming high quality data (Fig. 4.5). Transformation of the potential-field into a derivative map enhances edges or contacts by placing anomaly maxima at the point of the maximum horizontal gradient identified within the x- and y- orientations of the grid. However, the key assumptions made when transforming gravity and magnetic field data into the three orthogonal derivatives are: (1) the potential field measured at the surface is the vertical component of the field; (2) that the lithological contacts giving rise to the anomalies are abrupt, near-vertical, and isolated from other sources. The first assumption is essentially true for gravity and for magnetic data reduced to the pole (Blakely 1995). In reality however, geological contacts are rarely vertical and density and magnetization can vary in all directions in a geological unit. Computation of the first vertical derivative has been referred to as a data pre-processing step, particularly for gravity data before the interpretation of Euler and analytic signal.

Computation of the second vertical derivative as described by Blakely (1995) can be unstable. The second vertical derivative can be seen as a regional-residual separation technique (Blakely 1995) because it suppresses long wavelength anomalies related to regional influences.

Indirectly N-S and E-W directional filters have been found useful to locate suspicious N-W and E-W trending linear anomalies due to remaining levelling errors along the lines and tie-lines of the BAS-06 survey.

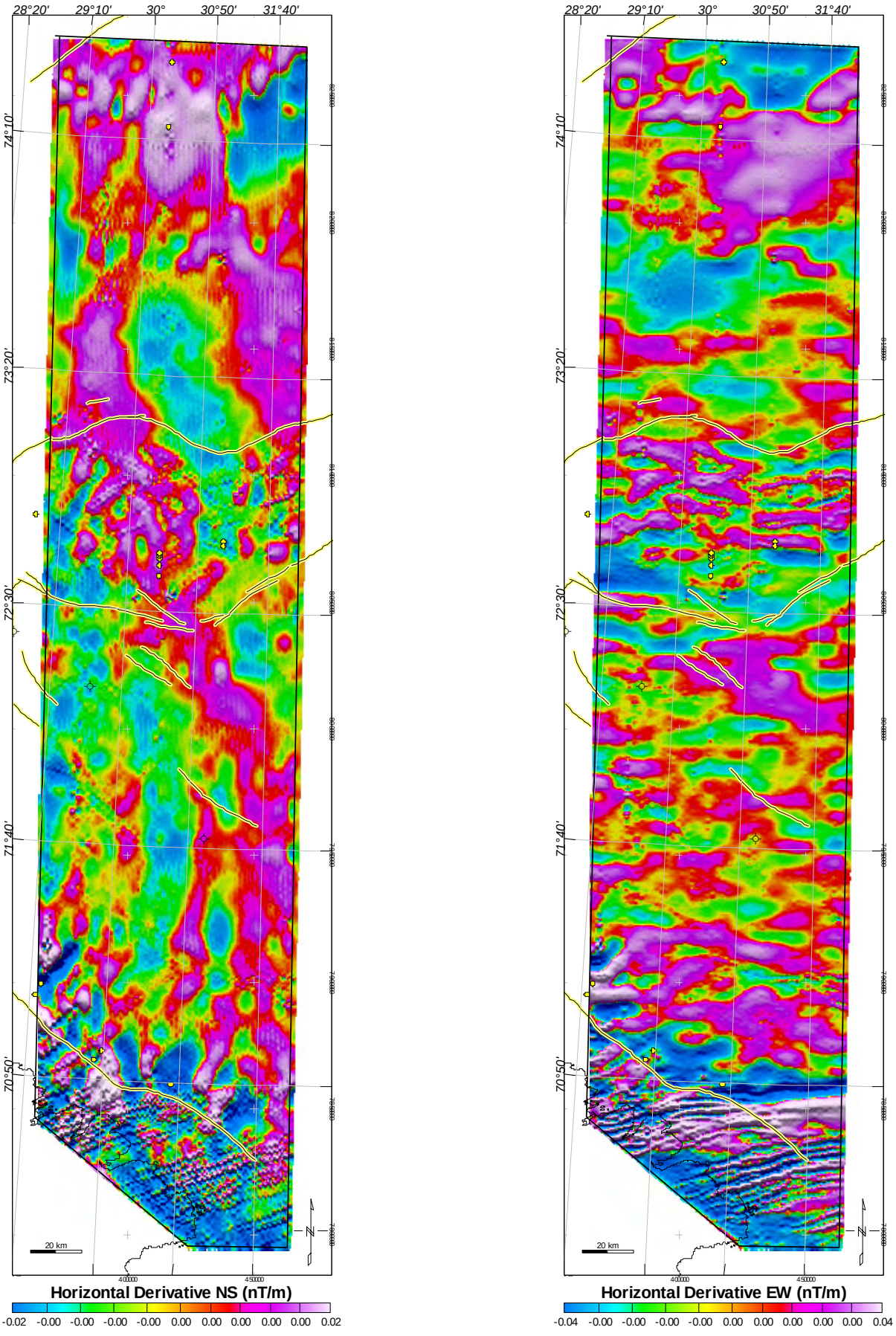

Figure 4.3 Directional horizontal derivatives of the BAS-06 dataset. The filters enhance the high frequencies along the N-S trend (left) and the E-W trend (right).

Quite similar to the way the first directional derivative defines the slope at any point on the surface, the terrain slope filter has been applied to calculate the slope at any grid node of the BAS-06. This means that across the surface, the gradient direction can change. Grid files of the terrain slope can produce contour maps that show isolines of constant steepest magnetic slope.

The terrain slope filter or total horizontal derivative filter, calculates the slope at any grid node on the surface. For a particular point on the surface, it is based on the direction of steepest descent or ascent of the magnetic field at that point. This means that across the surface, the gradient direction can change. The terrain algorithm can produce contour maps that show isolines of constant magnetic steepest slope. This operation is similar to the way the first directional derivative filter defines the slope at any point on the surface but is more powerful in that it automatically defines the gradient direction at each point on the map.

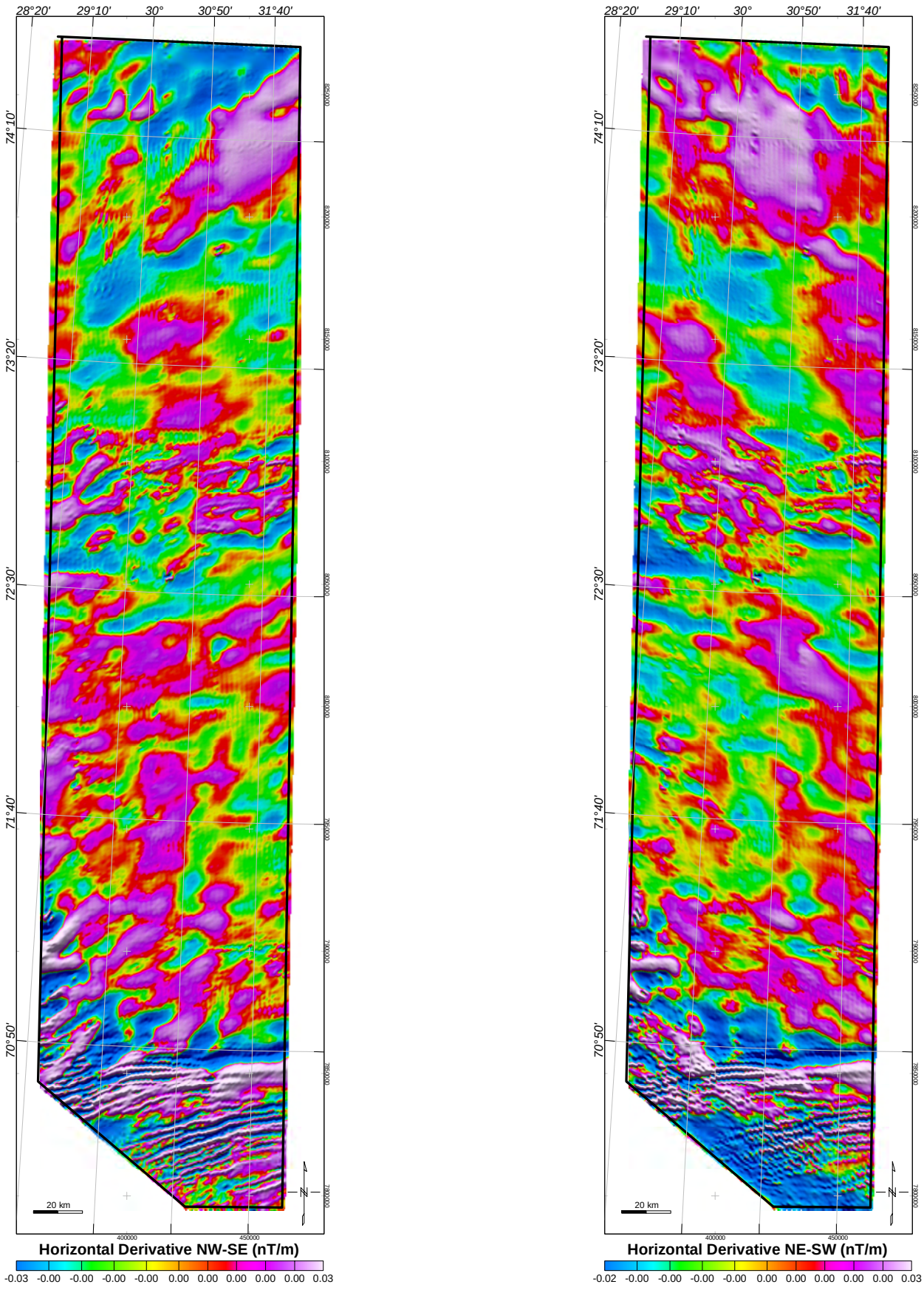

Figure 4.4 Directional horizontal derivatives along the BAS-06 area. The filters enhance the high frequencies along the NE-SW direction (left) and the NW-SE direction (right).

4.2.4 Analytic signal

The concept of analytic signal of magnetic anomalies was developed by Nabighian (1972). The analytic signal is calculated by taking the square root of the sum of the squares of each of the directional first derivatives of the magnetic field. The resulting shape of the analytic signal is independent of the orientation of the magnetisation of the source expected to be centered above the magnetic body. This has the effect of transforming the shape of the magnetic anomaly from any magnetic inclination to one positive body centered anomaly. Analytic signal has been utilized widely for mapping of structures and for determining the depth of sources (e.g. Roest et al. 1992; Hsu et al. 1996, Pilkington 2000, Ravat et al. 2002).

When interpreting the analytic signal it is assumed that the causative sources are simple near-vertical or step-like geological structures (Roest et al. 1992, Hsu et al. 1996). Therefore, the analytic signal has significant advantages over the simple derivatives and this application was utilized to map changes in basement structure, fabric and orientation. Synthetic modelling has proved that the maxima of the analytic signal are located over the edge of anomalous sources (Nabighian 1974, 1984, Roest et al. 1992). This simplification of the potential field, however, results in the compromise whereby during computation the sign of the original gravity and magnetic field is lost. Therefore, it cannot be determined whether the analytic signal anomaly has a higher or lower density or magnetic susceptibility contrast than its surroundings.

Significant structural data are lost during the calculation of the signal, for example, all dip information is removed (Nabighian 1974). The technique therefore requires interpretation in conjunction with other geophysical and geological information to maximize its potential. After calibration with known structures or other derived potential field products the analytic signal can be interpreted geologically with better confidence (Roest et al. 1992).

Conversely, the analytic signal was also suitable for detecting gridding artifacts arising from the levelling process of the BAS-06 or variations in line spacing because it enhances high-frequency edges (Fig. 4.6).

4.2.5 Automatic gain control (AGC)

Automatic gain control was used to convert waveforms of variable amplitude to a grid that gives an equal emphasis to signals with both low and high amplitudes (Mudge 1991). Like the previous derivatives filters, the AGC was useful to underline structural feature because it highlights trends with coherent alignments not apparent in true amplitude data (Fig. 4.6).

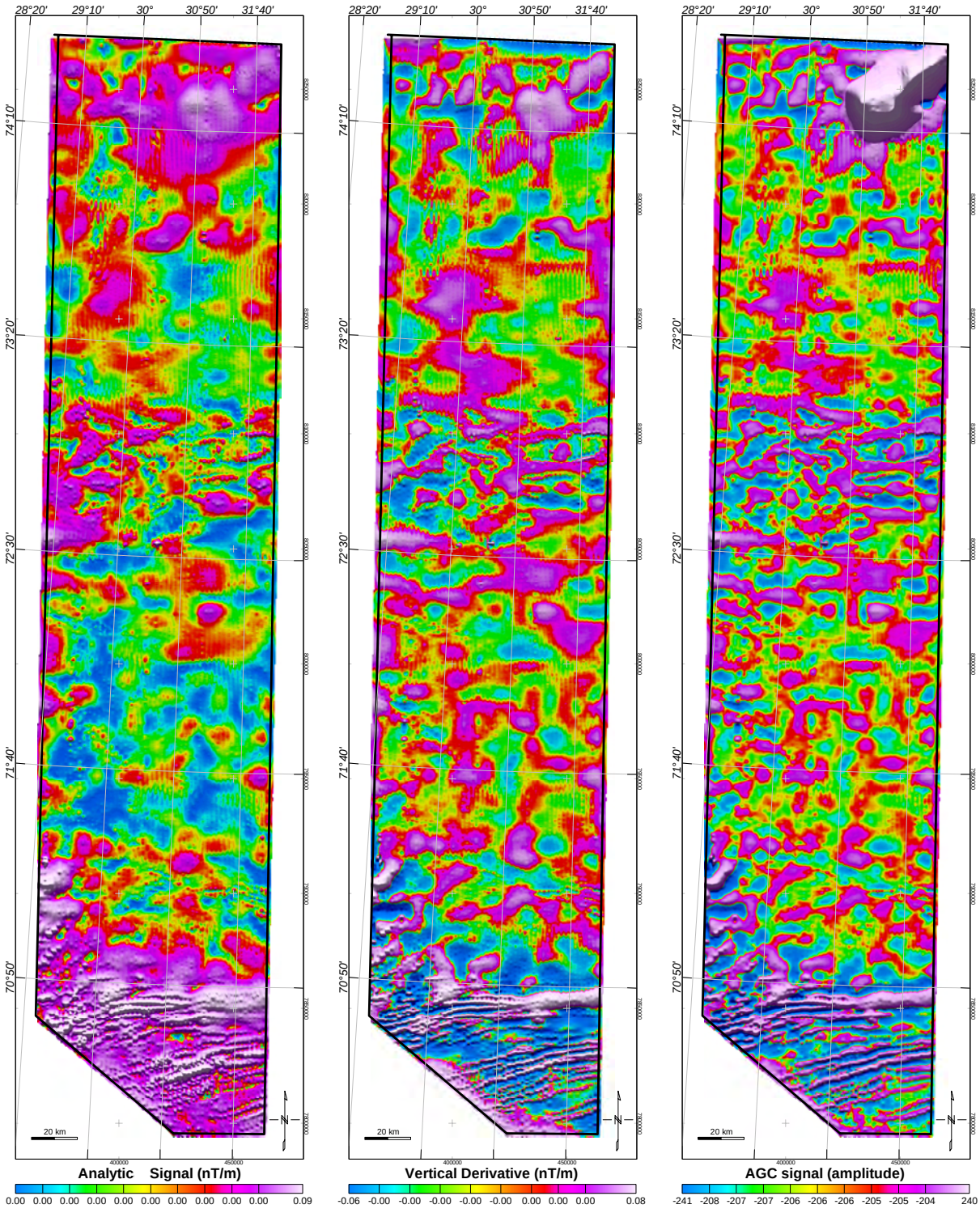

Figure 4.5 Analytic signal (left), first vertical derivative (centre) and AGC (automatic gain control) signal filters applied to the magnetic total field reduced to the pole.

4.2.6 Tilt derivative

The tilt angle is defined in terms of the ratio of the first vertical derivative of the potential field to the horizontal gradient of the field (Verduzco et al. 2004). This measure has the property of being positive over a source and negative elsewhere (Fig. 4.6). The tilt filter technique tends to enhance mapping of the subtle magnetic anomalies and maximizes the geometrical contrast of the internal basin structure (partly constrained by seismic). The tilt angle was compared with other edge detection measures such as the horizontal gradient, the second vertical derivative and the analytic signal and found to have added some advantage of responding well to both shallow and deep sources along the BAS-06 area (see later). Combined with its horizontal derivative, results were particularly useful for the structural interpretation along the BAS-06 (Fig. 4.6). The tilt angle results were combined and systematically compared with other filtered datasets to provide a set of interpretative maps presented and discussed later.

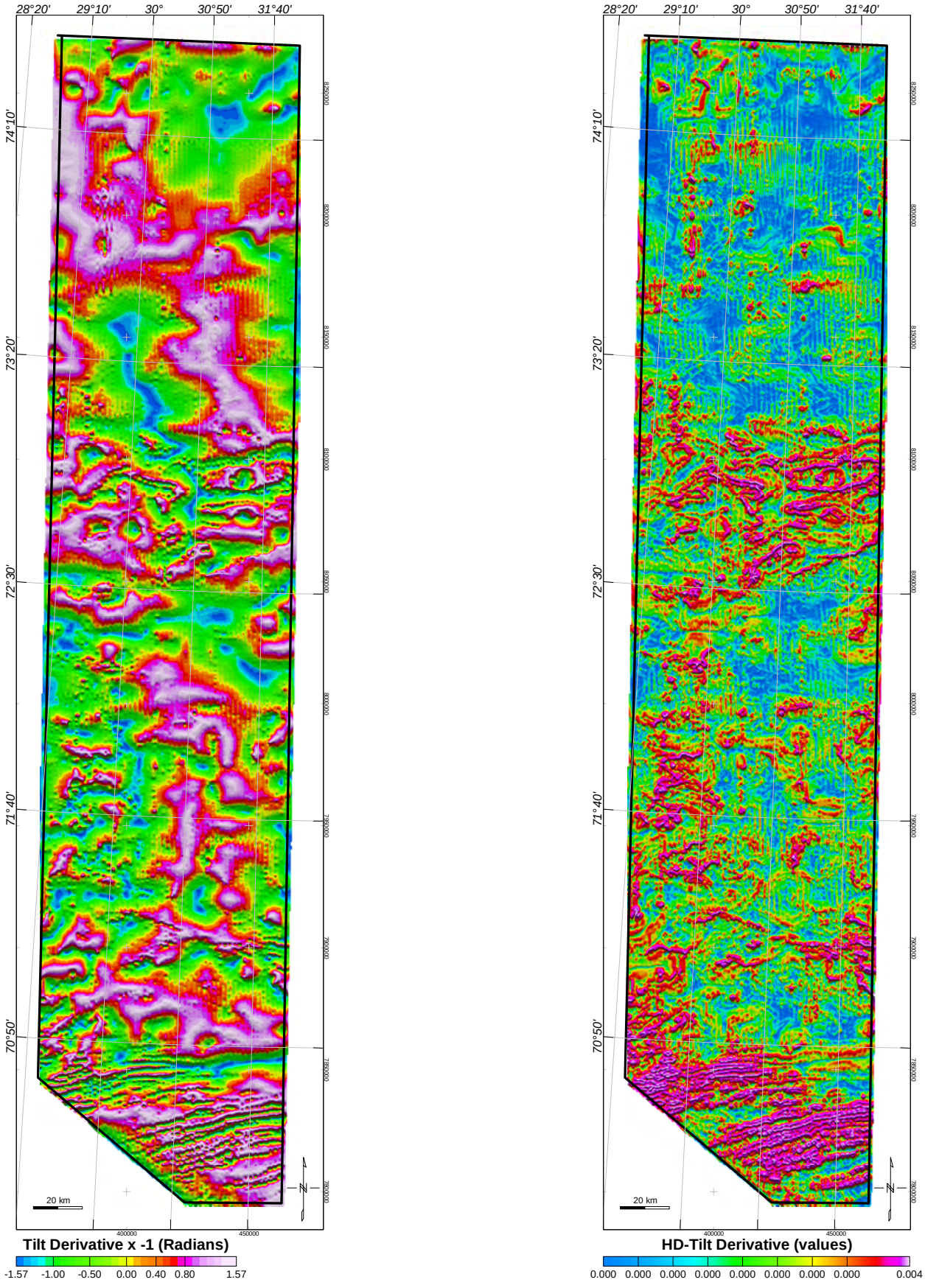

Figure 4.6 Tilt derivative of the magnetic total field reduced to the pole (x-1) (left) and its horizontal derivative (right). The different tilt patterns underline major magnetic units and major lineaments (N°135, N°70, N°45). Note already the marked pattern around the Nordkapp Basin.

4.3 Estimation of magnetic depth

4.3.1 Implications

Magnetic depth estimation plays an important role in magnetic interpretation. A complete quantitative interpretation of potential field data aims at estimating information about depth, dimension and contrast in the relevant geological units. However, keep in mind that such an interpretation suffers from inherent ambiguity. As a matter of fact, it is impossible to obtain all three types of information simultaneously without other a priori information. These methods usually work for simplified source geometries (dimensions) and are independent of the susceptibility contrast. The depths estimated by some methods can be used as the final, quantitative solution in some ideal situations (i.e., the anomaly is well isolated and the noise is insignificant or well removed).

Magnetic depth estimates are often a reasonable approximation to the magnetic basement (i.e., metamorphic/igneous). Basement depth (or equivalently, sedimentary thickness) is a primary exploration risk parameter. Estimates of basement depths are directly applicable to thermo-kinematical modelling and thermal maturity applications (e.g. heat flow estimation, source-rock burial-depth, distribution and volume).

4.3.2 Euler deconvolution

The Euler method uses Euler's homogeneity equation to construct a system of linear equations, and then determines through a least-squares inversion one time for one window the (vertical and horizontal) position of a single source (xo, yo, zo) for a given source geometry. It requires the use of the horizontal and vertical derivatives of the magnetic field if they are not observed. Thompson (1982) called the fall-off rate (i.e., the negative of the degree of homogeneity) the structural index (SI). Euler's homogeneity equation is valid for bodies of arbitrary shape, characterised by these indices. In practice, the Euler method assumes idealized structures such as contact, thin sheet (dike), vertical or horizontal cylinder and 3D sphere. Application of the technique throughout this study was completed using the Geosoft executable E3DECON.GX. The Geosoft E3DECON.GX algorithm is based on the method described by Reid et al. (1990). This section therefore briefly describes the theory advantages and limitations behind the technique and presents its applications along the BAS-06 survey area.

Euler 3-D deconvolution is a semi-automated technique enabling rapid qualitative interpretation and depth estimation of source depths from large gridded gravity and magnetic datasets (Reid et al. 1990, Ravat et al. 2002). The technique has considerable advantages. 1) It can operate on large

datasets extremely quickly; 2) provide a qualitative interpretation of geological structures; 3) provide depth estimates on the source of the anomalies 4) magnetic data do not need to be reduced to the pole (Reid et al. 1990) and 5) it is also insensitive to magnetic inclination, declination and remanence since these become part of the constant in the anomaly function of a given model.

The Euler technique assumes that the magnetic grid accurately represents the anomalous field. The absolute level of the anomalous field is however, rarely known. Thompson (1982) and Reid et al. (1990) assumed the anomalous field to represent the regional value. The Geosoft algorithm, however, computes the anomalous field and (x, y, z), and their uncertainties (standard deviations) within a data window, solving them through a least squares inversion method. The vertical and horizontal derivatives of the total field anomaly, to be inverted for x, y, z and anomalous field are advantageous because they automatically de-emphasise the regional field (Blakely 1995).

Euler deconvolution has been applied rapidly to the BAS-06 datasets, using the "moving window" technique (Reid et al. 1990). Recommendations suggest that the data window can be as small as 3 x 3 or as large as 20 x20 times the grid cell. Choice of the window size is particular to the quality of the dataset and the aim of the study. A 2D window size must be selected. It is an important consideration and depends upon the quality of the data, the distance between data sampling, errors introduced by the gridding process, the depth of investigation required and the size of the source. Ideally the window should be larger than the expected wavelength of any single anomaly but avoid containing multiple anomalies. Similarly the smaller the window, the more prone it is to noise (Ravat 1996).

The Euler technique produces a mathematical solution for every position of the window estimating the unknowns after each sequential movement. The minimum and maximum depths that can be resolved are related to the grid cell size and the window size selected highlighting the importance that the quality of dataset and the nature of the investigations which may be achieved when using regional datasets.

The pre-processing of the dataset used the analytic signal as the primary grid for Euler deconvolution. However, such procedures may increase the ratio of noise to signal within the grid, therefore, such pre-processing is limited by initial quality of the dataset, because noise will contribute to the scattering of solutions. The Geosoft manual and Hsu (2002) suggested that increased noise could be reduced by a simple upward continuation procedure. In the present project we used an upward continuation of 250 m to remove some remaining noise along the BAS-06. However this could have significant consequences upon the determination of source-to-window ratio and would complicate the depth interpretation of the deconvolution (Blakely 1995, Ravat, 1996, Ravat et al. 2002).

Synthetic tests (Ravat et al. 2002, Bainbridge et al. 2002, Blakely, 1995, Marson and Klingele 1993,

McDonald et al. 1992, Reid et al. 1990) indicate (1) that the method can locate with accuracy the outline and depth of a variety of simple geometrical shapes; 2) that the structural indices will cluster and determine the best structural interpretation. Although detailed as vertical contact, faults with a large throw may be best displayed with a structural index of zero (Table 4.1).

During the BAS-06 modelling, a suite of maps, encompassing all the different structural indices was required to accurately assess the different geological structures present within a study area particularly within complex regions.

Best results for BAS-06 have been obtained using indices of 0.5, 0 or 1 with windows sizes of 10 and 20 km. The more relevant solutions are displayed on Figs. (4.7-4.10)
Careful consideration of the distribution and clustering of Euler solutions is however required to discriminate which solution best represents the causative source at depth within the crust. We note that different structural index maps often produced similar clustering of solutions with BAS-06 that should not theoretically correspond to the particular structural index. This phenomenon may be explained by the gradients analysed by the chosen structural index, and the gradients associated with the anomaly being mapped.

Although in theory interpretation of the Euler solutions requires no pre-geological knowledge, Reid et al. (1990) acknowledge that this can be significantly beneficial. Reid (1995) acknowledged that the choice of structural index remains a limitation of the traditional Euler technique. These limitations arise as a product of some of the simplifying assumptions of the technique, which assume that the source is; (1) equivalent to a simplified geometrical feature (2) spatially homogeneous (3) independent of neighbouring magnetic sources (4) has a heterogeneous magnetization or density.

Along the BAS-06, geological structures are probably arbitrarily shaped sources, and therefore are not simply modelled or defined by the structural index. The fact that the sources may not be internally or spatially homogeneous (i.e. the density and shape of the source change with depth or along strike), or the source-to-observation distance increases (thus the anomaly shape changes with depth) or other sources impinge each others spatial positions is an inherent source of scatter (Reid et al. 1990, Ravat 1996, Keating 1998). Consequently it is necessary to examine a number of structural indices to compare results and clustering of solutions for several individual features. Alternatively, in such situations geological constraints from external data sources would be beneficial to the interpretation of the BAS-06 dataset in the future.

Complexities also arise with respect to the depth of burial of the source. Ravat (1996) noted that there was a strong inter-dependency between the choice of the structural index and the distance of the source-to-observation, and that with increased distance the results were biased towards the higher structural indices, explained by the exponential decay of a source anomaly with depth. It can

be predicted that with increasing depth the attenuation rate of the anomaly is less, therefore deeper sources may only be represented by higher values (Ravat 1996). The relationship between the source and the observation level are considerably altered following upward continuation of the observation level, increasing the possibility of mis-identification of the true structural index (Ravat 1996, Ravat et al. 2002).

Nevertheless, we found some correlation with the main trends underlined by the BAS-06. Comparison with the gravity anomalies also suggests some shallow sources around gravity highs and deeper sources along the main gravity low. This could confirm evidence for shallow or deep basement.

Structural Index	Magnetic field	Gravity field
0	contact	Sill/dike/step
0.5	thick step	Ribbon
1	Sill/dike	pipe
2	pipe	sphere
3	sphere	

Table 4.1. Summary of the structural indices for simple geometric models from a magnetic anomaly or gravity anomaly (After Ravat et al. 2002, Bainbridge et al. 2002, Blakely, 1995, Marson and Klingele, 1993, McDonald et al. 1992, Reid et al. 1990).

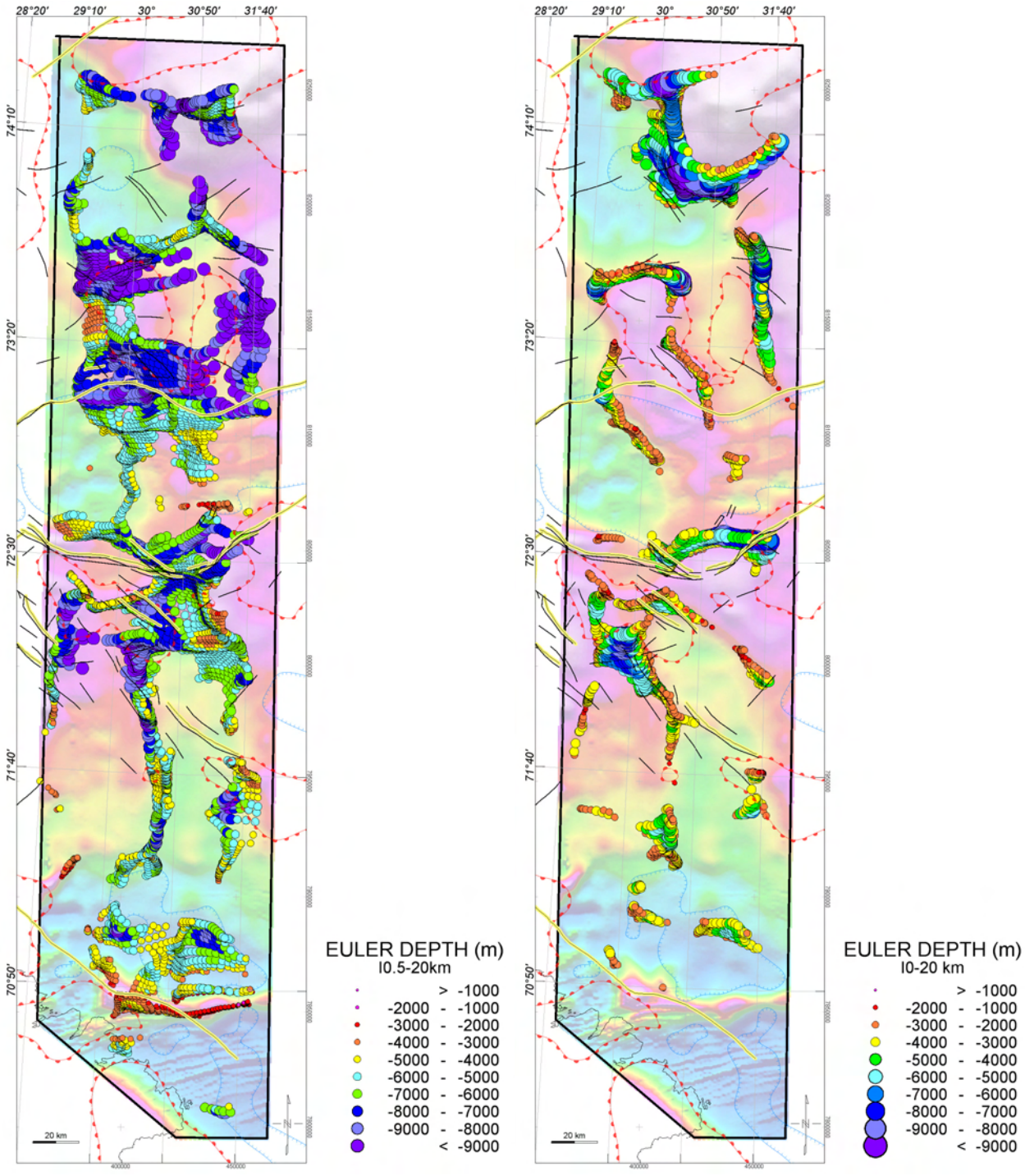

Figure 4.7 Result from Euler deconvolution over the BAS-06 using a moving window size of 20 km. Result using a structural index of 0.5 (left) and 0 (right). Contours draped on the total field outline the Bouguer gravity highs (in red) and lows (in blue).

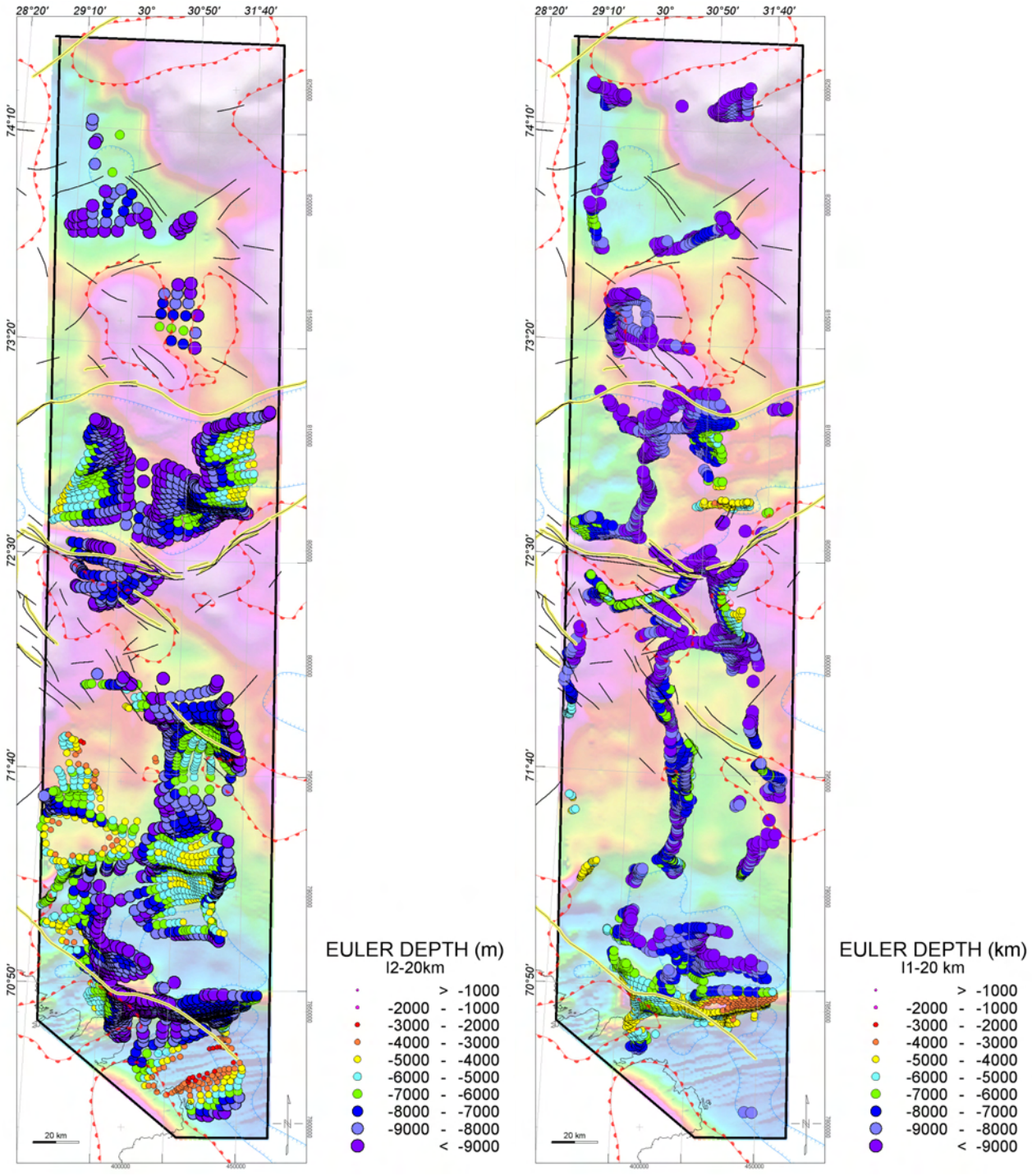

Figure 4.8 Result from Euler deconvolution over the BAS-06 using a moving window size of 20 km. Results using a structural index of 2 (left) and 1 (right). Contours draped on the total field map outline the Bouguer gravity highs (in red) and lows (in blue).

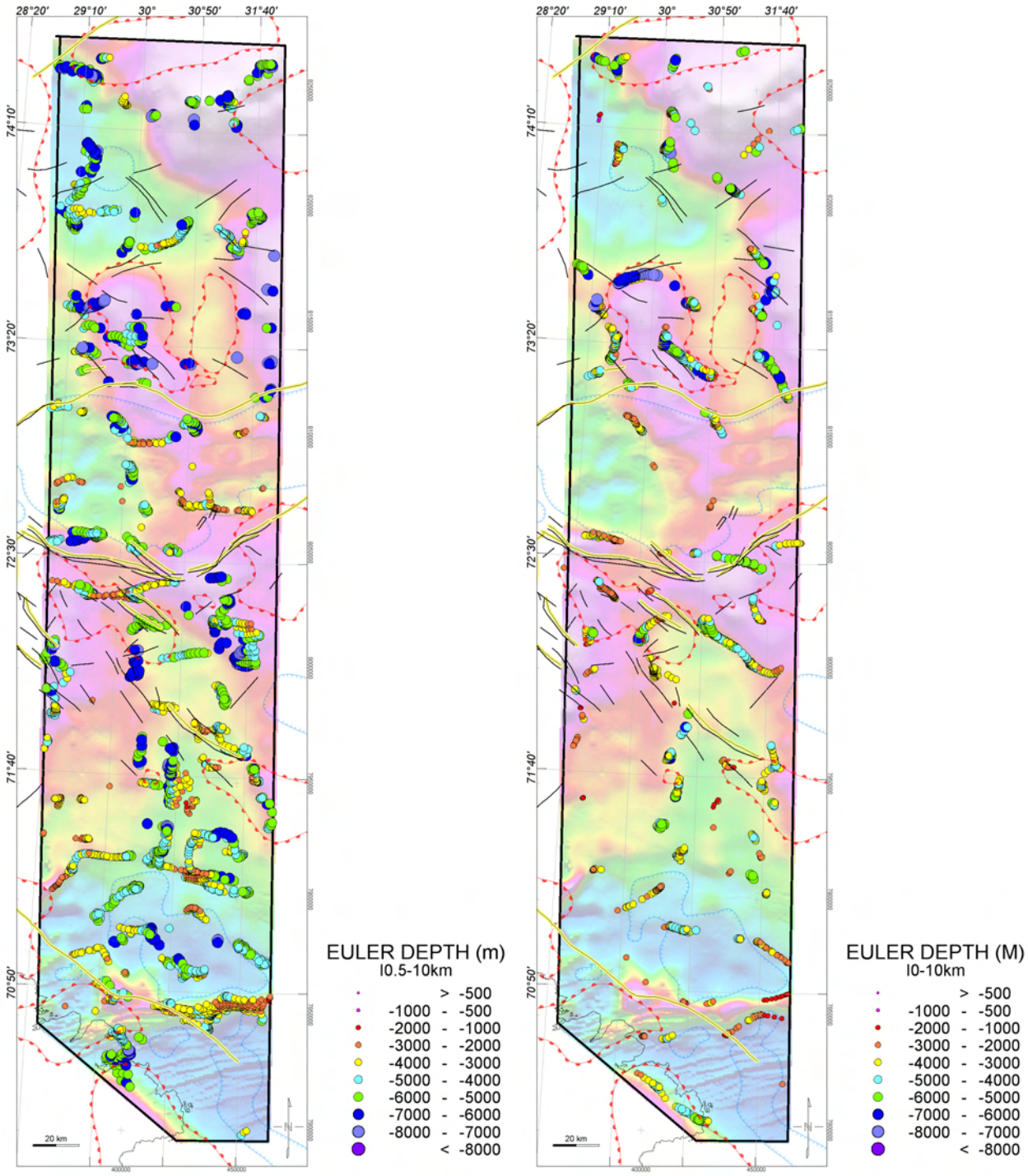

Figure 4.9 Result from Euler deconvolution over the BAS-06 using a moving window size of 10 km. Result using a structural index of 0.5 (left) and 0 (right). Contours draped on the total field map outline the Bouguer gravity highs (in red) and lows (in blue).

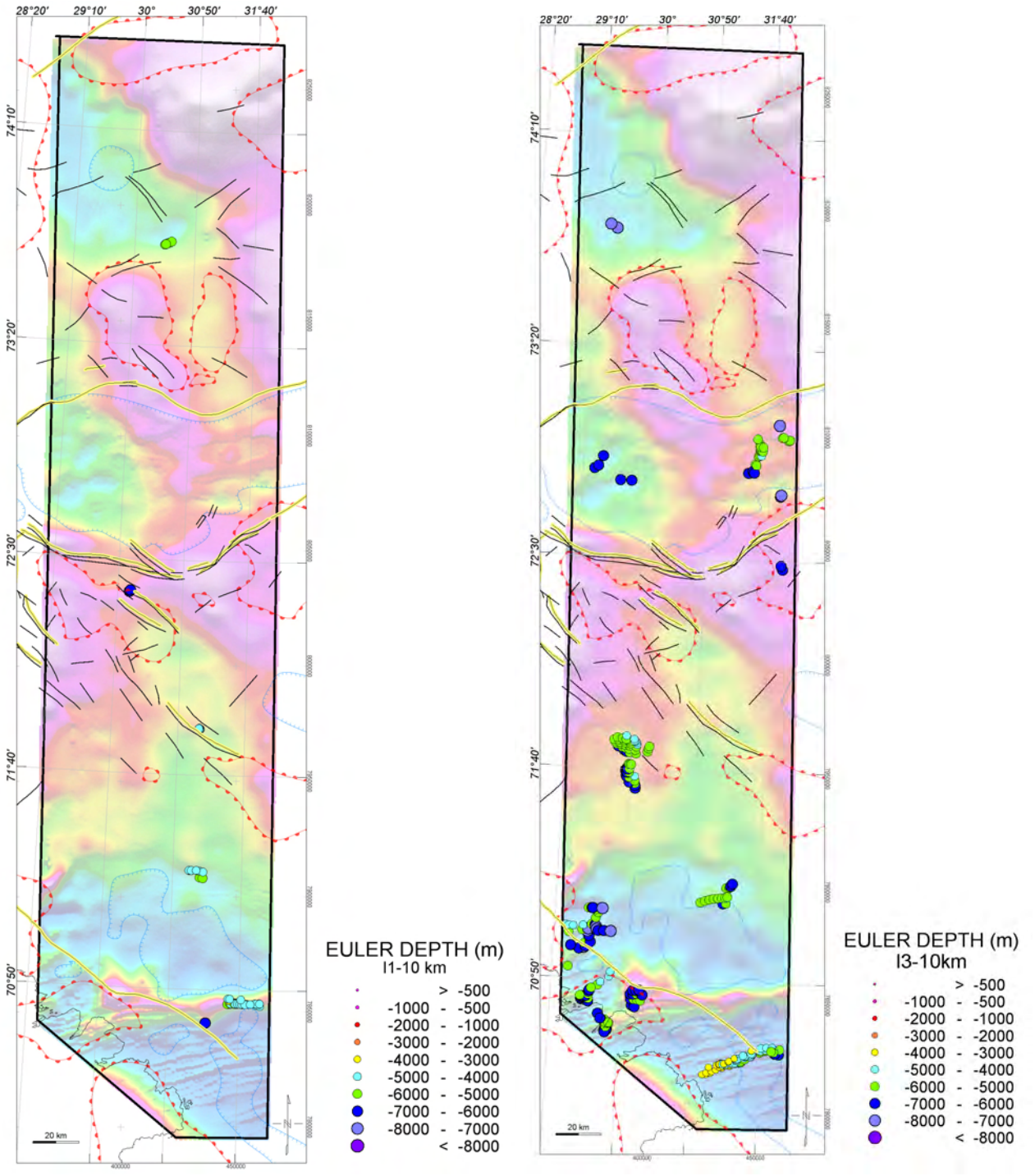

Figure 4.10 Result from Euler deconvolution over the BAS-06 using a moving window size of 10 km. Result using a structural index of 1 (left) and 3 (right). Contours draped on the total field map outline the Bouguer gravity highs (in red) and lows (in blue). Other black lines represent the fault observed at base Cretaceous level.

5 GEOLOGICAL FRAMEWORK AND PRELIMIBARY INTERPRETATION

Laurent Gernigon

Aeromagnetic interpretation involves the joint application of several datasets and the use of improved processing techniques. In order to enhance the signatures of the basement structures and lithological units, as well as faults, and salt diapirs above the older basement, a number of processed images derived from the total magnetic field have been interpreted. Geophysical and geological interpretations also include gravity data and a few released seismic lines, kindly provided by the Norwegian Petroleum Directory (NPD). They led to a preliminary interpretation of the survey area and to a discussion of basement and salt tectonic structures particularly highlighted by the new dataset. This preliminary work should lead into further research investigations at NGU. In the meantime, key aims of this chapter are:

1 to provide a preliminary interpretation of the structures, tectonic framework and lithology from the airborne geophysical results of the BAS-06.
2 to correlate and combine these results with the known geology of the study area to aid identification of structural features.
3 to delineate offshore continuation of existing basement domains mapped onshore.
4 to constrain rift-related basement and salt tectonic structures in the Nordkapp Basin.

5.1 Geodynamic setting - The Barents Sea

The BAS-06 survey covers a significant part of the Barents Sea. In order to better understand the geological meaning of the magnetic pattern, a short summary of the tectono-stratigraphic evolution of the study area is required and shortly summarised here. We refer particularly to Gabrielsen et al. 1990, 1992, Doré (1995), Johansen et al. (1993), Gudlaugsson et al. (1998), Larssen et al. (2005) and Worsley (2006) for further information and references about the geodynamic and paleogeographic framework of the Barents Sea.

The Barents Sea consists of complex structural features including platform areas, basement highs and sedimentary basin (Fig. 5.1). It has been affected by a long and complex tectonic history, which left its signature within the crust. The Barents Sea has been tectonically affected by major continental collisions and a complex rift history leading ultimately to continental breakup in Cenozoic time (Gudlaugsson et al. 1998, Faleide et al. 1993).

The tectonic and "basement" history of the Barents Sea is strongly influenced by the Early Proterozoic (Karelian) orogeny, which established the stable Russian-European platform adjacent to the Archean Baltic Shield (Alsgaard 1993, Gee et al. 2006). Accreted and superimposed, latest

Proterozoic (Baikalian) orogenic trends are oriented NW-SE, exemplified by the Kanin-Timan Ridge and the Kola-Kanin Monocline southwest of the Timan-Pechora and Barents Provinces. Timanian (formerly called Baikalian) basement comprises the western and central Timan-Pechora Basin Province and possibly part of the South Barents Basin Province (Gee and Pearse 2004, Gee et al. 2006). Timanian (or younger, Grenvillian) basement might be present in more northern regions as revealed by recent pattern of the crustal rigidity computed at the Barents Sea scale (S. Wienecke, personal communication 2007).

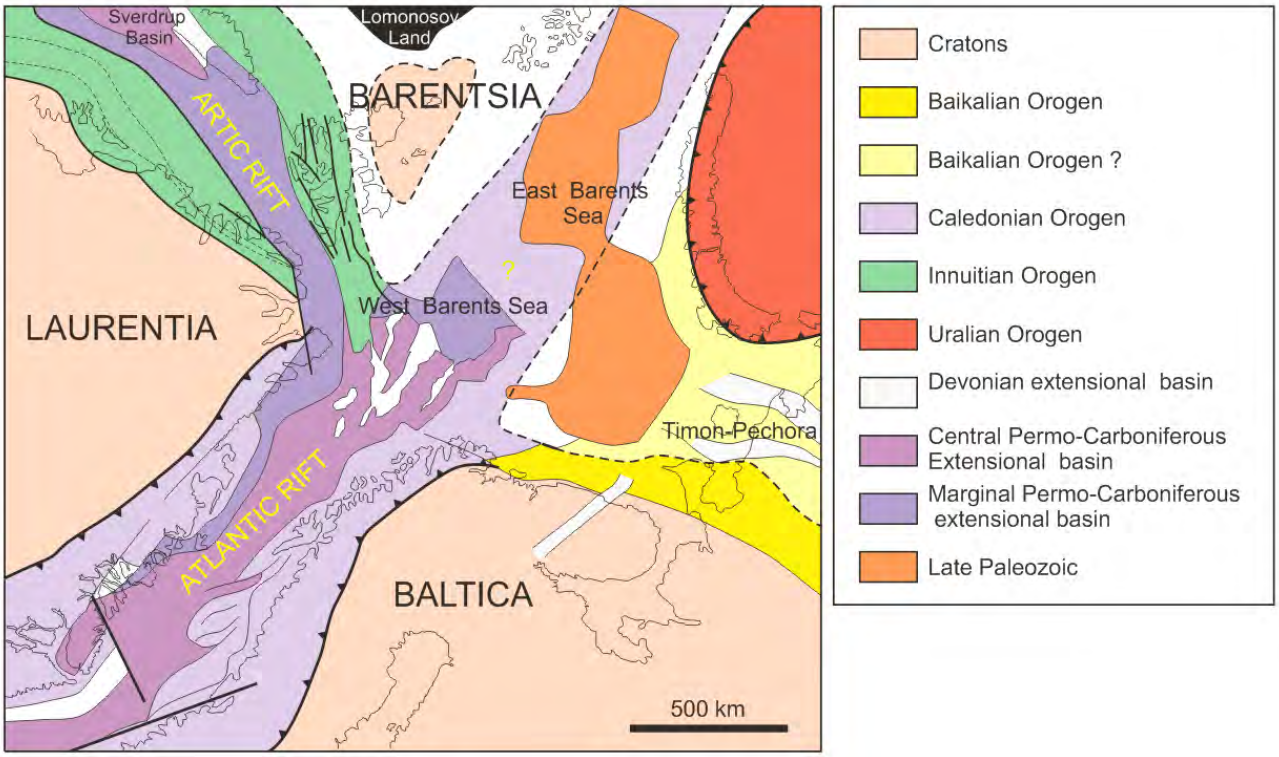

Figure 5.1 Regional paleotectonic and main orogens and rift zones of the Barents Sea area. Reconstruction to end-Permian time (after Gudlaugsson et al. 1998).

In the western Barents Sea area, the main collision event is the Caledonian Orogeny that is regarded onshore Norway to originate from two major tectonic phases (Fig. 5.1): 1) the Finnmarkian (Late Cambrian) and 2) the Scandian phase (Mid-Silurian-Devonian) (Roberts 2003). The Scandian Orogeny culminated approximately 400 Ma (million years ago). It represented the closure of the Iapetus Ocean, a major seaway occupying a position similar to, but somewhat oblique to, the present northeast Atlantic (Roberts 2003, Gee and Teben´kov 2004, Breivik et al. 2005, Gee et al. 2006). A remnant of the old Iapetus oceanic basin could have been preserved in this eastern Barents region, according to plate tectonic models (Trond Torsvik, personal communication, 2006). This collision resulted in the consolidation of the Laurentian plate and the Baltic plate into the Laurasian continent (Fig. 5.1). The eastern side of the Barentsian Caledonides are flanked by a Late Neoproterozoic Timanide foldbelt, recognised up to the Timan-Pechora and Novaya-Zemlya region.

The eastern part of the Barents Sea was subsequently affected by a youngest collision phase between the Laurasian continent and Western Siberia, which culminated in the latest Permian-earliest Triassic. The Urals mountain chain and its (probable ?) northern extension, Novaya Zemlya, mark the suture zone of this closure, which is younger in the Novaya Zemlya region.

The Late Palaeozoic and Mesozoic tectonic history of the Barents Sea was mostly dominated by extensional tectonics initiated by the end and collapse of the newly formed Caledonian and Uralian orogenic belts. Rift episodes have been documented in the Early-Middle Devonian, Carboniferous, Permian, Triassic and Late Jurassic-Early Cretaceous (Johansen et al. 1993). These events created the major rift basins in the Barents Shelf. While deposition of a continental nature took place locally during the Late Palaeozoic and Early Mesozoic in the syn- and post-orogenic collapse basins, marine sedimentation was by far the dominant factor from the Late Palaeozoic to the present day (Worsley 2006). A significant magmatic event, that affected the northern part of the Barents Sea is also recognized in Early Cretaceous time and likely part of a Large Igneous Province linking Greenland, Svalbard, Franz-Joseph Land and adjacent shelf areas before the continental breakup and ocean basin formation (Grogan et al. 1998, Maher 2001).

The transition to passive continental drifting between North Greenland and the Barents margin, and initiation of the Arctic-Atlantic oceanic connection, probably took place in mid-Cenozoic (Oligocene) times. Opening of the Nansen Basin, with the separation of the Lomonosov Ridge, a continental slice from the Barents margin probably began in the latest Cretaceous. Subsequent break-up and spreading into the Norwegian Sea, between Norway and Greenland, is thought to have commenced in the Late Paleocene-Early Eocene time. Later, serious uplift and erosion is documented in most of the Barents Sea area. Up to several kilometers of sediments were probably removed from this area during the Cenozoic (Nyland 1992, Faleide et al. 1996). Erosion and redeposition are thought to have been particularly intense during Plio-Pleistocene time.

5.2 First order regional crustal, gravity and magnetic trends along the BAS-06

Based on the new magnetic grid and comparisons between gravity and magnetic, the major trends along the survey area can be proposed (Figs. 5.2, 5.3 and 5.4). Both regional magnetic and gravity anomalies are usually most sensitive to variations in structure and composition of the crystalline basement. It was the major and viable assumption for the BAS-06 interpretation. Most of the bodies within the basement have distinctive magnetic signatures, characterized by their magnitudes, heterogeneity, and magnetic fabric. When calibrated with known onshore geology, basement structures can often be mapped from aeromagnetic data beneath the cover of sedimentary rocks.

Sub-cropping tilted sedimentary strata or folded sedimentary structures have low magnetic

susceptibilities but can also generate measurable magnetic anomalies (Gibson and Millegan 1998). Faults, carbonate mounds or other irregularities of the sedimentary strata can also influence the short wavelength magnetic signature. Small wavelengths attributes were extracted using the tilt derivative (TDR) approach (Verduzco et al. 2004). These operations suppress the longer-wavelength anomalies and emphasize both the effects due to shallow sedimentary cover and deeper basement structures. Because it was based on the second and higher derivatives, the local-wavenumber technique provided high-resolution images, in which the sub-domain structures and boundaries and magnetic lineations were displayed in more details.

The various magnetic and gravity attribute maps, interpreted in this report, describe the features and patterns of the basement blocks relative to their surrounding. We used a conservative term “structural contrasts” for the extended linear features observed in the maps, although many of these features could still be associated with significant basement blocks. The structural pattern of the basement as revealed from combined gravity and magnetic interpretations was characterized by a hierarchy of structural elements involving 1) large structural zones, 2) tectonic domains and 3) sub-domains and internal magnetic lineaments. For each domain, there also appear additional extended features that overprint some of these structures and are potentially related to deposition of basin sediments and salt tectonic.

Along the BAS-06 study area, 4 large tectonic domains affected by these inherited structures can be already proposed and described from North to South:

1 The Bjarmeland Platform
2 The Nordkapp Basin and surrounding margins
3 The Finnmark Platform Kola-Kanin Monocline areas
4 The onshore Varanger Peninsula and the near shore domain

The main boundaries that delineate units of the first structural class within the basin can be identified from correlating the aeromagnetic and gravity maps and their derivatives filters (Fig. 5.3, 5.4). Gravity and magnetic signatures most closely reflect the tectonic and structural characters of the area, and potential-field data also provide the necessary spatial continuity of coverage when seismic lines are missing.

The Bouguer gravity attribute map (Fig. 5.2) outlines the lighter and heavier masses within the crust. Because the structural features within the crystalline basement have significantly stronger magnetic than density expressions, and also because the BAS-06 magnetic line spacing was much closer, the resulting magnetic maps provide more detailed than the (released) Bouguer gravity map (Figs. 5.2 and 5.3).

Major basement domains should be expected when there is a pronounced expression both in

aeromagnetic and gravity data. Figure 5.4 illustrates the correlation between gravity highs and magnetic lows. Usually there is a good correlation and similarities between pronounced gravity and magnetic highs in most of the survey area, except along the Nordkapp Basin and in the southern and western parts of the Finnmark Platform.

It is also interesting to point out that most of the time; the magnetic signature could be associated with both shallow and deep structures as suggested by seismic observations combined with the potential field (Fig. 5.5). Since the earliest basement configuration and evolution is probably the first order factor for subsequent fault reactivation and subsidence pattern, it seems to be normal to observe several magnetic domains associated with several stacked structural levels.

Timanian and Caledonian trends dominate the basement architecture and influence the rift and basin configuration of the survey area. Caledonian influences are seen in the N-S structural grain of the western Barents margin and Svalbard, and the NE-SW grain of the southwestern Barents Sea and Finnmark (e.g. Doré, 1995, Roberts and Lippard 2005, Fichler et al. 1997). Old inherited structures usually appear to be the first order crustal parameters that control the rift or basin architecture (eg. Doré et al. 1997, Roberts and Lippard 2005). This is clearly highlighted by potential field data, themselves influenced by the basement configuration at the Barents Sea scale (e.g. Fichler et al. 1997). Along the survey area, the Bouguer anomalies underline the main crustal trends characterised by linear gravity highs or the regional alignment of the graben, usually fitting with regional long wavelengths gravity lows as observed along the Nordkapp Basin (M-NL1).

In this part of the Barents Sea, the NW-SE and NNW-SSE trending gravity and magnetic pattern could be inherited from the Timanides structural grain, recognised along the Kola-Kanin Monocline structure stretching up to the Timon-Pechora Basin on the Russian side. NW-SE regional and crustal trends are particularly prominent on the Finnmark Platform area. Farther west, rifted basins such as the Hammerfest and Nordkapp Basins follow NE-SW Caledonian trends. They were initiated by late Palaeozoic extension, and like the Russian basins were later a major site of Triassic deposition (Roberts and Lippard 2005). More stable platform areas, the Bjarmeland and Finnmark platforms, bound these basins to the north and south, respectively, but NNW-SSE and N°70-°80 alignments can be observed in the northern part of the BAS-06.

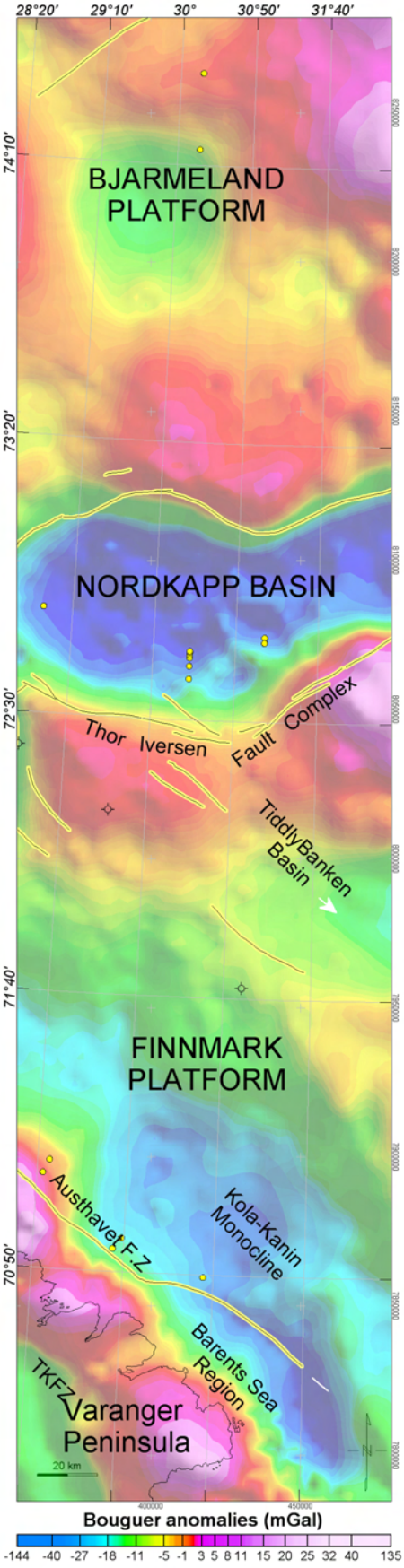

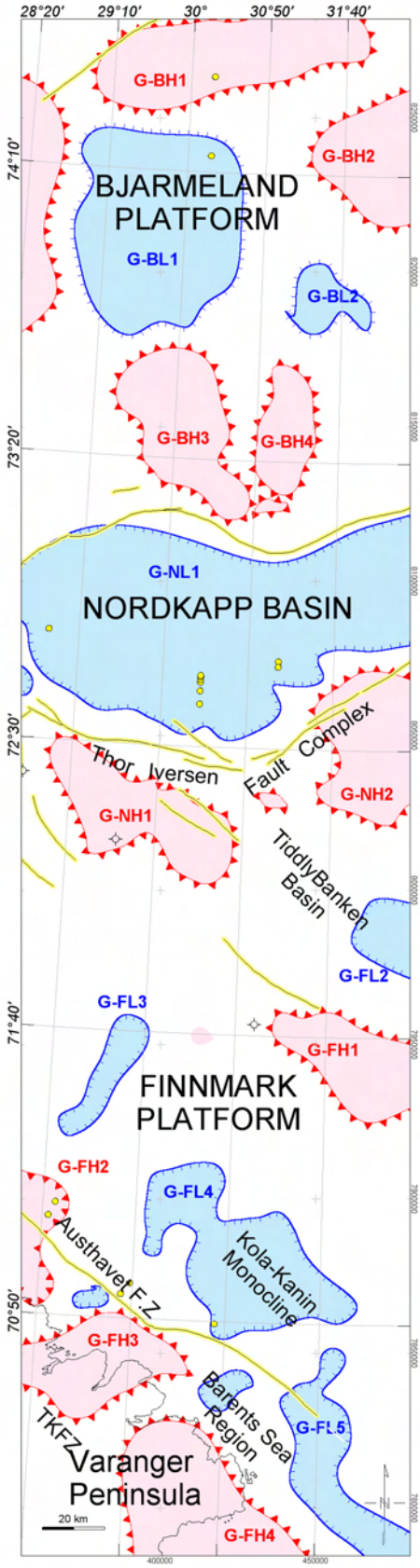

Figure 5.2 Bouguer anomalies along the BAS-06 survey area and interpretation of the main anomaly highs and lows. Black and yellow lines underline the main structural features of the area (NPD). Black lines alone represent the faults mapped at base Cretaceous level (NPD/NGU compilation).

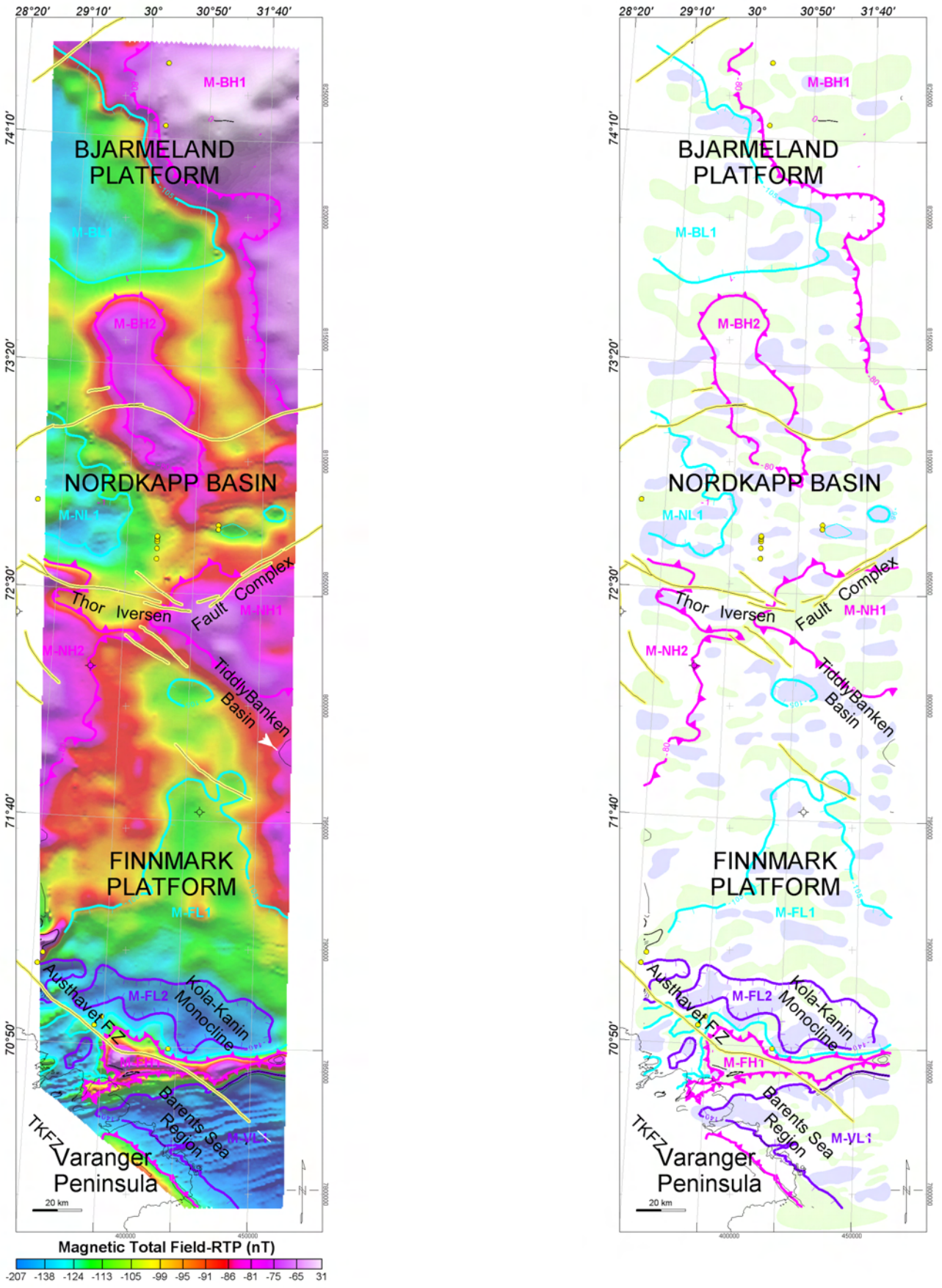

Figure 5.3 Magnetic total field (left) and outline of the main anomalies (right). Green and purple polygons outline the positive and negative magnetic anomalies after 30 km high-pass filtering.

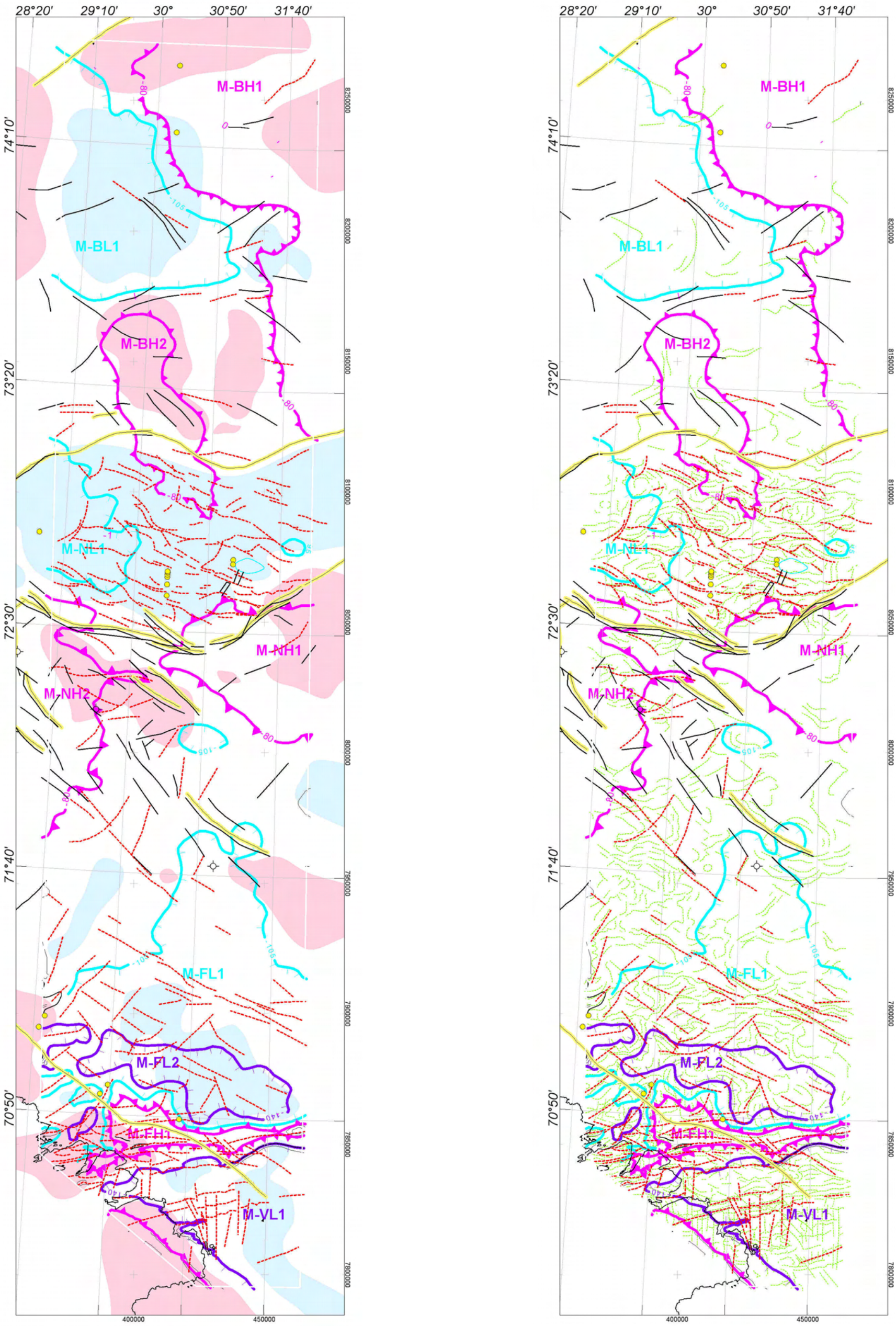

Figure 5.4 Interpretation maps and main magnetic lineaments of the magnetic field. Map on the left includes the main gravity highs (pink polygons) and lows (light blue). The dashed green lineaments on the right represent the magnetic foliation deduced from the horizontal derivative of the tilt derivative (HD-TDR) calculated from the magnetic total field, reduced to the pole. The dashed red lines represent the main magnetic lineaments. The TDR filters suppressed the longer-wavelength anomalies and emphasize both the effects due to shallow sedimentary cover and deeper basement structures.

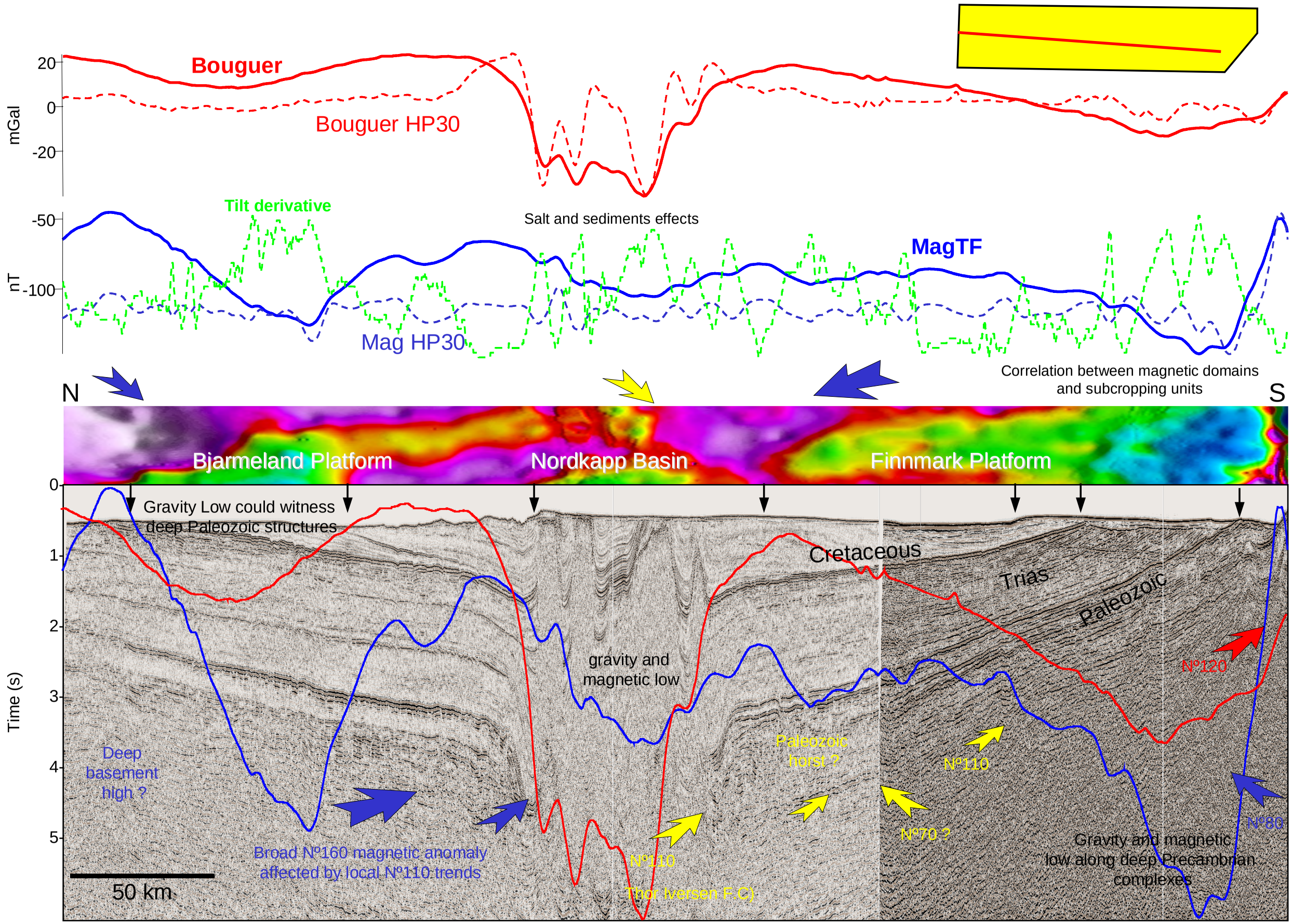

Figure 5.5 North-South seismic transects and potential field anomalies across the main tectonic and potential field domains covered by the BAS-06 survey.

5.3 The Bjarmeland Platform

The Bjarmeland Platform includes the extensive platform areas east of the Loppa High and north of the Nordkapp Basin. The platform was established in the Permian, but subsequent uplift and erosion tilted the Palaeozoic and Mesozoic sequences towards the south so that unconsolidated Quaternary sediments overlie successively older rocks towards the north. Five exploration wells have been drilled on the Bjarmeland Platform, but only in the southern part of this large platform. Two of them have been drilled in the transitional area between the platform, Nordkapp and Hammerfest Basins. Both of these wells reached the Upper Palaeozoic (7226/11-1 and 7124/3-1), the former demonstrating mid-Carboniferous onlaps of the basement (Larssen et al. 2005).

The southern part of the Bjarmeland Platform is characterised by a regional NNW-SSE (M-BH2) and NE-SW (M-BH1) striking anomaly highs and adjacent low magnetic domains (M-FL1) stretching more or less continuously down to the Nordkapp Basin. Magnetic lows and highs coincide locally with similar gravity anomalies (Figs. 5.3 and 5.4) but the NNW-SSE and NW-SE trends are more clearly defined on the BAS-06 dataset. The broad NNW-SSE positive anomaly (M-BH2) is prominent in the central part of the platform and could coincide with the G-BH3 gravity high on the northern flank of the Nordkapp Basin. Inside the broad positive anomaly, smaller N°80-N°120 oriented wavelength lineations appear close to the graben slope. They coincide with the northern border fault zone of the Nordkapp Basin and probably represent deep-seated basement faults (Fig. 5.5).

Most of the anomalies probably reflect deep and old features, not clearly imaged by the seismic data available in our study (Fig. 5.5). The broad N°160 striking anomaly (M-BH2) could fit with strong amplitude seismic reflections observed on the northern flank of the Nordkapp Basin but seismic imaging is still too poor to develop this idea at the present stage. NE-SW seismic lines were also missing during this study and consequently, we could not get an optimal orientation for an accurate structural investigation. However, the N°110 trends may suggest (Devonian-Carboniferous?) faulting of the magnetic unit M-BH2. We note also, that the magnetic pattern also coincides well with the boundaries of major Mesozoic subcropping units as suggested by the seismic transect (Fig. 5.5).

5.4 The Nordkapp Basin and surrounding margins

The Nordkapp Basin is a fault-controlled graben located along the northeast-southwest trending Palaeozoic rift system that extends eastwards from the Hammerfest Basin to the disputed area between Russia and Norway (Gabrielsen et al. 1990, Nilsen et al. 1995). This structure is well constrained both by the gravity and the new magnetic data (Figs. 5.2 and 5.4). The Nordkapp Basin

is bounded by the Bjarmeland Platform to the north and the Finnmark Platform to the south and is divided into a northeastern and southwestern segment; the latter is recently covered by a similar aeromagnetic survey (SNAS-06, NGU report Number 2006.089) (Løvaas et al. 2006).

The central part of the Nordkapp Basin, underlined by the BAS-06 survey, is characterised by a regional gravity low (G-NL1) surrounded by broad gravity highs (G-BH1, G-NH1, G-NH2), locally influenced by major fault zones suggested by NW-SE trending gravity and magnetic anomalies (Fig. 5.4). The main regional orientation of the Nordkapp Basin, also suggested by the Thor Iversen Fault Complex, is mostly N°100-110 to N°70-80 oriented and coincides with local small to medium magnetic wavelength trends (Figs. 5.4 and 5.5).

Compared to the old grid compilation based on the 1970 data, the new grid changes the regional magnetic picture of the Nordkapp Basin a lot and provides additional information (Fig. 5.6). Significant differences are observed. Further to the BAS-06, new trends, lineaments and other magnetic features appear in most parts of the saliferous basin. Local magnetic influence due to salt will be treated in details in a separate chapter and we focus here on the major architecture of the graben. In the old NGU compilation, NW-SE trends appear now as artefacts following the NW-SE orientation of the old raw magnetic profiles, poorly levelled and roughly interpolated.

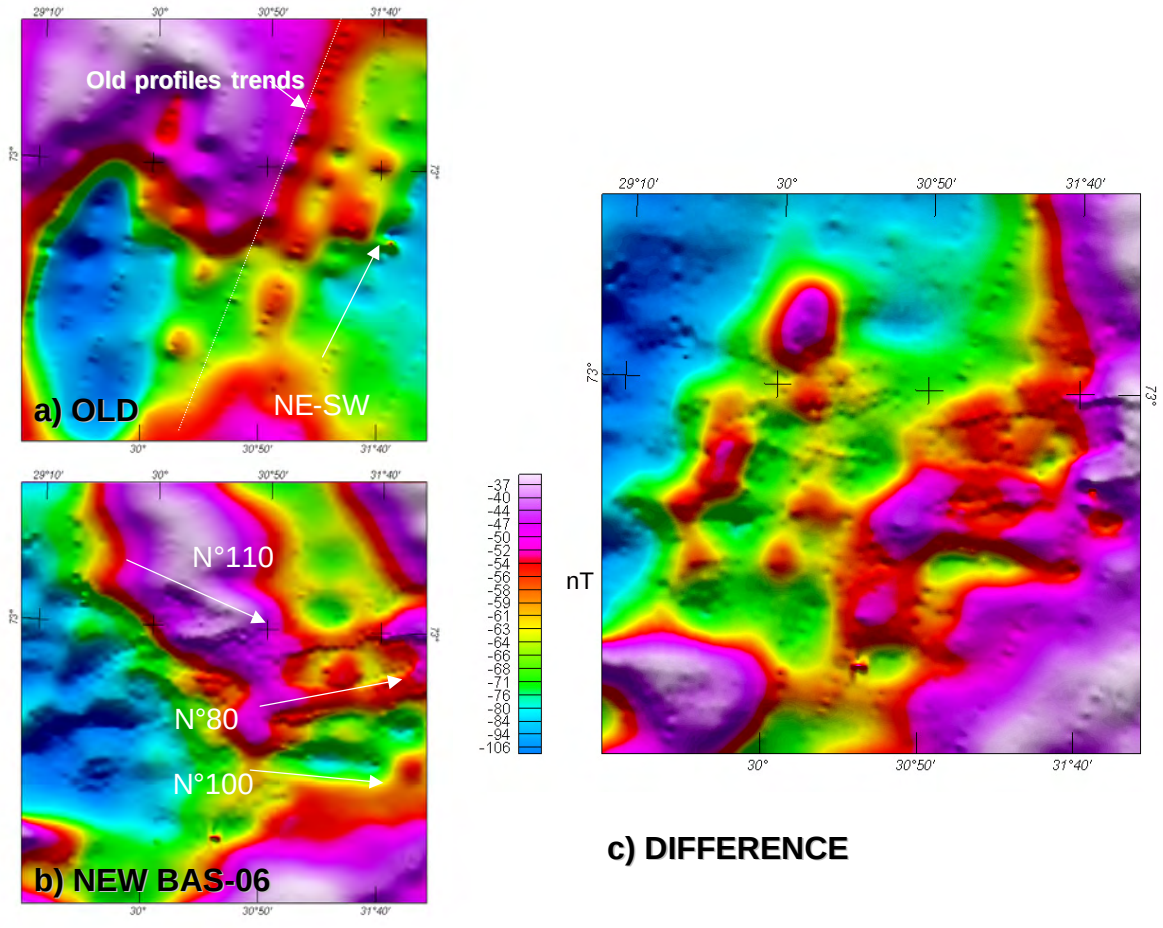

Figure 5.6 Vintage aeromagnetic compilation from the Nordkapp Basin area (a) compared with the new dataset (b). The difference is obvious and significant (c).

New trends are now observed with the magnetic survey and suggest a more complex crustal and basin architecture of the Nordkapp Basin, clearly divided in sub-magnetic segments at the level of the survey.

The western part of the central Nordkapp Basin is characterised by a lower magnetic domain (M-NL1) compared to its eastern part (Figs. 5.3, 5.6). However, no clear and similar changes appear in the gravity signature. However, the eastern part represents a narrower graben, where more linear and elongated magnetic trends are observed. The structural style variability of the Nordkapp Basin from west to east and the contrasting E-W magnetic pattern of the Nordkapp Basin can be explained by the interaction between rift deformation affected by oblique pre-existing deep features and/or pre-existing grabens. A large 20 km wide relay zone can be particularly observed both on the gravity and magnetic trends. This transfer zone coincides with the progressive narrowing of the Nordkapp Basin from west to the east. The relay zone also coincides with the southern prolongation of the broad NW-SE magnetic anomaly M-FH2 observed on the magnetic total field from 72° up to 73°40´N. This large anomaly about 40 km wide is disrupted at the level of the Nordkapp Basin and probably characterises old basement or Paleozoic striking features, which influenced the graben architecture development during successive rifting episodes. Anomaly M-NH1, in the southern part of the Nordkapp Basin could represent the initial prolongation of the magnetic unit M-FH2 before subsequent rift-induced dislocation. Our modelling (cf.chapter 7) also suggests a shallowing of the top basement from west to east on either side of this major relay zone; confirming that the crustal architecture varies laterally in the Nordkapp Basin area.

Between the Nordkapp Basin and the Finnmark Platform a transitional domain is characterised by both gravity (G-NH1 and G-NH2) and magnetic highs (M-NH2 and M-NH3). The Thor Iversen Fault Zone lies on the northern flank(s) of theses anomalies (Figs. 5.2, 5.3, 5.4). The Thor Iversen Fault Zone is a prolongation of the Troms- Finnmark and Måsøy Fault Complexes and represents a regional fracture zone at the scale of the Barents Sea. These principal fault trends were characterised by peak faulting activity at specific times, and many can be linked fairly confidently with known faults on the Finnmark mainland (Gabrielsen 1984, Gabrielsen et al. 1992; Jensen and Sørensen 1992). The NE-SW offshore fault trend is known to have been operative in Devono-Carboniferous time exploiting the Caledonian structural inheritage (Faleide et al. 1984, Gabrielsen et al. 1992, Bugge et al. 1995). Basin-bordering movements continued through the Permo-Triassic interval and appear to have extended into the late Mesozoic. Many such NE-SW-trending faults can be traced onshore, in Finnmark (Roberts and Lippard, 2005). The existing faults in Finnmark, especially in western areas, were subjected to successive reactivations in Permo-Triassic and, notably in the Jurassic-Late Cretaceous (Roberts and Lippard 2005).

With the new survey, we suggest that the N°100 trend of the Thor Iversen Fault Zone could be connected with the prolongation of one of the regional trends which defined the Tiddlybanken Basin and West Kola Graben described by Ivanova (2001). Some linear trends of the Euler

deconvolution solutions (Fig. 4.7, 4.8 and 4.9) also suggests that the N°60 segment of the Thor Iversen Fault Zone could extend further southwest towards the Måsøy Fault Complexes and could explain the geometry of the gravity "spur" (G-NH1) southwest of the median ridge located between the central and south Nordkapp Basin.

5.5 The Finnmark Platform - Kola Kanin Monocline

The BAS-06 covers the hinge zone between the Finnmark Platform and the Kola-Kanin Monocline. North of the Varanger Peninsula, the deep part of the Finnmark Platform is characterised by an underlying rift topography with fault blocks containing siliciclastic sediments of Early Carboniferous age; these were onlapped in the mid-Carboniferous by minor carbonate evaporites in certain intervals (Bugge et al. 1995). Exploration wells have been drilled on the Finnmark Platform, all reaching the Upper Palaeozoic (7120/12-4 on the western platform and 7229/11-1, 7128/4-1, 7128/6-1 and 7228/9-1 in the east) (Larssen et al. 2005). The Paleozoic is overlapped by Triassic and Cretaceous units, tilted to the north and truncated in the southern part of the platform (e.g. Bugge et al. 1995) (Fig. 5.7).

The magnetic signature of the Finnmark Platform is complex and probably involves both shallow and deep magnetic sources (Figs. 5.5, 5.7). It is, however, difficult to distinguish between all the factors especially because they interact. Subsidence pattern, bathymetry and shape of the sediment are often controlled by the deep basement architecture of the platform and, similar to the Bjarmeland Platform some correlation also exists between deep structures and subcropping units. Nevertheless, the deep contributions are certainly most important to explain the amplitude of the gravity and the magnetic total field. Small wavelength features highlighted by filtering (High-pass or tilt derivative) may represent the lithologic contrast of shallow faults rooted or controlled by deeper crustal faults or shear zones (Figs. 5.3 and 5.7).

In the southern part of the new survey, a broad, NW-SE elongated gravity low (G-FL4) is observed to the north of the Varanger Peninsula coinciding with a northwestern prolongation of the Kola-Kanin Monocline (Fig. 5.2). The NW-SE regional trends also coincide with well-known onshore Archean and Precambrian megastructures (Karpuz et al. 1995) further discussed in the next chapter dealing specifically with onshore-offshore relationships.

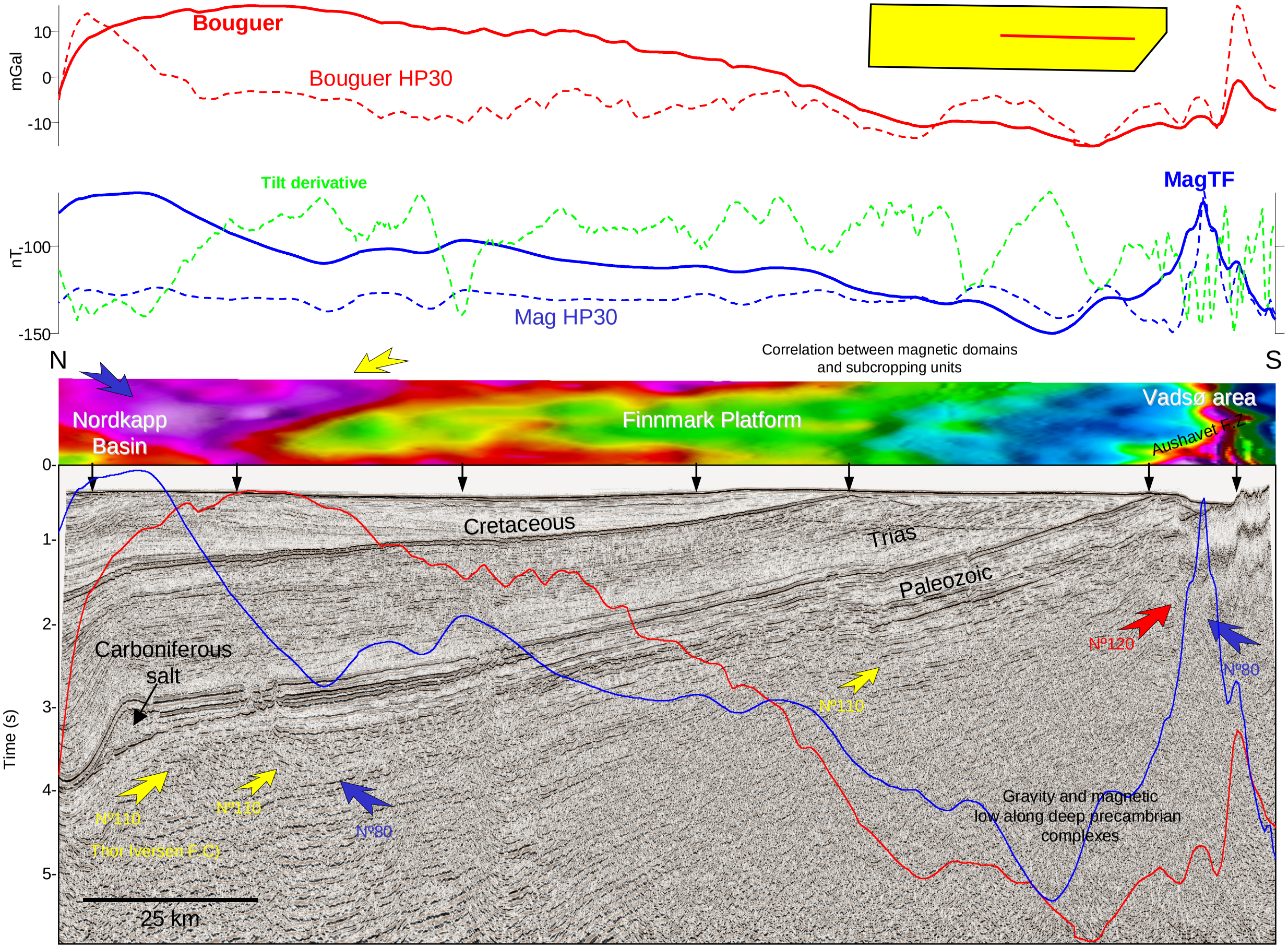

Figure 5.7 North-south seismic transect, gravity and magnetic total field across the Finnmark Platform.

South of the Finnmark Platform, a relatively low gravity and magnetic region compared to the whole survey is observed (G-FL4, M-FL2). Figure 5.3 shows that the northern boundary of the magnetic low region also fit with some seismic sequences boundaries. Figures 5.5 and 5.7 show that the limit between the low and high magnetic region coincides approximately with the base of the Cretaceous.

In the southern part of the platform, the new aeromagnetics highlights new positive trends and structures. NW-SE to N°70 trending lineaments, with high frequency, are clearly observed in the northern part of the Varanger Peninsula (Fig. 5.3). They coincide with discrete gravity changes in the Finnmark Platform and can be correlated with onshore trusted and folded structures described in detail in the following chapter. South of 71°20´, in the western part of the survey, a dominant NE-SW linear and narrow strong anomaly may represent an intrusion between gravity anomalies G-FH2 and G-FL3.

Deep seismic and wide-angle surveys are quasi-inexistent along the BAS-06. However, a Russian seismic transect (AP-1-95) is located approximately 100 km east of the BAS-06, north of the Ryabachi Peninsula (Ivanova 2001, Ivanova et al. 2006) (Fig. 5.8). This wide-angle transect is almost parallel to the 2D seismic section described in figure 5.7 and provided constrains for the meaning of the broad and regional NW-SE gravity trends. Some structures can be carefully extrapolated towards the BAS-06 region.

The Kola-Kanin Monocline represents a thick Riphean-Vendian (?) complex, expected to extend in the southern part of the BAS-06. The gravity regional low could roughly represent the potential field expression of the West Varanger Graben, which is part of the Kola-Kanin Monocline. The thickness of the Riphean metasediments maybe as much as 10 km on the Kola-Shelf but probably less north of Varanger Peninsula (cf. modelling chapter). Theses formations underlie the Paleozoic and Mesozoic sediments that pinch-out on the southern flank of the monocline.

Major crustal faults, are interpreted by Ivanova et al. (2006) could coincide with the NW-SE and NNW-SSE magnetic lineaments observed along the Finnmark Platform. Some of them correlated with the trends of the Austhavet Fault Zone and the Trollfjorden-Komagelva Fault Zone (TKFZ) lying from the whole Varanger Peninsula up to the Pechora Basin in Russia (e.g. Ivanova 2001). On the Varanger Peninsula, the Barents Sea region reflects net gravity changes (eg. Karpuz et al. 1995). The northern part of the NW-SE Austhavet Fault Zone roughly coincides with the transition between gravity highs (G-FH3, G-FH4), and the gravity low area G-FL4. This fault zone could coincide with the Karpinsiy Fault Lineament described by Ivanova (2001) (Figure 5.8). On the Russian side, the Karpinsiy Fault Lineament is interpreted as a major deep and steeply dipping thrust fault, where the Riphean complexes of the Timanides (Balkalides) are thrust over their platform analogues (Simonov et al. 1998).

A more prominent N°80-trending high amplitude and elongated magnetic anomaly (M-FH1) is particularly observed north of the Varanger Peninsula, and merge locally with the Austhavet Fault Zone. This magnetic anomaly clearly delimits two magnetic domains in the southern part of the Finnmark Platform and coincides also with discrete trends in the gravity signature.

Parallel to the Varanger Graben (Fig. 5.8) is the West Kola Graben described by Ivanova et al. (2006) between 71° and 72° which? lies in the trend of the Tiddlybanken Basin. It represents old and deep Cambrian-Silurian, Devonian and Carboniferous depocenter observed up to the Fendynski High (Ivanova 2001, Ivanova et al. 2006). This complex is also affected by small Devonian inversions according Ivavova et al. (2006). The faults reach locally 10 km depth and have been reactivated during subsequent rift events. Some of the old Palaeozoic systems can extend toward the BAS-06 survey area and may have extended obliquely across the Nordkapp Basin before the subsequent Mesozoic rift episodes. Broad NW-SE elongated magnetic highs observed on both sides of the Nordkapp Basin may represent the northern prolongation of the old and deep structures described by Ivanova (2001).

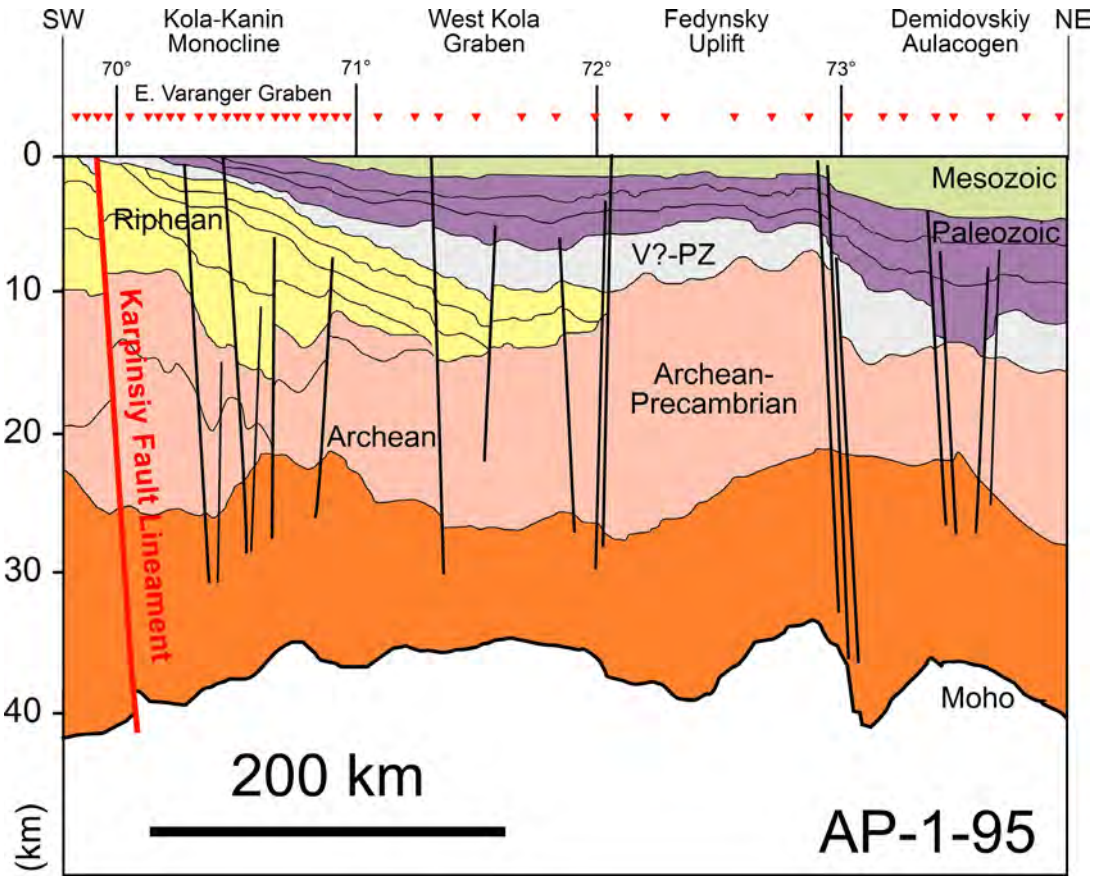

Figure 5.8 Geological section along the regional profiles AP-1-95 (after Ivanova 2001, 2006). This section illustrates the deep structures of the Kola-Kanin Monocline.

5.6 Varanger Peninsula and near shore domain. Onshore-offshore relationships

Part of the BAS-06 survey overlaps the northern part of the Varanger Peninsula (Fig. 5.9). This overlap allows us to constrain and understand the meaning of the magnetic anomalies using onshore-offshore relationships.

The principal features of the bedrock geology of the Varanger Peninsula are described on the NGU 1: 500,000 bedrock geology map by Siedlecka and Roberts (1996) and the 1:250.000 sheet of Vadsø (Siedlecki 1980) partly digitised and draped on the BAS-06 magnetic grid to provide the geological input in our interpretation (Figs. 5.10-5.15) (a .pdf of this map can be found on the archive DVD). The previous magnetic aeromagnetic compilation of the Varanger Peninsula (Olesen et al. 1992) has also been merged with the BAS-06 to provide an onshore extent of the new survey (Fig. 5.10). To better illustrate the onshore structures and its implication for the BAS-06 interpretation (and reciprocally), a NW-SE trending geological section has been realised during this project (Fig. 5.11). The structures can also be compared with the different maps described in the following section. It has been compared with a magnetic profile extracted along the southernmost part of the BAS-06. Values of rock susceptibilities sampled and measured by NGU in that area were projected along the onshore transect.

5.6.1 Onshore Geology

South of the BAS-06, the Varanger Peninsula is characterised by sequences of old sedimentary rocks, which range from Late Precambrian to Early Cambrian. Previous remote sensing and magnetic analysis of the Peninsula assumed that major penetrative NW-SE, NNW-SSE to NNE-SSW and NE-SW lineaments were originating from Archean to Proterozoic crystalline basement features (Karpuz et al. 1993, 1995). The NW-SE lineament zones are particularly significant in both remote sensing and potential field data and probably represent the oldest weakness zones in this part of the Fennoscandian Shield (Karpuz et al. 1995). Structural investigations suggested that some of the features were formed due to either strike-slip or dip-slip reactivation of the major fault zones since Late Archean time (Siedlecka and Roberts 1992, Karpuz et al. 1993, 1995)

The Varanger Peninsula is divided into two regions separated by the major Trollfjorden-Komagelva Fault Zone (TKFZ), which marks a clear metamorphic, structural boundary (Siedlecka and Roberts, 1992) (Figs. 5.9 and 5.10). The Barents Sea Region (BSR) lies to the north part of the TKFZ and the Tanafjorden-Varangerfjorden Region (TVR) represents the southern part of the Varanger Peninsula. The TKFZ is also highlighted by net gravity and magnetic changes between TVR and BSR (Figs. 5.9 and 5.14).

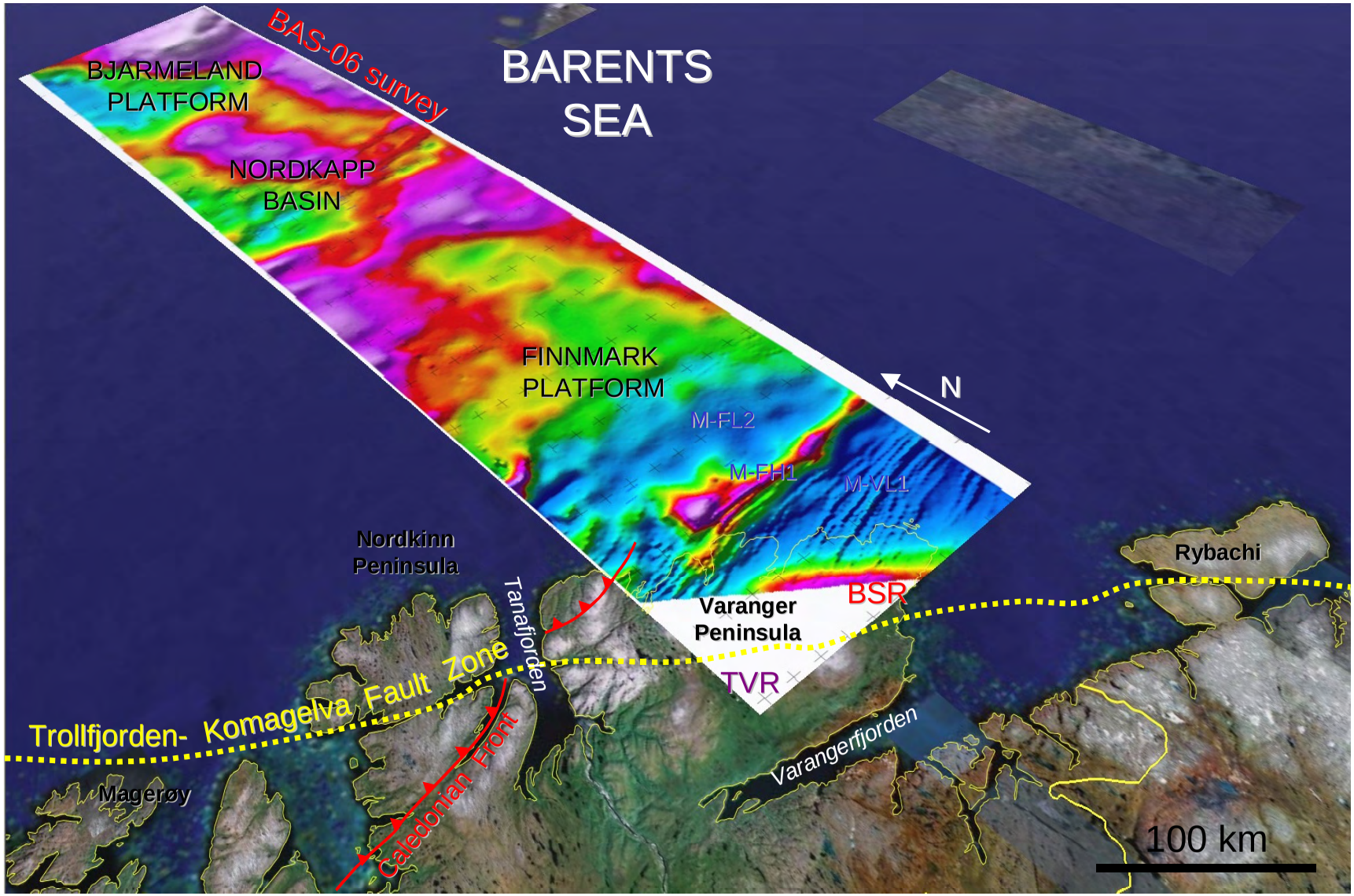

Figure 5.9 Satellite elevation model of the Varanger Peninsula and onshore-offshore relationships with the BAS-06. BSR. Barents Sea Region; TVR. Tanafjorden-Varangerfjorden Region. M-FL2; M-FH1; M-VL1 represents the main magnetic domains discussed in this chapter.

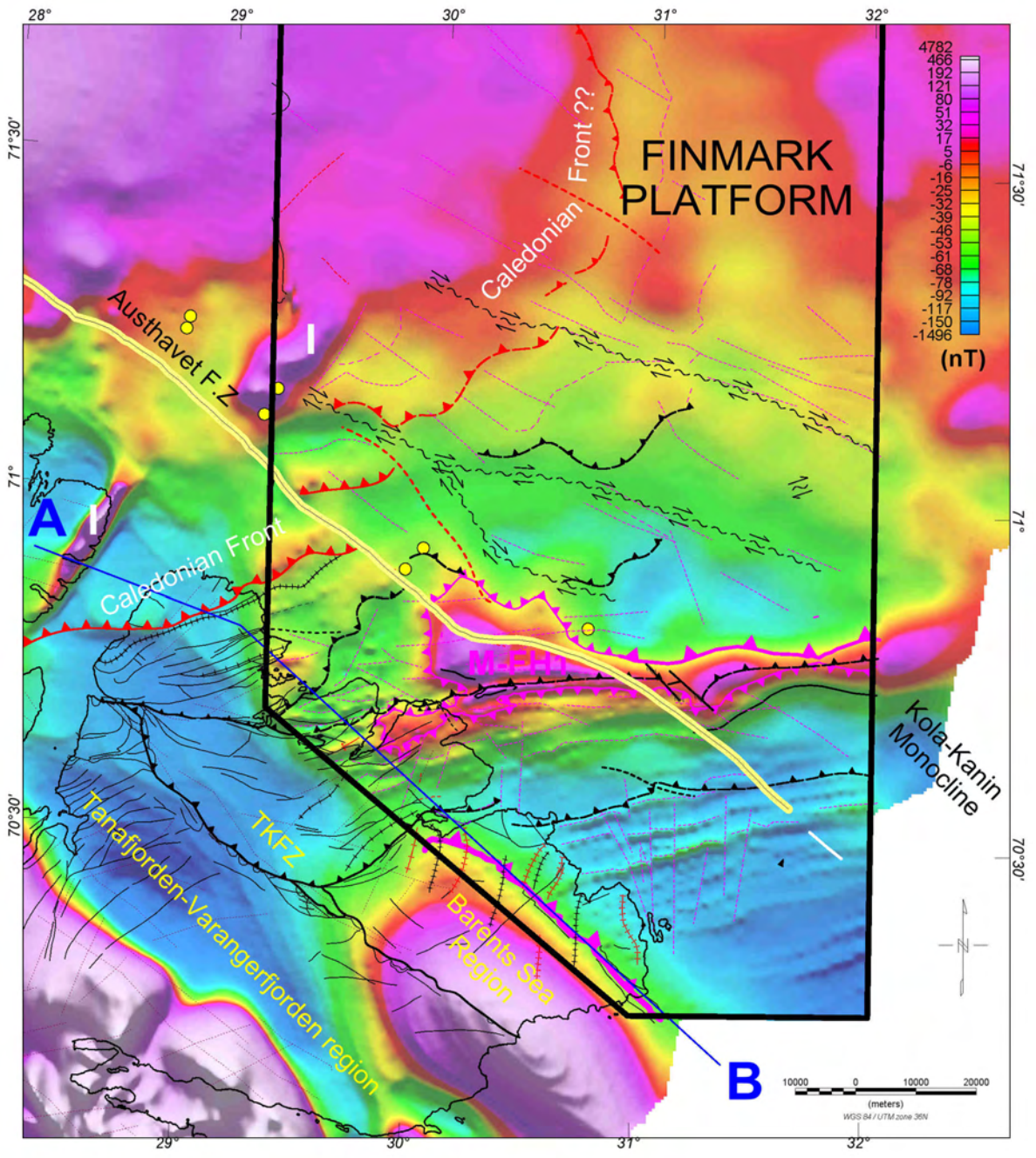

Figure 5.10 BAS-06 survey and surrounding magnetic data (e.g. Olesen et al. 1992) on the Varanger Peninsula. I: high amplitude magnetic anomaly, which could represent a mafic intrusion shifted by the Austhavet Fault Zone.

The regional significance, the structure and evolution of the TKFZ, was previously discussed by Siedlecka and Roberts (1992) and Karpuz et al. (1993, 1995). The fault zone is almost parallel to the Kola Kanin Monocline axis and extends to the east from the coast of the Kola Peninsula in Russia to the Rybachi-Sredni Peninsula. A western extension in the Barents Sea has also been proposed by Gabrielsen and Færseth (1989).

South of the TKFZ, the Tanafjorden-Varangerfjorden Region (TVR) consists of up to 3.8 km of Late Riphean to Early Cambrian successions lying unconformably upon the Karalian metamorphic

complex (Siedlecka and Roberts, 1992). To the north, the Barents Sea Region (BSR) represents about 9 km of Late or possibly Mid-Riphean to Early Vendian sequences resting unconformably upon the Barents Sea Group is the Vendian Lockvikfjellet Group, overthrusted by the Berlevåg Formation, to the west. In contrast to the formation of the TVR, only affected by diagenesis, the allochtonous sequences of the BSR group have been metamorphosed under lower greenschist facies conditions.
The metasedimentary sequences of the BSR were deposited in a basin bounded to the south by the TKFZ, the latter probably acted initially as a major basin border fault (Siedlecka and Roberts 1992). Subsequently, major strike slip deformation was expected in Late Precambrian to Early Ordovician, with subsequent deformation in the Paleozoic and Mesozoic (Lippard and Robert 1987). Rice et al. (1989) proposes a strike-slip movement of 400 km along the TKFZ, associated with Caledonian thrusting However, Karpuz et al. (1995) suggest that the displacement could be less than 250 km. Finally, Jensen and Sørensen (1992) consider also a post-Caledonian (pre-Vendian ?) dextral movement along the TKFZ of less than 5km associated with a Late Palaeozoic rifting phase in the Barents Sea.

The structure of the Varanger Peninsula was strongly influenced by the Caledonian Orogeny (Roberts 1972, Karpuz et al. 1995). In the BSR, there is a general decrease of the intensity of the deformation from NW to SE (Roberts 1972). The Northwestern part represents a thrust and fold belt system overturned to the SE at moderate angles. Metadolerite dikes are profuse in this area (Roberts 1972) but no maps of all the dikes have been produced or published so far. In the NW, the folds and thrust faults are essentially NE-SW, close to the Caledonian front.

5.6.2 Onshore-offshore relationships and new insights from the BAS-06 dataset

Aeromagnetic and gravity investigation of the Varanger-Vadsø Peninsula have previously been investigated by Åm (1975), Chroston (1986), Olesen et al. (1990). Åm (1975) interpreted the thickness of the Late Proterozoic sedimentary cover in the region from less than 1 km in Varengerfjorden to 7 km in the northeastern part of the Varanger Peninsula. As previously suggested, the Riphean-Vendian (?) formations of the BSR likely extend offshore along the Kola-Kanin Monocline and the southern part of the Finnmark Platform (Ivanova et al. 2001, 2006).
Some specific uncertainties can be pointed out regarding magnetic lineaments and their character in that area. Differences in overburden thickness also give different conditions for lineament identification, offshore Varanger Peninsula. Large areas with a thin overburden provide a good spatial and dynamic resolution of the magnetic pattern and hence, lineaments are more easily identified. Thick overburden increasing from the Finnmark Platform to the Nordkapp Basin could partly decrease or hide the magnetic signature. Some interpreted lineaments are closely correlated to the faults and structures shown on published maps of the area (e.g. NPD shape files) and this indicates that the processed magnetic data could confirm most of the previously mapped faults.

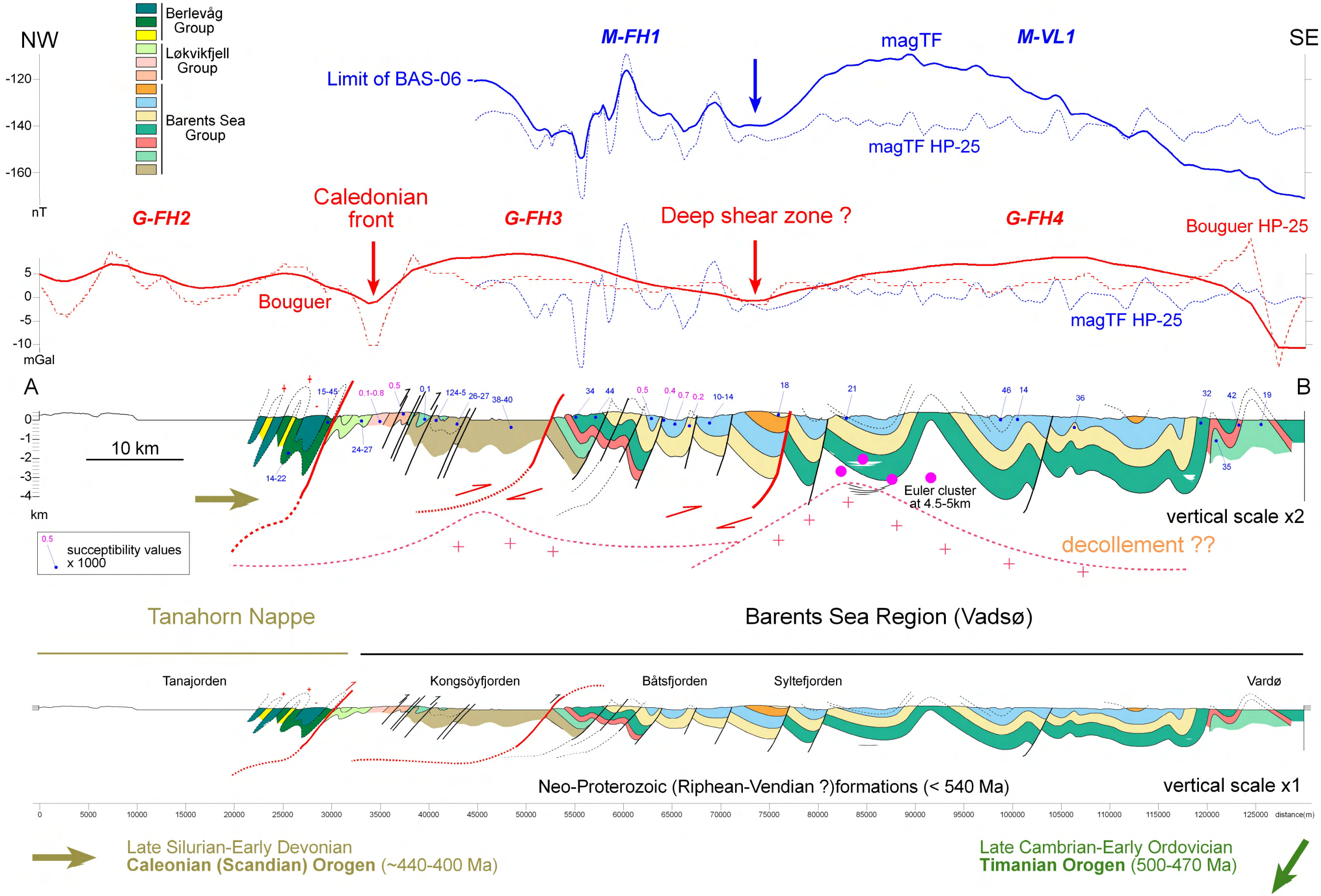

Figure 5.11 NW-SE geological transects from Tanafjorden to Vardø combined with Bouguer gravity and magnetic total field. Transect AB located on figure 5.10.

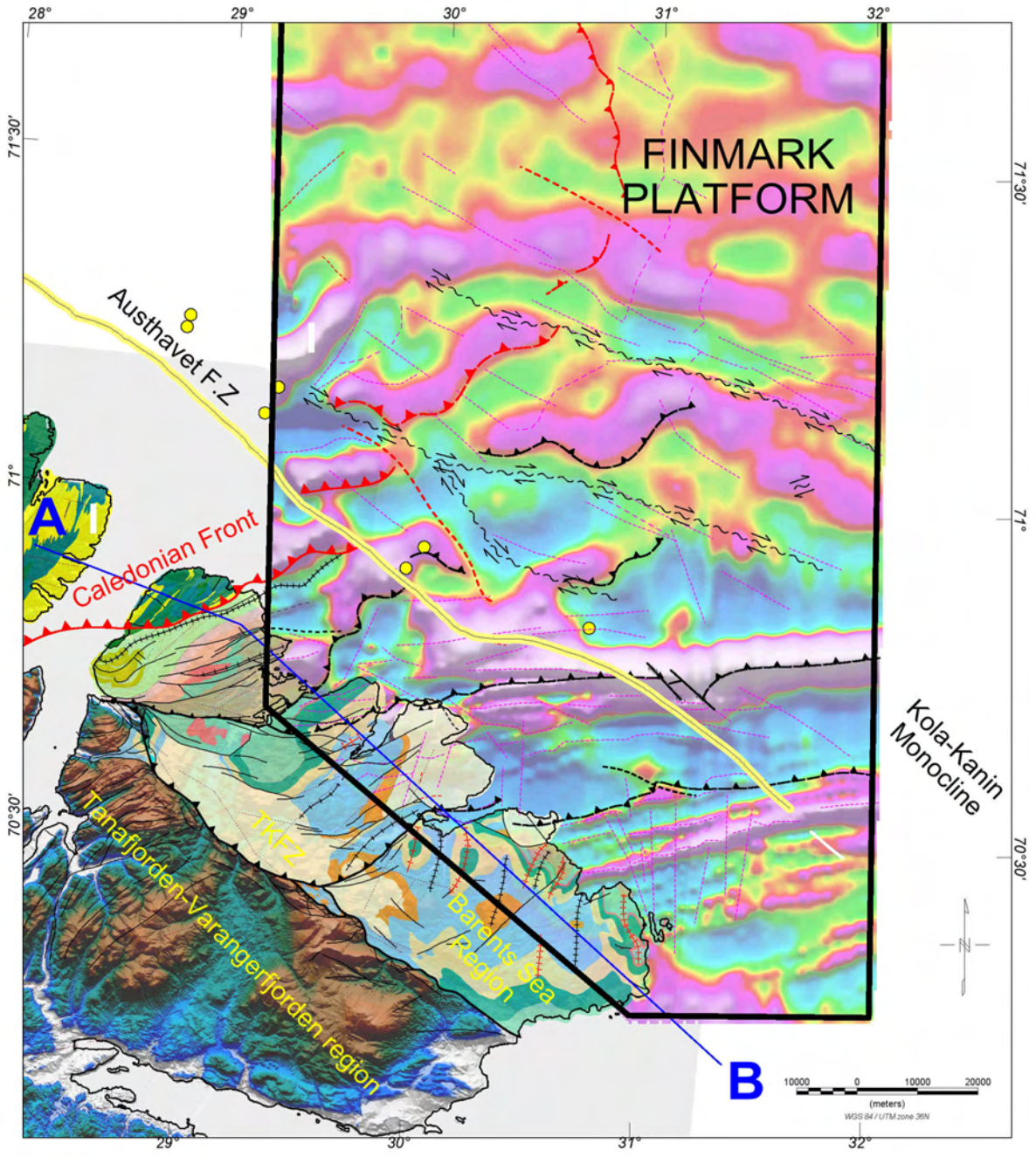

Figure 5.12 Magnetic total field (HP-30 km) compared with the bedrock geology observed in the Barents Sea Region (from the M. 1:250.000 bedrock map of Siedlecki, (1980). The greater part of the Varanger Peninsula, particularly in the west and north, is underlain by the metamorphic allochthon of the Caledonides (Roberts and Gee 1985, Roberts 2003). Southwest of the survey area, the Bervelåg Formation of the Gaissa-Tanahorn Nappes represents the Caledonian Front lying near Tanafjorden in the northwestern part of the Varanger Peninsula (Siedlecka and Roberts 1992, 1995). Main onshore-offshore relationships can be proposed. TKFZ: Trollfjorden-Komagelva Fault Zone. The main lineaments have been highlighted on the BAS-06. An extension of the Caledonian Front (red symbol) can be proposed. Sigmoidal magnetic pattern can reflect strike slip accommodation of the deformation on the Finnmark Platform. Geological legend and structures are described on Fig. 5.11.

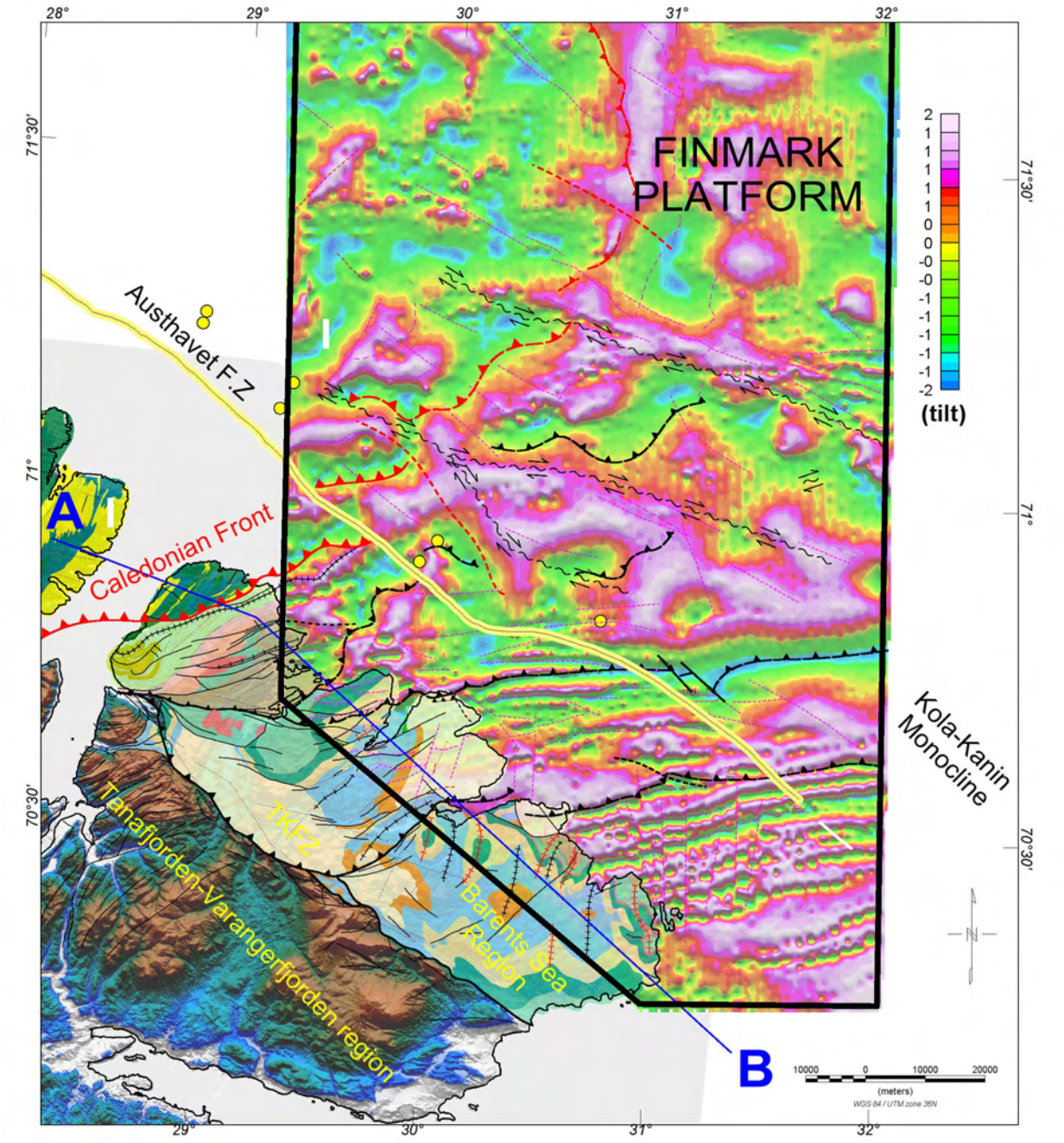

Figure 5.13 Tilt of the magnetic total field (HP-30 km) compared with the geology observed in the Barents Sea Region. The tilt derivative filter provided more structural details and illustrated the onshore prolongation of the different faults or sedimentary units described in the Barents Sea Region. The tilt filter highlighted the NW-SE trending lineament and the Caledonian Front on the Finnmark Platform. Note that the trace of the Austhavet Fault Zone (NPD-shape file) could be re-interpreted locally.

Conversely, some lineaments related to new fault zones appear to be more complex in the southern part of the Finnmark Platform.

Along the transect (Fig. 5.11), good relationships with the deformed sediments of the BSR have been observed. In contrast, deformation of the TSR is less intense with NE-SW trending anticlines and synclinal features but with minor thrusts found locally in the western part of the TSR.

New N°70 trending lineaments, with high frequency, have been clearly observed in the northern part of Barents Sea Region (M-FH1). The clear magnetic layering observed in this near shore area correlates very well with structural features observed onshore in the BSR (Figs. 5.12, 5.13, 5.14). The high frequency content is linked with the main fold and overthrust structures of the BSR. The magnetic layering, observed offshore (M-FH1, M-VL1) can be explained and reflect the main faulted block distribution of the Barents Sea Region, which most likely represents an intensely fractured area containing hematite (?) or later intruded by dikes. Using a high-pass and derivatives filters; we also showed that the tilt (geological tilt) of some sedimentary layers influence the magnetic signal.

The amiabilities of the large magnetic and gravity wavelengths coincide with major structural domains underlined by our geological transect (Fig. 5.11). The primary structural boundary coincide with the Caledonian Front. The Caledonian Front and related overthrusts coincides with NNE-SSS to NE-SE trends observed in the southwestern part of the BAS-06. It is characterised by a NW-SE gravity low. Close to the front, the magnetic anomalies coincide with fault-propagation folds and thrusts gradually steepening through the vertical toward the SE (Karpuz et al. 1995). Offshore the Varanger Peninsula, their magnetic trends vary mainly from NW-SE close to the Caledonian Front to N°70-N°80 further to the east. The main N°70 magnetic anomaly N-FH1 correlate with the formations and overthrusts observed between Kongsøyfjorden and Båtsfjorden (Fig. 5.14). It represents a set of thrust faults with probably a strike-slip component. It could be connected with a deeper shear zone. In its central part, the N°70 striking anomaly M-FH1 is affected by the Aushavet Fault Zone. However, the N°110-trending Austhavet Fault Zone does not significantly displace the N°70-N°80 lineations as can be observed in the low magnetic domain M-VL1.

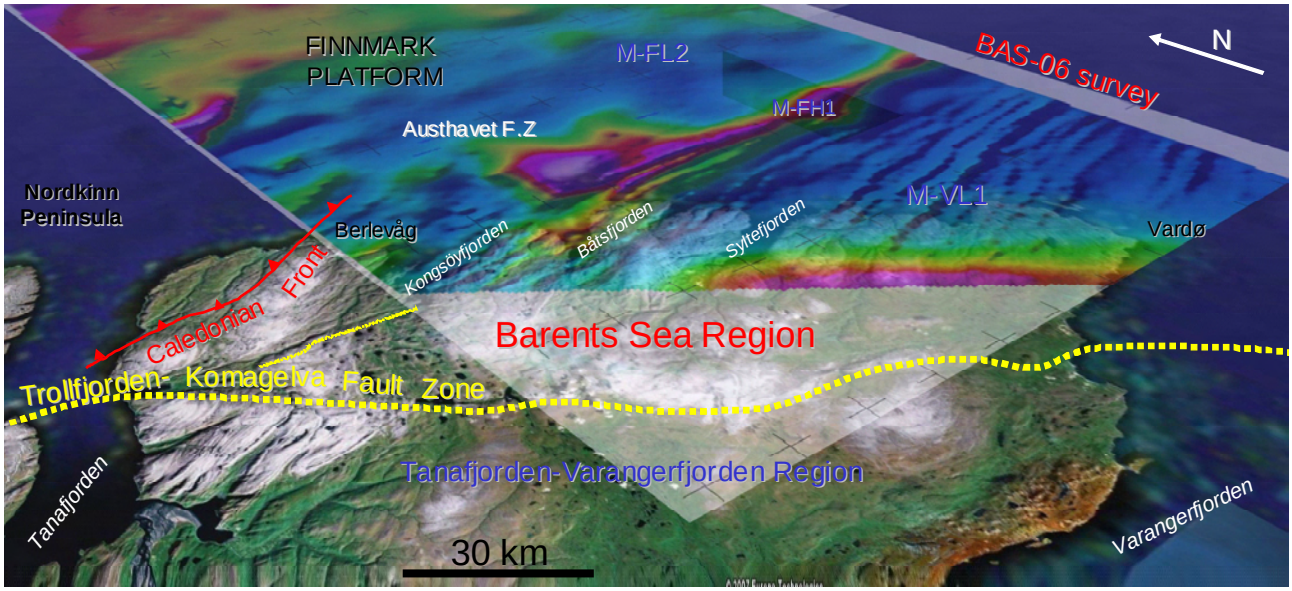

Figure 5.14 Onshore-offshore relationships in the Barents Sea Region. A main magnetic positive anomaly M-FH1 between low magnetic domains M-FL2 and M-VL1 runs in the prolongation of overthrusted structures and faults observed onshore between Kongsøyfjorden and Båtsfjorden.

A second and major structural and geophysical change is observed at the level of Syltefjorden. A gravity low in the central part of the Barents Sea Region (Between G-FH3 and G-FH4) also reflects a major change in the magnetic total field signature (Figs. 5.11 and 5.15). We believe that this gravity low coincides with a major crustal boundary, which may divide the BSR in distinct crustal blocks. It could represent a deep Proterozoic fault or shear zone, likely reactivated during the Caledonian event. This boundary can be extrapolated offshore and seems to coincide with a discrete subdivision in the well-layered magnetic pattern. Euler solutions for these areas suggest that the N°70-80 magnetic lineation observed in the southern part of the BAS-06 lie at depths deeper than 2 to 3 km increasing to the southeast in the M-VL1 magnetic area (Figs 4.7, 4.8 and 4.9). In the M-VL1 area, the main magnetic trend is still N°70 but several N-S lineations were underlined by enhanced filters. They slightly disrupt the N°70-80 layering pattern. This boundary also coincides with contrasting gravity lows anomalies with different trends (Fig. 5.15).

Southwest of this stripped zone, deformation in the onshore part is less intense and mostly affected by anticlines and synclines, instead of inverse and thrusts features, prominent in the northwestern part of the peninsula. The trends of the onshore structures also change between Syltefjorden and Vardø with a dominant N-S orientation of the folded structures (Figs. 5.11 and 5.12).

At a regional scale, the eastern part of the BSR shows a significant magnetic change with a prominent magnetic anomaly not observed in the northwestern part of the Varanger Peninsula (Fig. 5.10). The correlation between potential field and the structural contrasting style observed onshore, suggest a major crustal boundary. The meaning of this anomaly was already discussed by Karpuz et al. (1995). This anomaly coincides with the southeastern segment of the TKFZ and could originate at a depth of 5 km (Åm 1975). With the new survey, we also got some clusters of Euler solutions at similar depth of 4.5-5 km (Fig. 5.11). According to Karpuz et al. (1995), the spatial coincidence with gravity anomaly G-FH4 may suggest the presence of a possible basement high or intrusion at depth along this part of the Varanger Peninsula.

Compared to the contrasting N-S structures described in the southwestern part of the Varanger Peninsula, the main dominant magnetic trends still remain N°70 on the BAS-06 and can be followed event beneath the N-S folded structures (Figs. 5.13 and 5.14). This could be explained by late dislocation and rotation of fault blocks. Some folds with facing reversal polarity (Fig. 5.11) may also suggest a possible backthrusting process, which could explain the trend differences between the magnetic lineations and the N-S axis of the folds. A deeper thrust system involving a trailing imbricate fan above a deeper detachment could influence such a conjugate faulting and folding. A deeper blind-thrust hypothesis is suggested in our transect (Fig. 5.11).

Between the Syltefjorden and Vardø, the folding is likely Caledonian in age (Silurian - Early Devonian time) but an older compressional phase related to the Timanian Orogen (Cambrian-Silurian), can not be excluded in that area (D. Roberts, personal communication 2007). The N-S

trend of the onshore folds could also be explained by this older compressional phase but more onshore investigations and more data are probably required to valid this hypothesis.

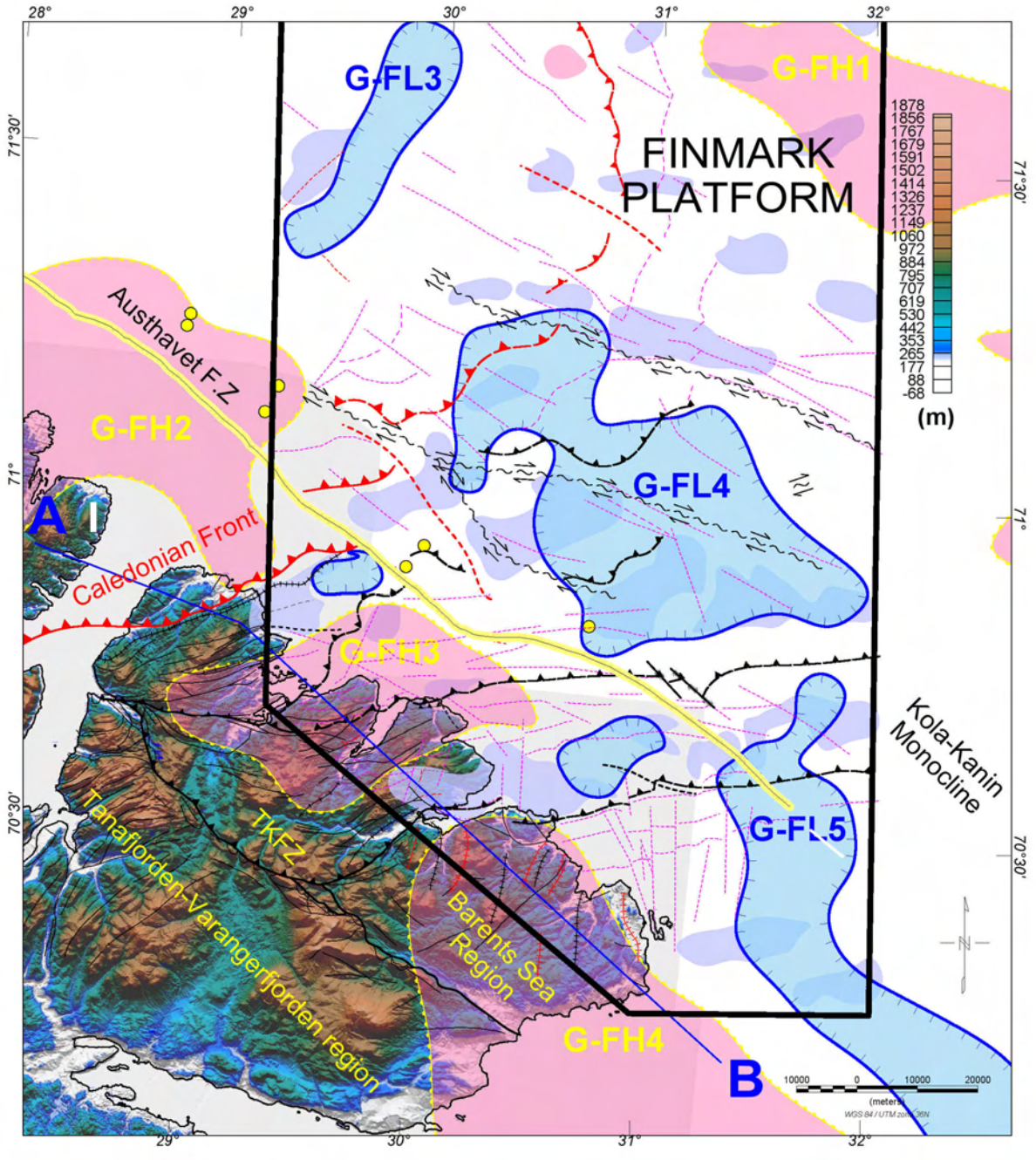

Figures 5.15 Onshore offshore relationships along the Varanger Peninsula. G-FH2, G-FH3 and G-FH4 represent gravity highs and G-FL3, FG-FL4 and G-Fl5 underline the main gravity lows in the area. The main magnetic lineament, interpreted as offshore extension of overthrusts, inverse faults and folds described in the Barents Sea Region also coincide with local gravity changes.

6 SALT AND MAGNETIC FEATURES. EXAMPLES FROM THE NORDKAPP BASIN

Laurent Gernigon

It is the first time, with the NGU SNAS-06 survey (Løvaås et al. 2006), that an aeromagnetic survey with such a resolution covers the Nordkapp Basin and its salt diapirs (Fig. 6.1). In this chapter we show that magnetics can aid and support the interpretation of salt and sub-salt features in the Nordkapp Basin. Some can argue that salt geometries of the salt domes are well known due to good seismic coverage in this area but we think that magnetic data could be useful to refine or assist the seismic interpretation. Magnetic data can particularly highlight discrete fault zones or transfer zones not always detected with conventional 2D seismic data. It can be used to constrain the top magnetic basement as well (cf. chapter 7).

Even though salt diapirism has been studied intensively for many years (the mechanism and geometry of flow and base of salt diapirs are not always yet satisfactorily resolved by seismic data). The shape of the salt still remains a key issue for location of potential exploration wells on the edge of overhang features (Fichler et al. 2007). Gravity and magnetic data can be used to improve velocity models below salt, where velocities derived solely from seismic data and boreholes information are typically interpolated over large distances (Bain et al. 1994). Dynamic linking between seismic, gravity and magnetic interpretation allows multiple seismic interpretations to be tested and either eliminated or corroborated (Flanagan et al. 1988, Bain and Weyand 1993, Prieto 1993, Fichler et al. 2007).

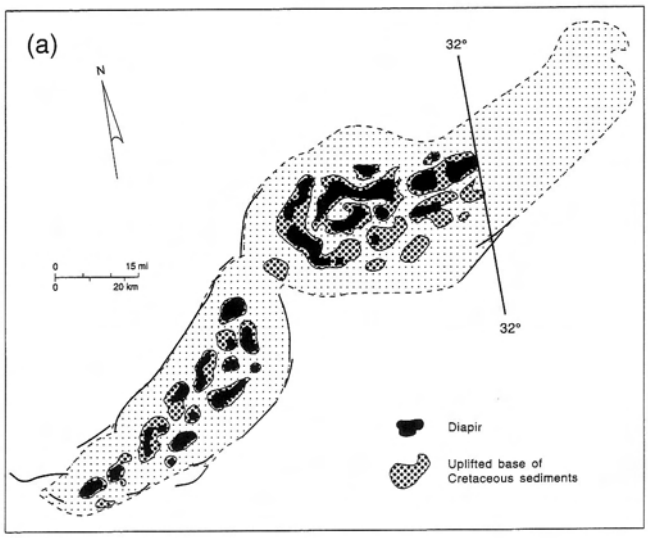

Figure 6.1 Structural map of the Nordkapp Basin showing salt diapirs and main faults zones after Nilsen et al (1995). Black fill represents subcrops of diapirs at or near Plio-Pleistocene erosion surface. Hatched areas represent uplifted base Cretaceous sediments. Note that east of 32°E lies the disputed area.

Key examples of the magnetic implications are presented in this chapter. Interpretation of magnetic features influenced by salt tectonics in this part of the Barents Sea could be relevant, cost effective and certainly strategic for a future survey in the disputed area between Norway and Russia or along similar but under-explored saliferous basins suspected in the Barents Sea area.

6.1 Salt tectonics in the Nordkapp Basin

The BAS-06 covers the central part of the Nordkapp Basin, between the median ridge and the disputed area (Figs. 6.1 and 6.2). The initial sedimentary basin probably formed during post-orogenic collapse and regional extension in Late Devonian-Early Carboniferous (Rønnevik and Jacobsen 1984, Gudlaugson et al. 1994). Poor seismic resolution makes determination of Palaeozoic thicknesses uncertain although in contrast to the Hammerfest Basin, they were surely significant (Larssen et al. 2005). The pre-salt sediment is believed to consist of coaly alluvial siliclastics of the Billefjorden Group (Larssen et al. 2005). Renewed rifting episodes occurred in the mid-Carboniferous, associated with a change to a more arid climate. During Late Palaeozoic, the Nordkapp Basin was the site of extensive salt deposition overstepping a wider area (e.g. Hammerfest Basin, Tromsø Basin, Svalvis Dome, Maud Basin, Ottar Basin, Finmark Platform) (Gabrielsen et al. 1992, Johansen et al. 1993, Breivik et al. 1995).

The thick Upper Carboniferous-Lower Permian evaporites could consist of two salt units, tentatively of Bashkirian-Kasimovian and Asselian age (7229-8-1 well) (Rønnevik 1981, Faleide et al. 1984). The original salt thickness in the Nordkapp Basin is estimated to have been between 2000-2500 m in the South Nordkapp Basin and to be about 4000 m in the central and Eastern Nordkapp Basin (Jensen and Sørensen 1992, Koyi et al. 1993). The Permian succession above the salt is believed to comprise mainly cold water carbonates, siliciclastics and cherts as observed in Svalbard (Larssen et al. 2005, Bugge et al. 2002). The well (7228/9-1S) drilled on the margin of the Nordkapp Basin penetrated the Upper Palaeozoic succession; it terminated in mobilised halite of the Gipsdalen Group. A second well (7228/7-1) drilled recently in the basin itself, penetrated Triassic sandstones abutting a late Palaeozoic salt body (Larssen et al. 2005); this well probably encountered an allochthonous block of Permian carbonates, apparently moved out of place as a result of later halokinesis. In addition, IKU-SINTEF shallow cores penetrated various parts of the Paleozoic and Mesozoic successions, providing important stratigraphic and sedimentological informations, but are not completely released (Bugge et al. 1995).

During the Early-Mid Triassic (Anisian?), an overall westward and northwestward prograding system supplied from the south and the east, affected an area already in shallow marine conditions (Bugge et al. 2002). Along the BAS-06 study area, salt expression is characterised by numerous diapirs and salt pillows initiated during that period (e.g. Gabrielsen et al. 1992, Nilsen et al. 1995, Koyi 1993). During the Early-Mid Triassic, increased subsidence and thickening of the sedimentary

section has been proposed as the triggering mechanism for salt diapirism. Dengo and Røssland (1992) and Bugge et al. (2002) suggested that massive deposition could cause differential loading and triggered diapirism. However, Nilsen et al. (1995) proposed that reactive Early Triassic diapirism could have simply rised by fracturing of the salt overburden as suggested by sand-silicon modelling (Vendeville and Jackson 1992). Nilsen et al. (1995) showed on seismic data that there was no major differential subsidence of the Nordkapp Basin at that time. We favour the later interpretation.

Normal faulting and thinning of the salt overburden could be Late Smithian-Early Spathian in age (Gabrielsen et al. 1992, Nilsen et al. 1995). Later, the diapirs pierced the overburden and rose actively. The movements of Palaeozoic salt began in the Early Triassic and since then the diapirs have undergone several phases of development. Gravity gliding phases occurred during Mid-Later Triassic and Late Cretaceous time. Later episodes of active salt reactivation were postulated from Late Jurassic to recent time. Nilsen et al. (1995) related the last salt diapirism to mid-Tertiary compression; which could explain the “squeezed” diapirs geometries and the folded structures observed in intra-salt basins. The Nordkapp Basin was subsequently uplifted and eroded in Plio-Pleistocene time allowing the salt features to subcrop and to be reached by the shallow IKU drillholes described in detail by Bugge et al. (2002).

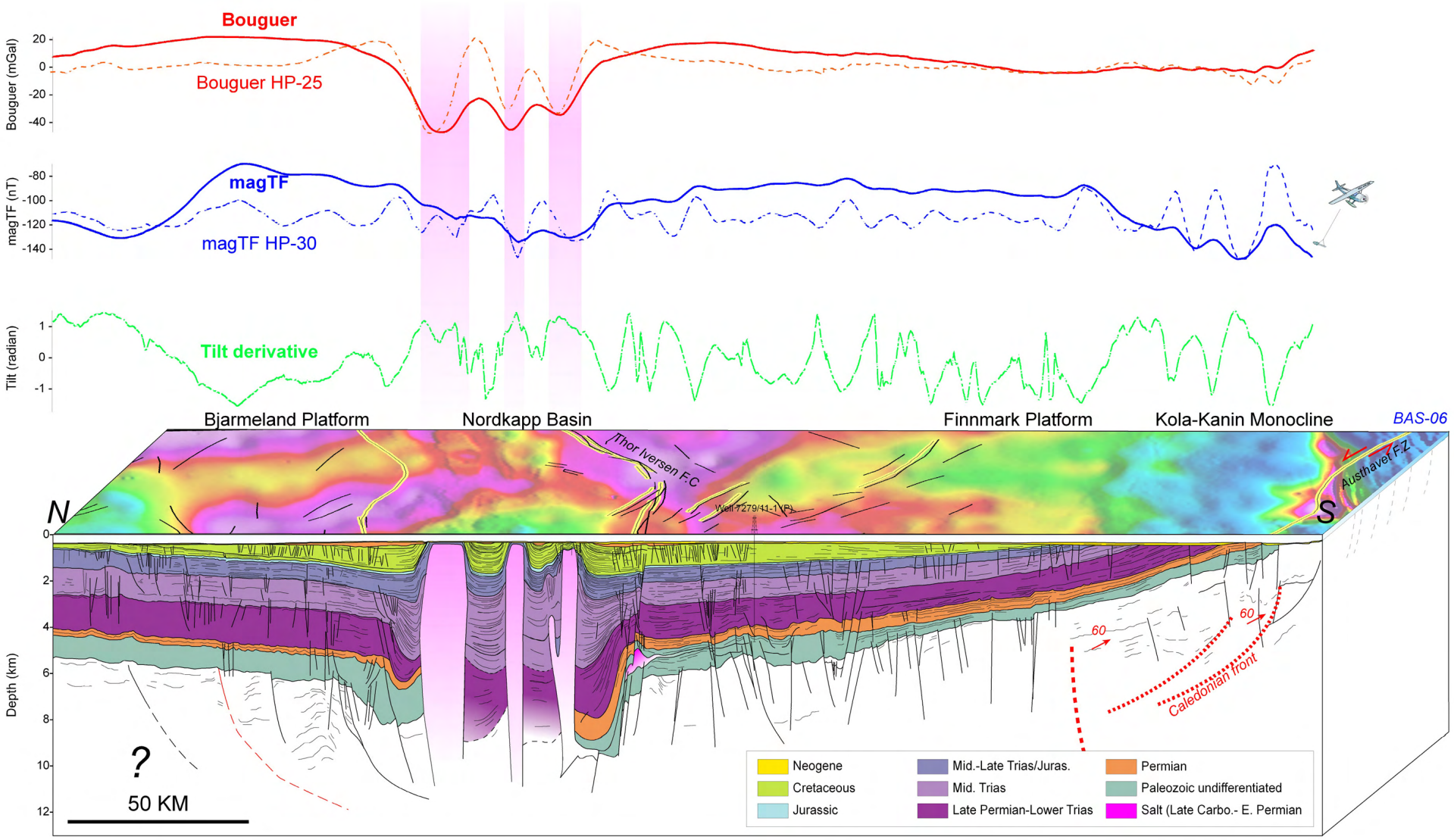

Figure 6.2 3D basin architecture and main sedimentary units of the Nordkapp Basin and surrounding areas compared with potential field data.

6.2 Magnetic expression of the salt domes in the Nordkapp Basin

6.2.1 Magnetic anomalies

A multi-disciplinary integration can also provide valuable information where seismic data alone may be difficult to interpret. In this study, integrated gravity, magnetic and seismic modelling has been used in the Nordkapp Basin to provide information about salt geometries (Fig. 6.2).

A first spectral analysis shows that the frequency content of the BAS-06 contains more spectral information at medium to high wavenumbers (=medium to short wavelengths) than the vintage data (Fig. 6.3) The slope analysis of the power spectrum (Spector and Grant 1970) suggests that the top of most of the main magnetic sources, highlighted by the spectrum are shallow (< 3 km).

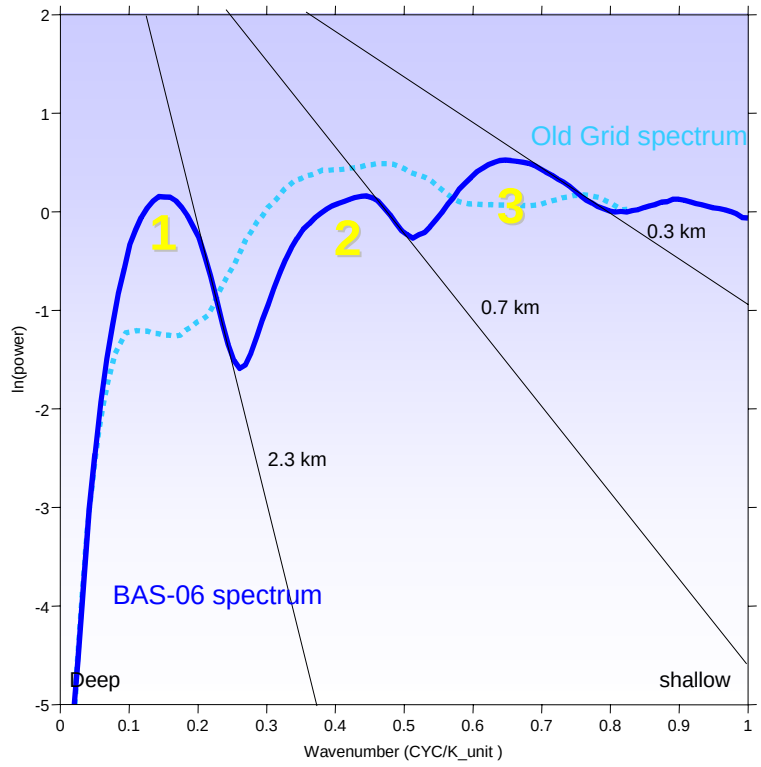

Figure 6.3 Power spectrum analyses of the 2 grids displayed in Fig. 5.6. The curves illustrate the spectral response of the magnetic total field along the same area but of two different grids. There is higher energy power in the BAS-06 at medium to low wavelengths (~high wavenumbers). At low wavenumbers, the peak or the deep null can mean that only the top of a thick magnetic layer is observed (Naidu and Mathew 1998) and the related spectrum cannot characterise the bottom of this layer due to small window size.

Shallow salt is probably the key element, which explains why anomalies are observed on surface. According to Flanagan et al. (1988), the use of magnetics data for mapping salt interfaces is of most benefit with salt features shallower than about 4500 m, owing to small magnetization contrast to be detected. This is the case in the Nordkapp Basin where most of the salt diapirs reach near surface (Figs. 6.2, 6.4)

The magnetic responses due to salt structures in the Nordkapp Basin are usually characterized by small, low amplitude (<4-5 nT), negative magnetic anomalies, where the diapirs reach the near surface (Fig. 6.2). Figs. 6.4 to 6.5 show that a combination of both gravity and magnetic data can provide useful information about the salt diapirs distribution and geometries. Figs. 6.2, 6.8 and 6.9 highlights comparison with seismic data. These responses were identifiable in high-resolution total magnetic intensity aeromagnetic data even for a line-spacing of 2 km. Results from the higher resolution SNAS-06 survey (South Nordkapp Basin 2006, acquired by NGU before BAS-06), shows that the magnetic picture can be improved using higher line-spacing. The 2x6 km specification already provides reasonable and good results both at basin and crustal scale and remains a good compromise for further reinvestigations of the entire Nordkapp Basin.

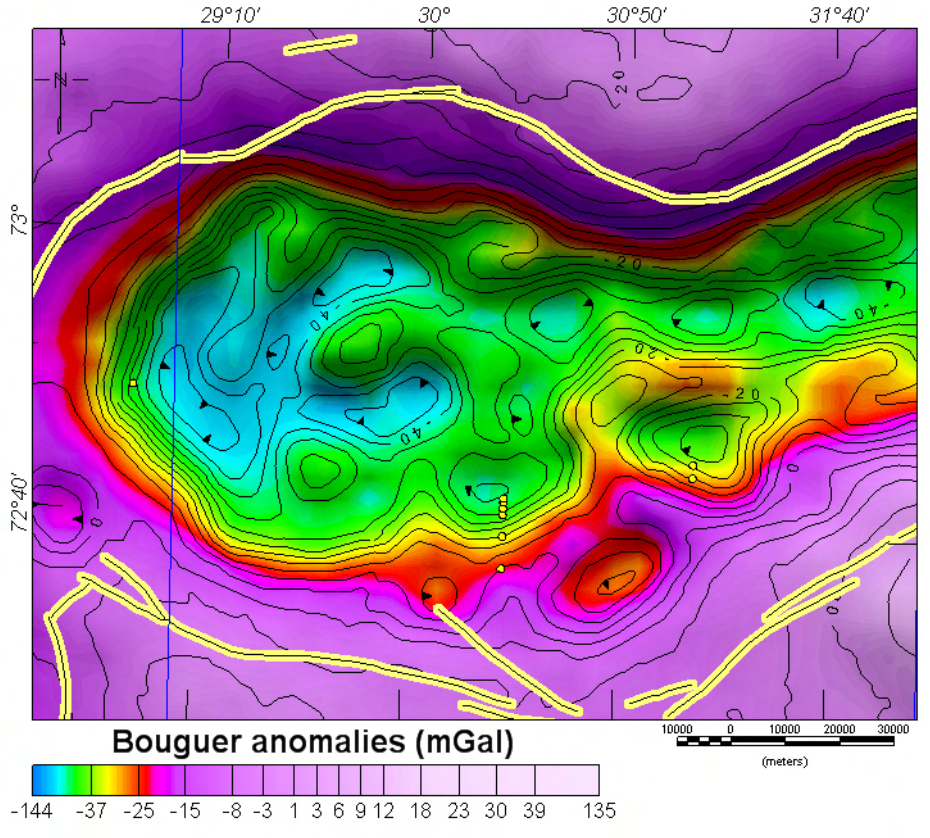

Figure 6.4 Bouguer anomalies (Skilbrei et al., 2000) around the Nordkapp Basin superimposed with their high-pass filter at 30 km. The round-shaped gravity lows usually coincide with salt features observed on seismic lines. Yellow lines represent NPD faults (Gabrielsen et al. 1990). Yellow circles represent the SINTEF Petroleum Research shallow wells.

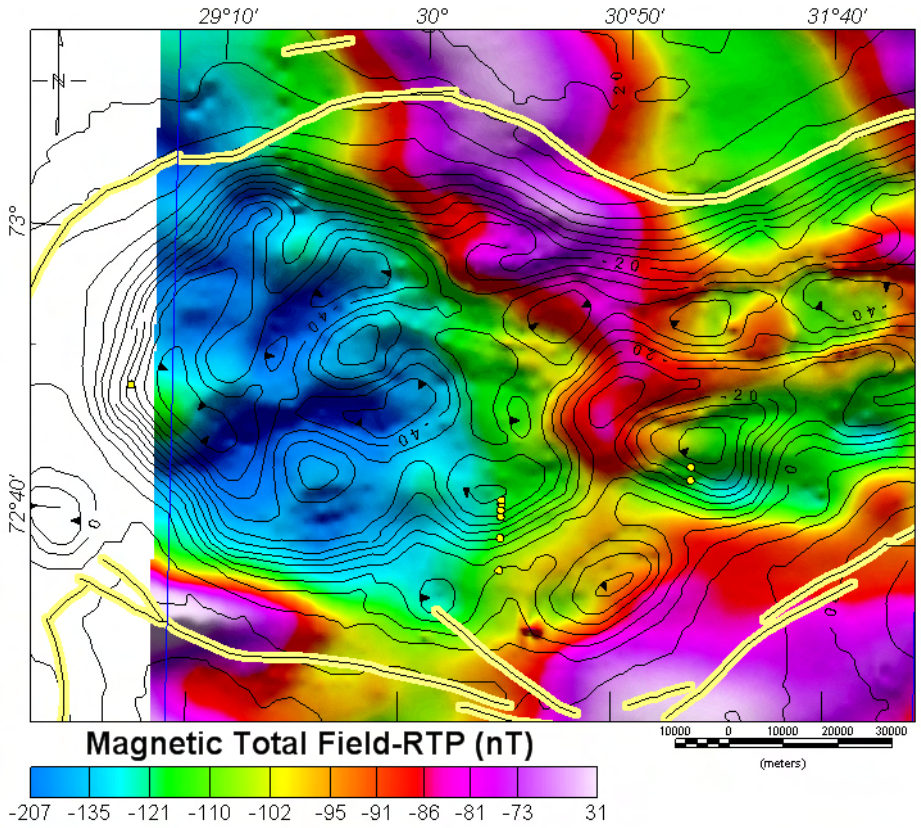

Figure 6.5 Magnetic total field reduced to the pole in the northern Nordkapp Basin. For comparison, the contour of the Bouguer Gravity anomaly (HP-30 km) have been superimposed on the magnetic field.

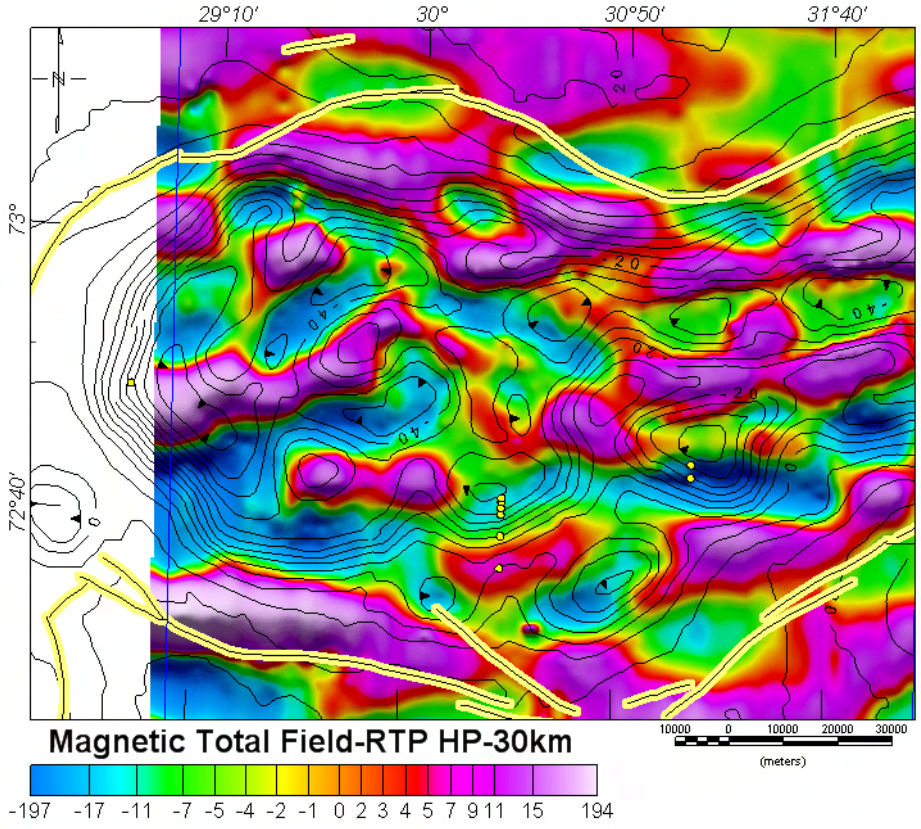

Figure 6.6 High- pass filtering at 30 km of the total field. Features related to salt domes and faults are better depicted. Except for a few elongated anomalies, the magnetic lows fit with the gravity lows.

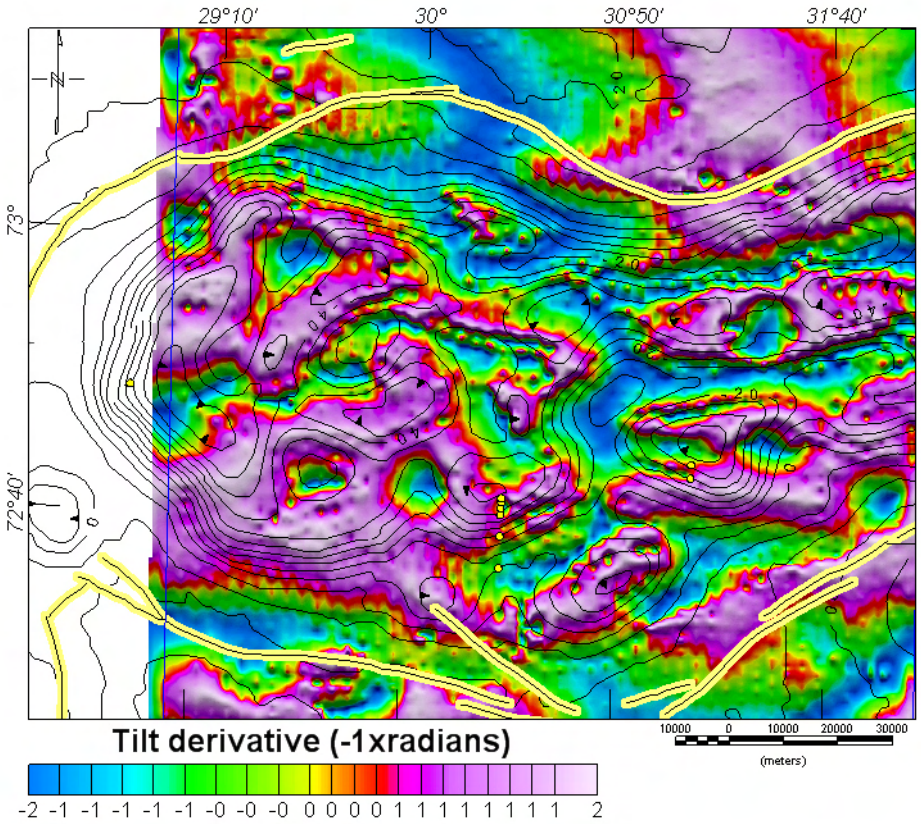

Figure 6.7 Tilt derivative filter of the magnetic field reduced to the pole with surperimposed Bouguer gravity contours.

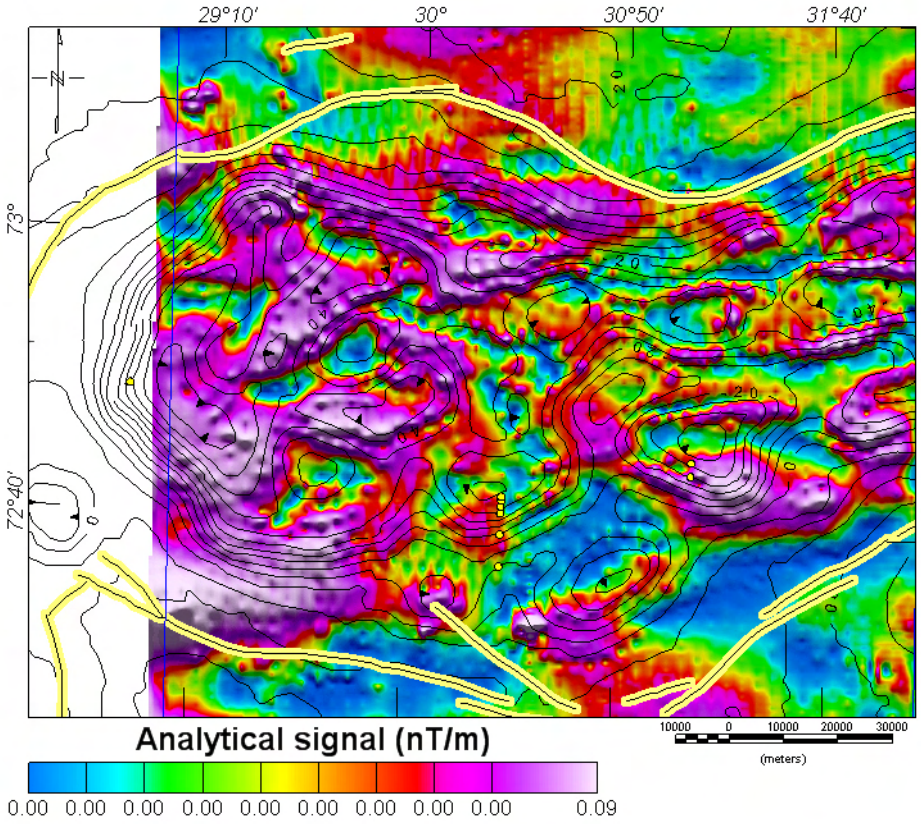

Figure 6.8 Analytic signal of the magnetic field reduced to the pole with superimposed Bouguer gravity contours.

The magnetic total field along the Nordkapp Basin area can be enhanced by a range of linear filtering techniques, which selectively enhances specific anomalies due to one or several types of geological sources (Figs 6.6, 6.7 and 6.8). The dimensions of the domes are very similar to those interpreted from our sparse 2D seismics and the gravity Bouguer lows (Fig. 6.9). High-pass filtering of the data has been used to remove the long wavelengths component of the magnetic total field. High pass filtering with 25 to 30 km cut-off wavelengths allowed us to highlight short wavelength (15-20 km) anomalies mostly linked to salt diapirs (Fig. 6.6). A Good correlation between gravity lows and salts diapirs imaged on seismics can be observed (Fig. 6.10).

After reduction-to-the-pole correction, local misfits between magnetic and gravity anomalies are however, observed. They could represent sub-salt faults or a shift of the main anomalies, due to shape variation between the shallow and deep parts of the diapirs. We also note that the salt features influence the present day bathymetry. Trends, lineaments, and axis deduced from both gravity and magnetic data also coincide locally with bathymetric highs and lows (Fig. 3.8).

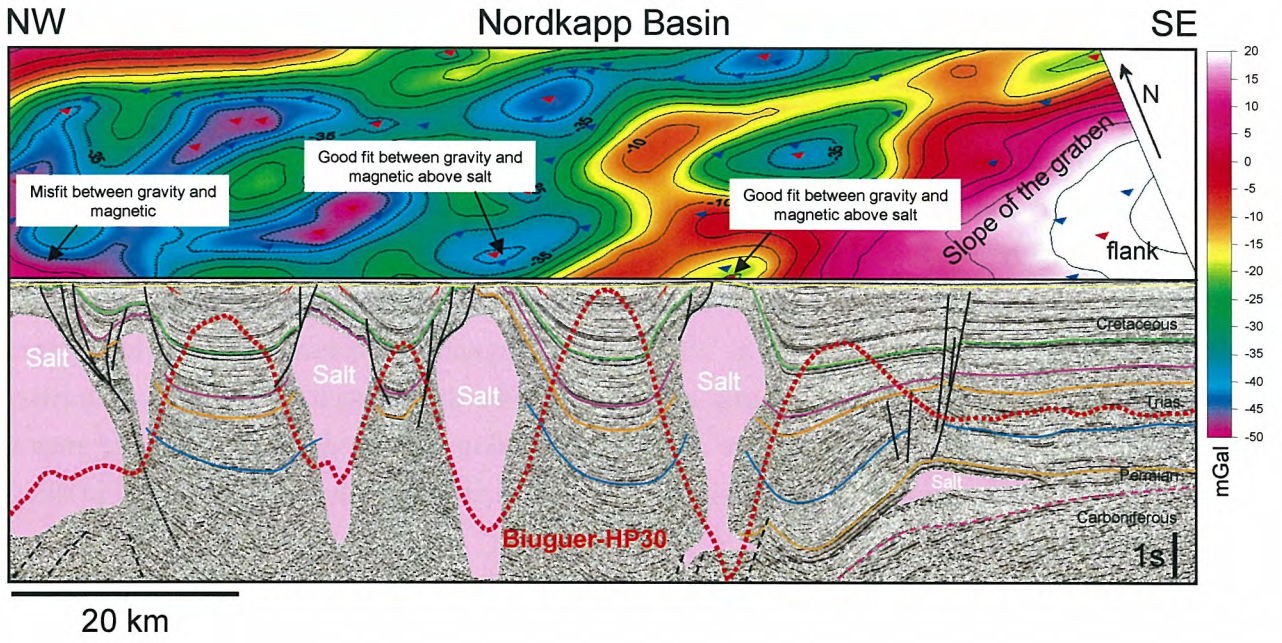

Figure 6.9 Seismic section showing salt diapirs combined with gravity Bouguer anomalies (HP-30 km). A Good correlation can be observed and salt diapirs coincide with clear gravity lows.

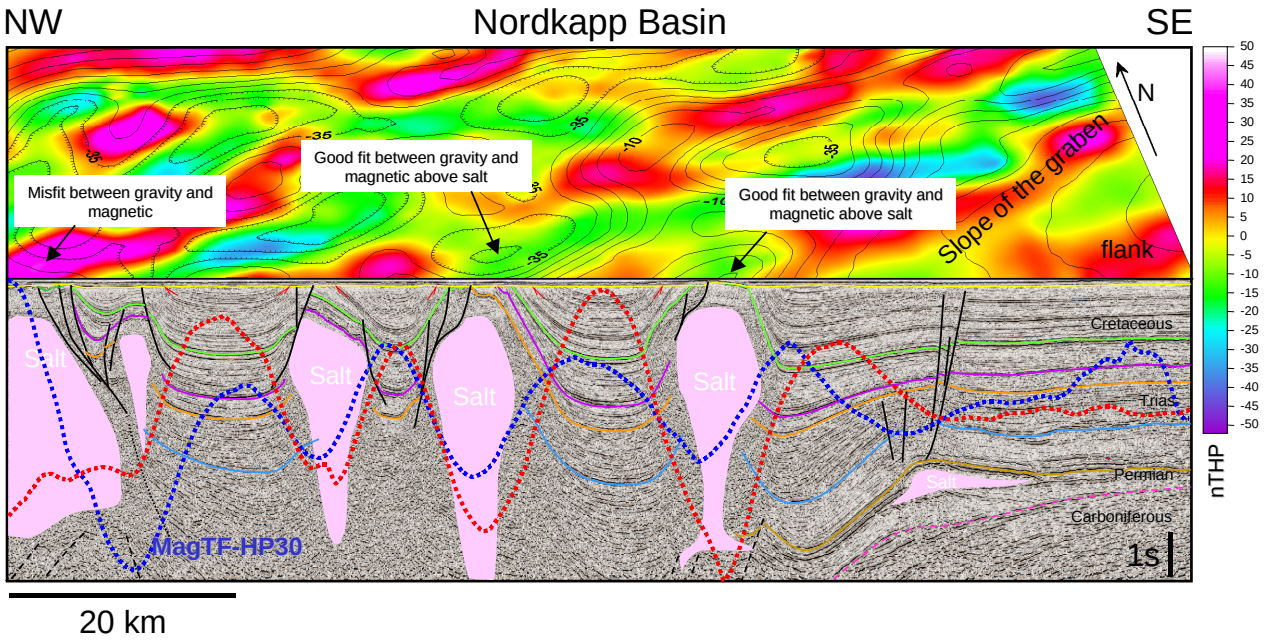

Figure 6.10 The same seismic section showing salt diapirs combined with magnetic anomalies (HP-30 km). A good correlation can be observed and salt diapirs locally coincide with both gravity and magnetic lows. Note, however, that magnetic and gravity lows do not coincide with diapirs in the left part of the section.

The observed magnetic salt response is most likely related to many physical effects. It can be explained by the summation of 1) the negative signal due to the salt body and 2) the positive responses due to the sands and shales, tilted during active and passive diapirism. The lithology of the exhumed and eroded sedimentary section in the Nordkapp Basin consists of minor sandstone, carbonate, shale and salt (Bugge et al. 2002). The magnetic signature of these rock types is dependent on their relative content of iron and especially Fe-oxides such as magnetite (Lauritsen et al., 2007). The lack of shale/sands due to a salt intrusion can produce this specific magnetic susceptibility contrast. Similar magnetic signature and interpretation have been proposed in the Gulf of Mexico (Saad 1993).

The diamagnetism of the salt (halite) is a peculiar form of magnetism. It is the result of changes in the orbital motion of salt electrons in the presence of the externally applied magnetic field. Interaction between the Earth magnetic field and the salt creates an induced magnetic force that changes the centripetal force on salt electrons, causing them to either speed up or slow down in its orbital motion. The induced magnetism opposes the external magnetic field and explains the peculiar magnetic signature of the Nordkapp Basin salt diapirs. In the absence of local susceptibility measurements, we utilized published salt magnetic susceptibility for our magnetic modelling modelling (see Chapter 7). Salt is usually slightly diamagnetic (minor negative susceptibility), but virtually zero or non-magnetic. Salt magnetic susceptibility average equal to -10×10^{-6} SI units or for comparison, an average susceptibility of shale is 640×10^{-6} SI units. Sandstone has exhibited an

average susceptibility of 439 x 10^{-6} SI (Nettleton 1976, Flanagan et al. 1988, Prieto 1993). Bulk magnetic susceptibilities ranges from -12.10^{-6} (SI) to +750. 10^{-6}, exceptionally reaching 14. 10^{-3} (Hrouda et al. 2001).

6.2.2 Lineaments and magnetic foliation

Variation of the magnetic field can be enhanced by further linear and non-linear derivative filtering algorithms which selectively enhances specific trends or outlines one or several geological sources. Along the BAS-06, interesting features appeared after calculation of the total horizontal derivative of the tilt derivative of the magnetic total field, initially reduced to the pole (HDR-TDR-RTP). The HDR-TDR-RTP is independent on the total magnetic field amplitude and is theoretically independent on the geomagnetic inclination and is theoretically successful to define edges of magnetic bodies (Verduzco et al. 2004). Using these filters to highlight magnetic lineaments; trends and foliation appear as linear and/or curvilinear magnetic, edges, minima and maxima in the magnetic field. Along the Nordkapp Basin, terrain slope, analytical signal and other derivatives filters also provided the best images for structural interpretation. A joint interpretation of the magnetic features and lineaments has been realised in detail along this area (Figs. 6.11, 6.12, 6.13, 6.14). The maps illustrate the magnetic lineaments identified with respect to the clarity in which they appear but also, in some cases, involving a judgement regarding the specific geological situation (previously described) and the possible cause of the lineaments around the basin. This includes NS or EW trends of remaining levelling errors as well.

Using HDR-TDR-RTP, curvilinear magnetic features have been identified, digitised and interpreted as shallow to mid-depth lithologic contrasts, which defined the mini-basins deformed and squeezed between the salt diapirs. Locally, symmetry appears in theses trends (Fig. 6.11). They have been interpreted as synforms and antiforms axes of the mini-basins or salt dome themselves. Good correlation between gravity, magnetic and seismic data support locally this interpretation but could not be checked everywhere here due to our poor seismic coverage. Similarly first derivative and terrain slope filters applied to the 30km high-pass magnetic total field also proved to correlate with the main structural axis observed on the seismic data.

Using the TDR and HD-TDR filter, we interpreted several NW-SE lineaments in the Nordkapp Basin. The Euler solution suggested also major alignments including NE-SW, NW-SE and NS trends. The Euler trends do not always follow the dominant NW-SE lineament underlined by the TDR filter (Figs. 6.11, 6.12).

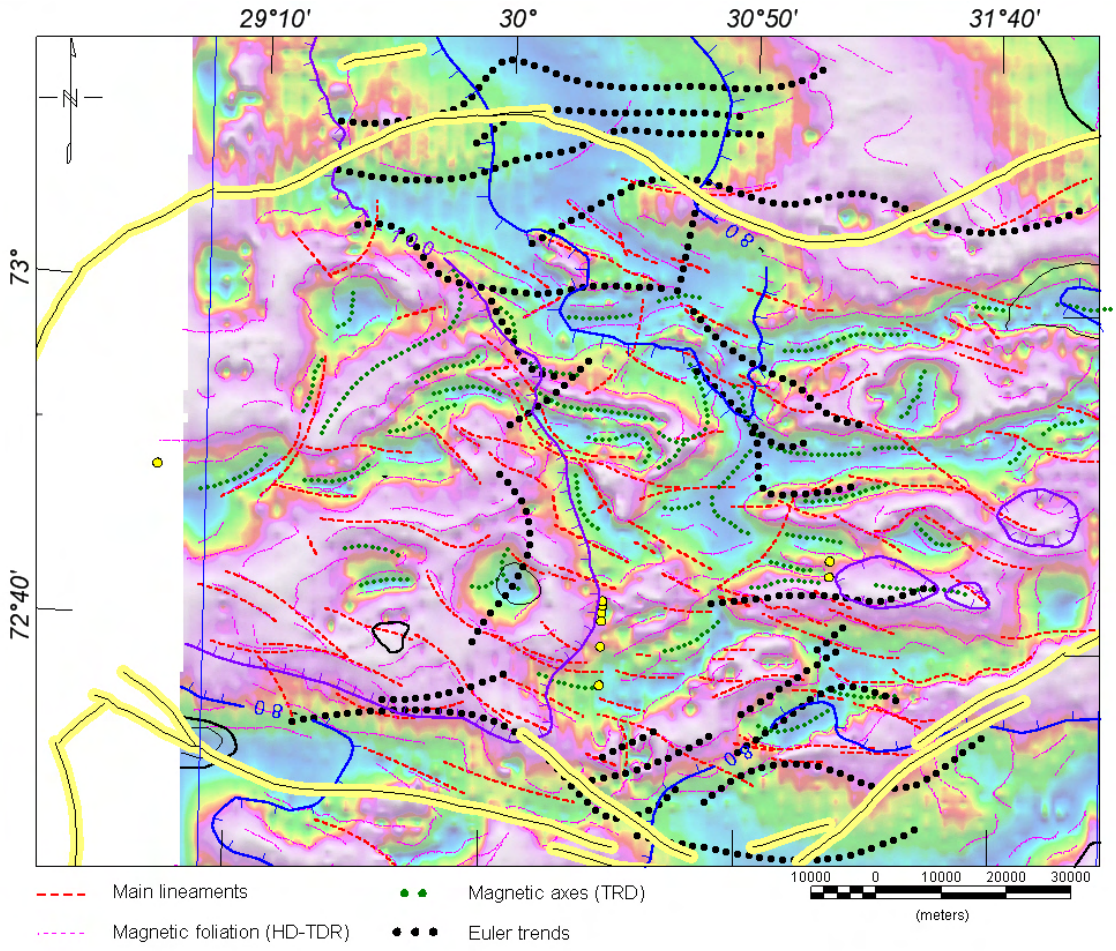

Figure 6.11 Magnetic lineaments and foliation interpreted from the tilt derivative of the magnetic total field (background) and its horizontal derivative (HD-TDR). The contour lines outline the magnetic total field values. Faults outline from NPD (Gabrielsen et al. 1990) and IKU wells depicted in yellow.

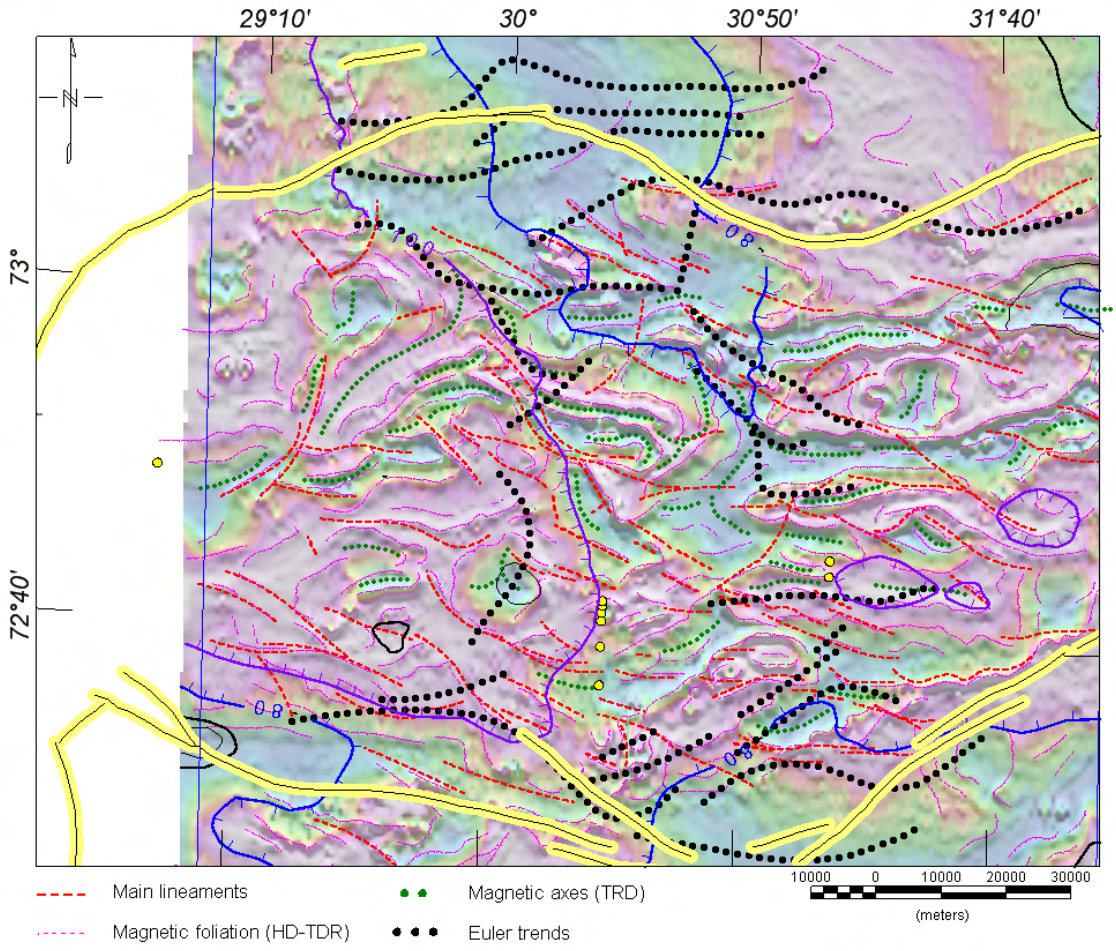

Figure 6.12 Magnetic lineaments and foliation interpretation draped on a composite map including the tilt derivative of the magnetic field and its horizontal derivative.

Lineaments can be related to fracture zones or to rock types with low magnetization and in that sense could be characterized as magnetic connections. It has been pointed out that narrow rock types of low magnetic intensity can be a likely explanation for magnetic foliation. Banded magnetic pattern fits with the general shallow bedrock structures and faults. As a matter of fact, the filters confirm that the surrounding and deformed sedimentary contribute to the total field anomalies due to the rising salt. The rising dome strongly deforms the surrounding sediments and locally the magnetic minimum is related to a magnetic maximum influenced by the dip of the sedimentary layers, dragged towards the salt dome.

The curvilinear magnetic pattern, associated with the salt domes are locally disrupted by the NW-SE linear trends, interpreted as faults, transfer zones and complex relay and branching patterns of salt domes and walls. Usually, relay patterns also fit with gravity lineaments and form where one salt body dies out along strike and one or more neighbouring walls or diapirs rise.

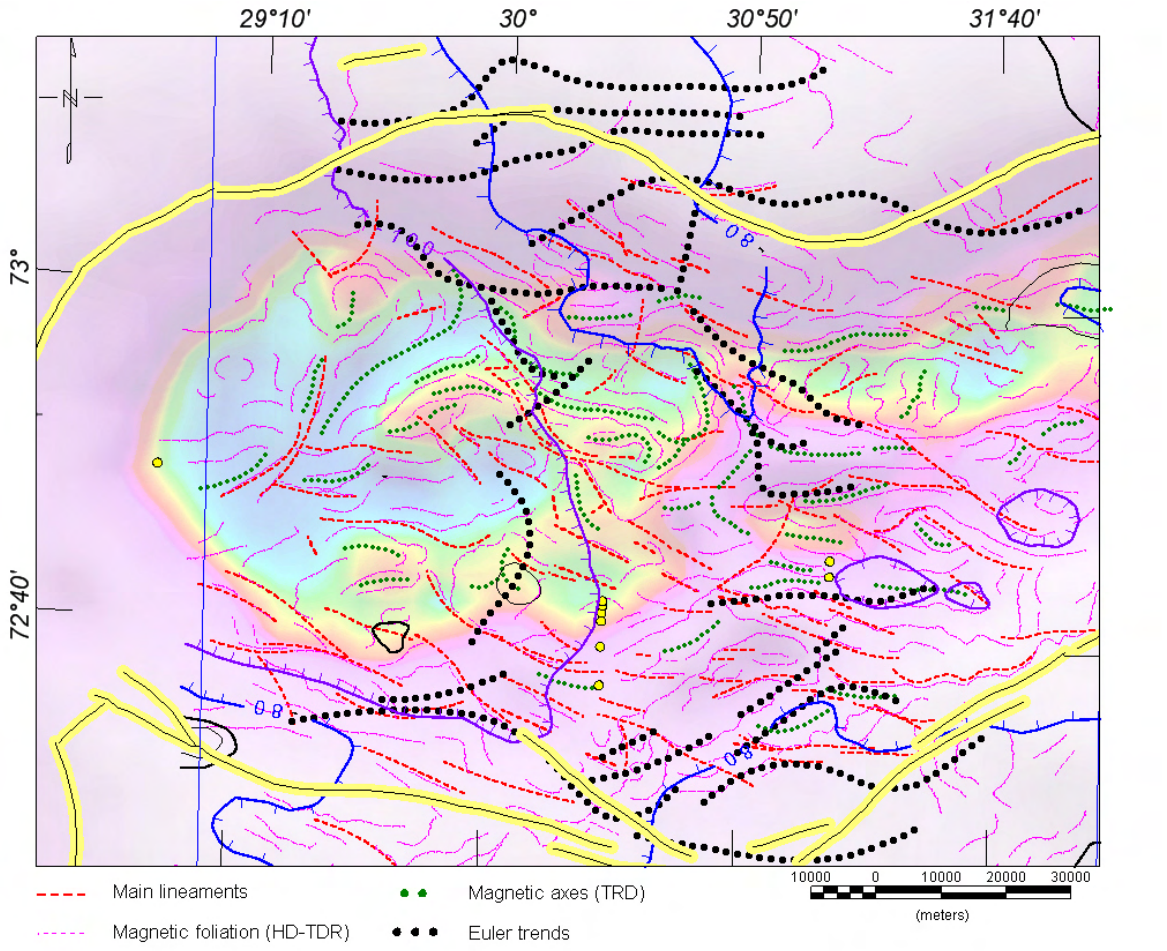

Figure 6.13 Magnetic lineaments and magnetic foliation draped on Bouguer anomalies. The black dashed lines represent the major lineaments underlined by the Euler solutions.

6.2.3 Strike and dip of the dragged sediments

We also find interesting comparisons between seismic data and the tilt derivative filtered versions of the magnetic total field RTP (TDR-RTP). Location of the salt dome, intra-salt basin and the symmetry/asymmetric nature of the structural features can be investigated with this technique. A long wavelength version of the TDR-RTP coincides with the salt dome and an asymmetry of the TDR-RTP signal coincides with similar structural asymmetry observed on seismics (Figs. 6.14, 6.15). When using the slope of the TDR-RTP and a vector flow map of the TDR-RTP, we can conclude and observed, that the vector flow maps of the tilt derivative could locally fit pretty well with the strike, dip and steepness of the sedimentary layers, dragged by the salt. This is useful to constrain the geometry of the mini-basins that are squeezed between salt domes. More correlation with seismics should confirm this hypothesis, but comparison with our sparse seismic database is already quite convincing (Fig. 6.15).

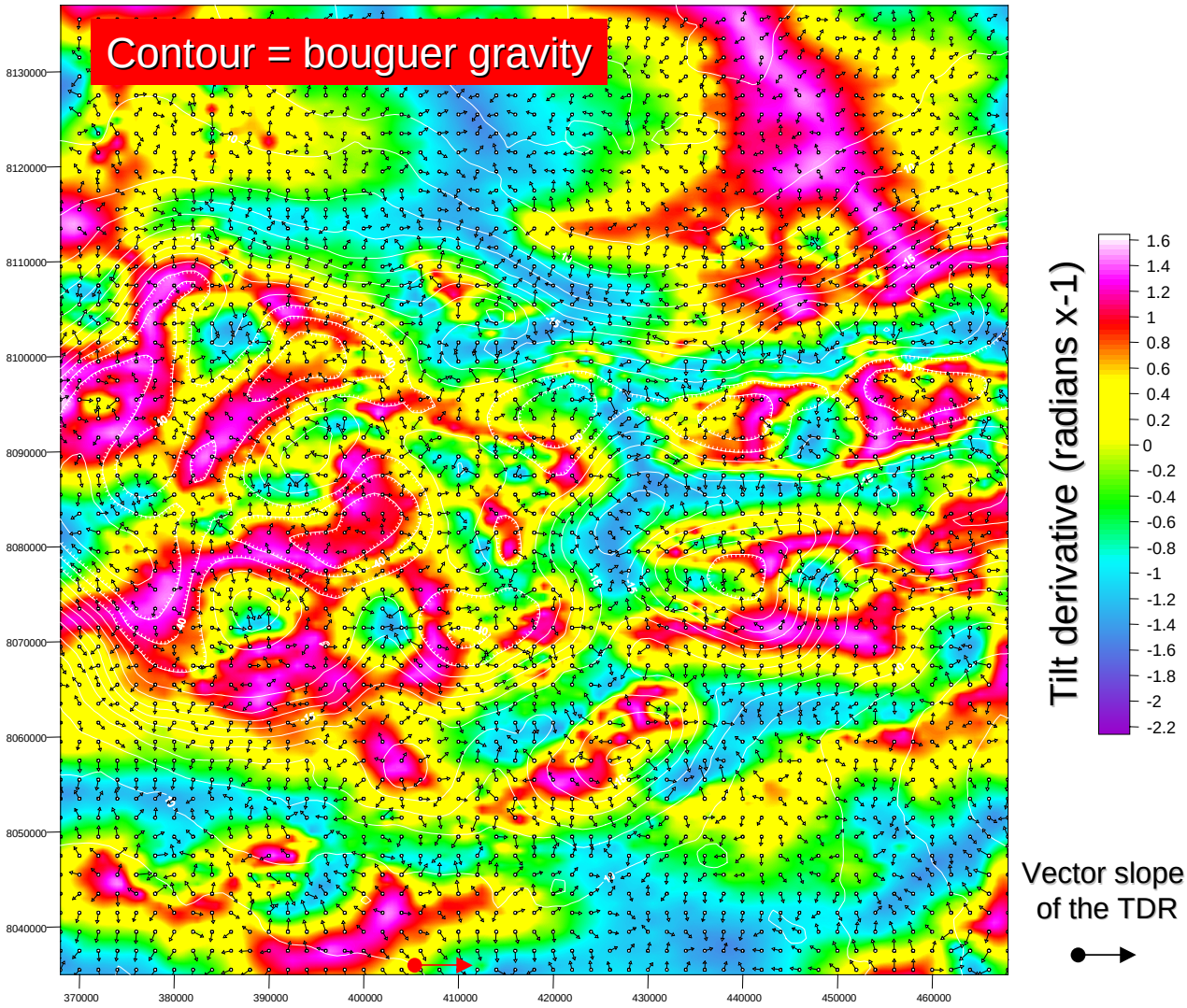

Figure 6.14 Tilt derivative of the magnetic field (TDR) and vector slope of the TDR. The arrow symbol points in the downhill direction and the length of the arrow depend on the magnitude, or steepness, of the TDR slope. This kind of map can provide structural indication about the geometry of the sedimentary strata deformed by the salt diapirs.

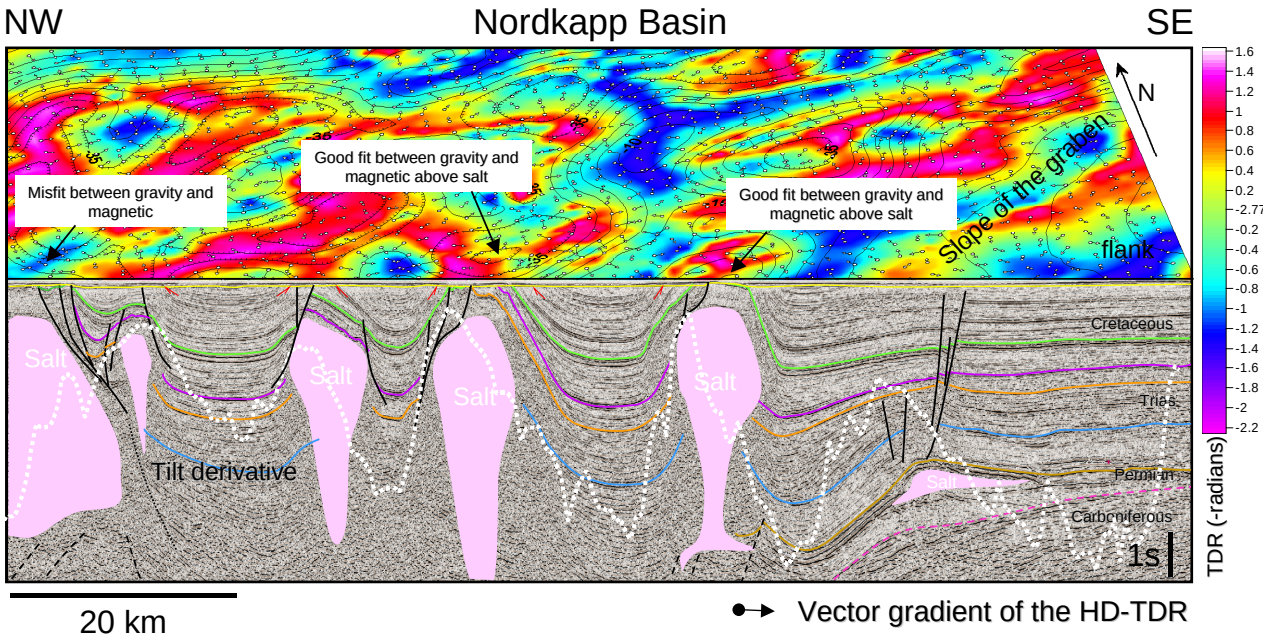

Figure 6.15 Seismic section combined with the tilt derivative of the total magnetic field. The tilt variation fits pretty well with the strike, dip symmetry and steepness of the sedimentary layers dragged by the salt. Contours represent the Bouguer anomalies (HP-30 km).

6.2.4 Overhanging of salt diapirs

Most often, subsalt seismic imaging does not allow us to fully appreciate the real shape of the salt diapirs at depth. Magnetic data can be useful as an independent indicator of salt overhang (Fig. 6.16). However, there are few papers about the magnetic interpretation of salt overhang and the magnetic implication to solve this kind of problem and to our knowledge it remains an interesting but complex open question. Saad (1993) suggested that a magnetic anomaly of the salt dome is usually sharper than the gravity anomaly and that is usually centred over the shallowest part of the salt mass (Fig. 6.16 and 6.17). Conversely, the gravity anomaly can be broader and has its centroid located over the center of the total salt mass, including consequently a deeper effect. If the magnetic signature is not affected by magnetic side effects, an offset between the magnetic and gravity anomaly axes could indicate that the shallow salt is not coincident with the centre of the salt mass. A significant implication could be that the shallow salt dome overhangs are offset from the central stock. Therefore comparison between gravity and magnetic data could be useful to get a rough interpretation of the overhang geometry associated with salt diapirs. Fig. 6.17 illustrates how the 3D salt configuration could produce different gravity and magnetic responses.

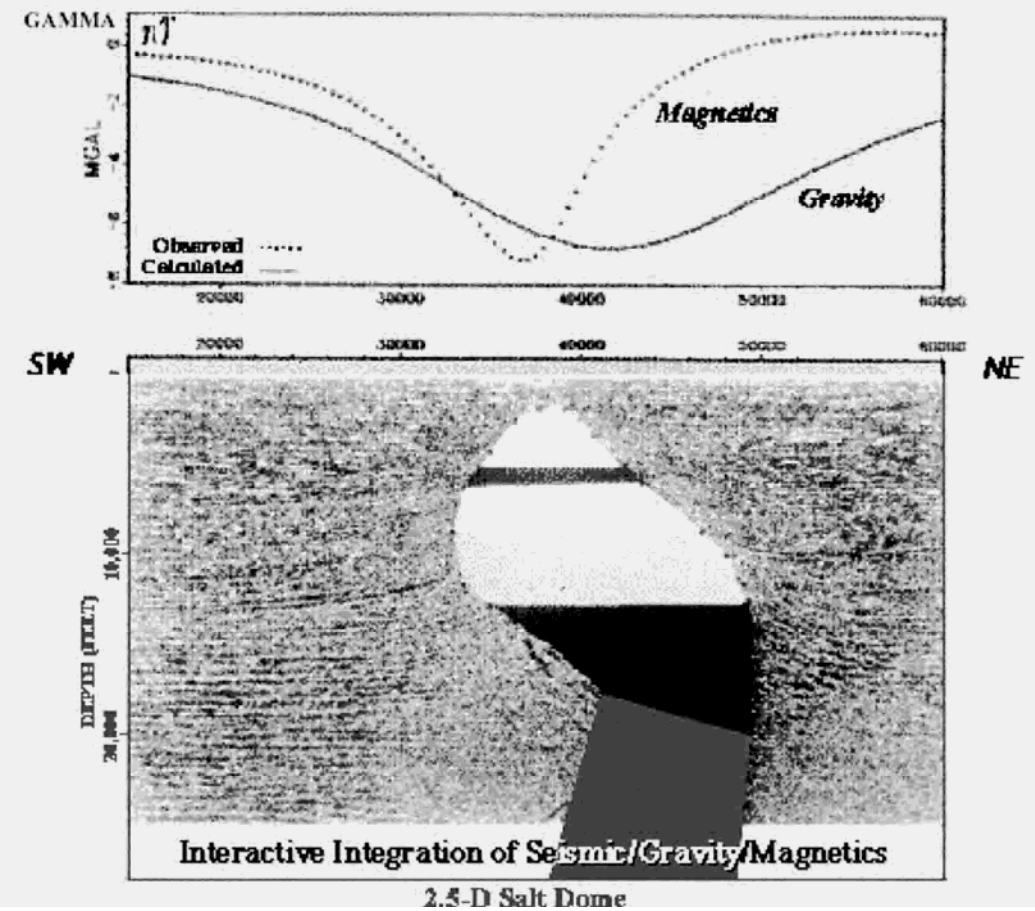

Figure 6.16 Salt overhang model and potential field responses (Saad 1993).

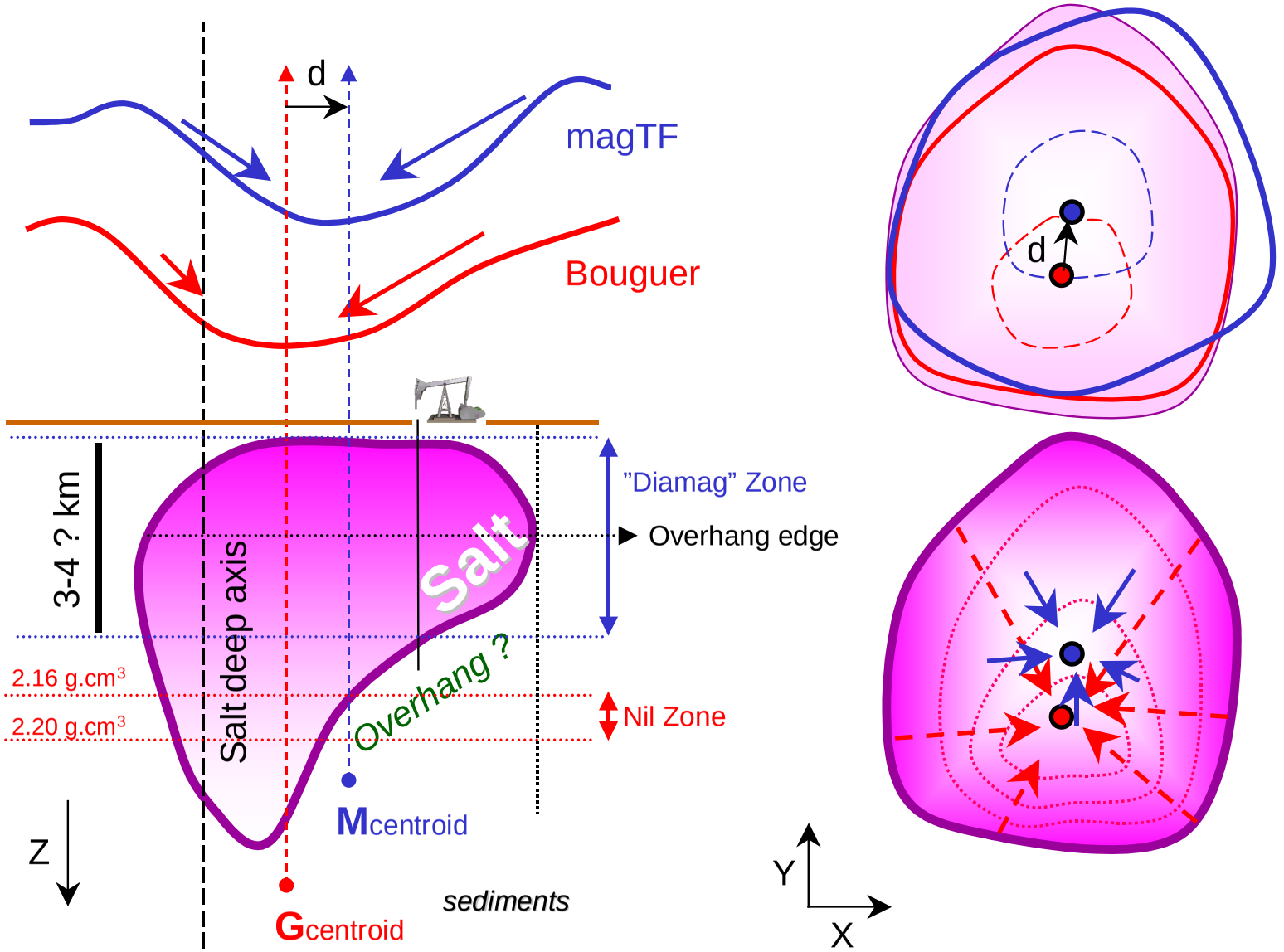

Figures 6.17 Salt with overhang geometry and expected gravity and magnetic signatures. The distribution of the gravity and magnetic centroids points (in 2D map projection) could constrain the orientation of potential overhands and salt overlaps for specific and simple cases.

Differences between the centroids point (in 2D map projection) of the gravity ($G_{centroid}$) and magnetic ($M_{centroid}$) anomalies due to salt diapirs can be used to aid in the identification of overhanging salt features, independently of the seismic data (Saad 1993). Gravity and magnetics can support interpretation of salt overhang and steep flanks, and can differentiate between rooted and non-rooted salt (Fig. 6.17).

The respective positions and differences between the $G_{centroid}$ and the $M_{centroid}$ points could precise the orientation and geometry of the overhangs. An increasing distance between G_{apex} and the M_{apex} can approximate the relative amount of salt overlapping the sediment. Similarly, comparison between gravity and magnetic axis also provides further particulars on the salt structure. An offset between G_{apex} and the M_{apex} can often be readily observed on both maps and profiles and can be used as a rough but first indication of overhangs.
To illustrate these differences $G_{centroid}$ and the $M_{centroid}$ have been calculated directly from the magnetic (total field RTP+ HP30 km) and gravity grids (Bouguer HP-50 km) using an inverse peak finding methods. Both gravity and magnetic grids have first been multiplied by -1 and the Geosoft peak-finding routine was run to find the deflection of adjacents inflection points automatically detected inside a moving window (Montaj Grav/Mag Interpretation manual, Geosoft 2005). These solutions indicate the location of the $G_{centroid}$ and the $M_{centroid}$ points, plotted on the map (Fig. 6.18).

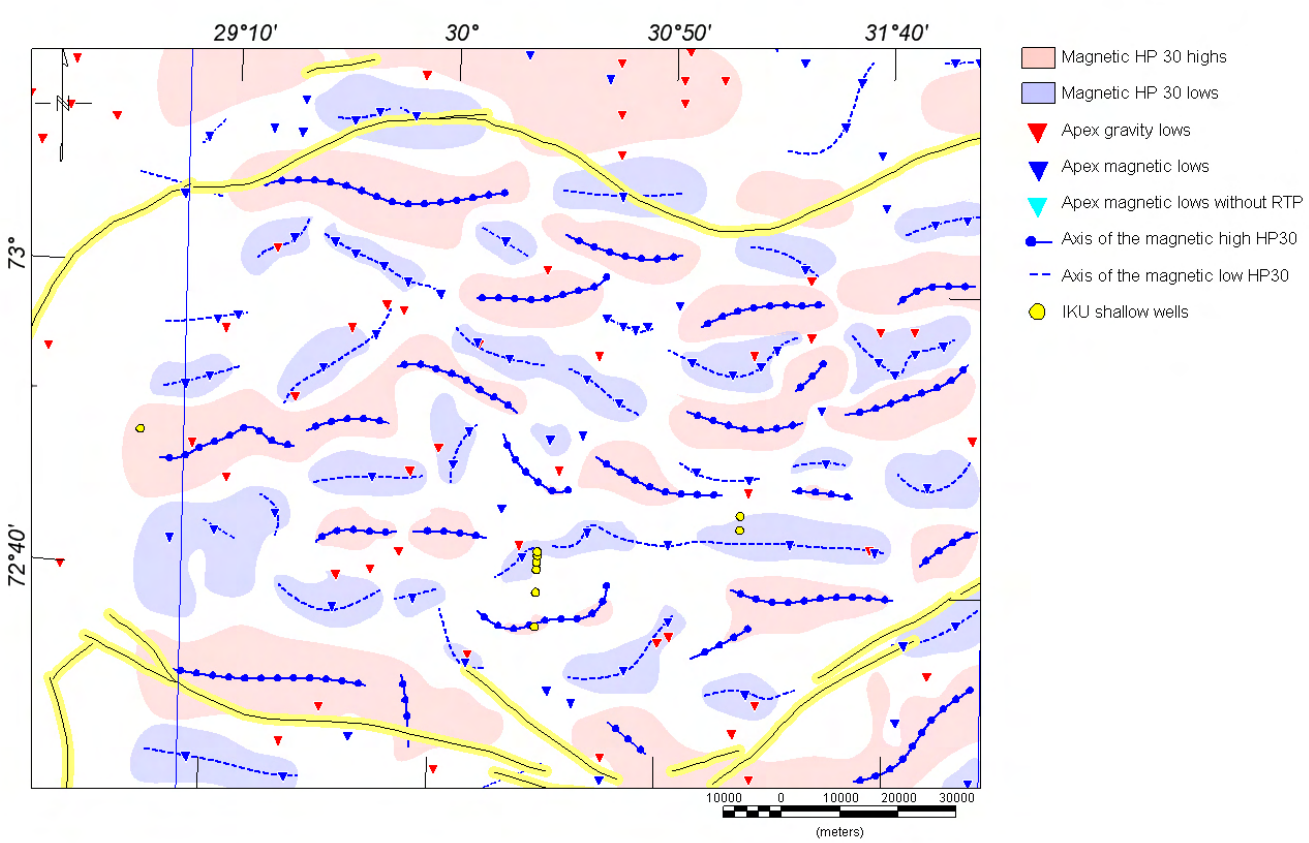

Figure 6.18 Main contours, trends and central apex and of the magnetic anomalies processed with a 30 km high pass filtering.

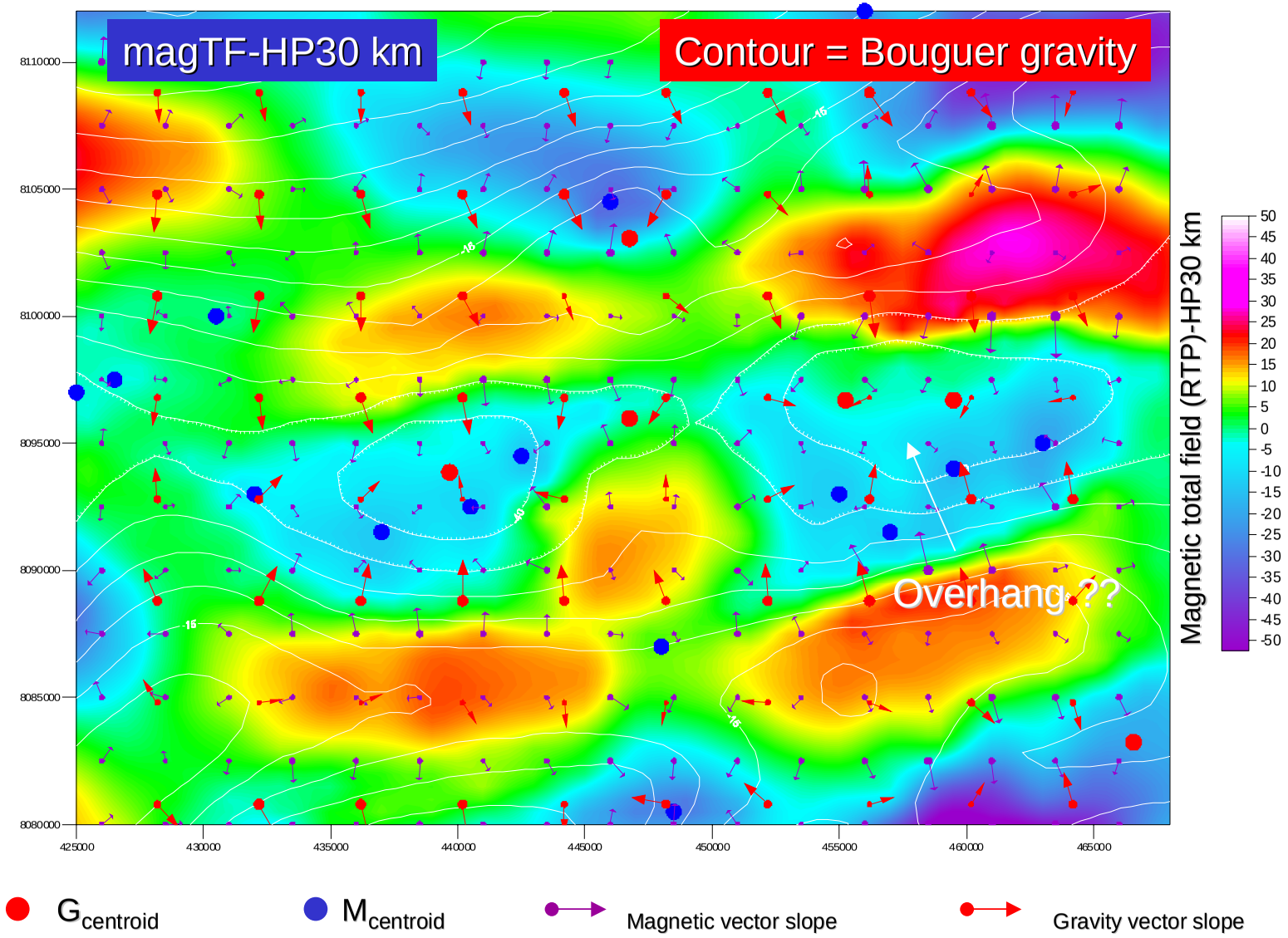

Figure 6.19 Example of magnetic and gravity centroids and slopes in the eastern part of the Nordkapp Basin. Local shifts between the gravity and magnetic centroids could indicate the presence of overhang.

A vector map of the gravity and magnetic field illustrates the gravity and magnetic flows toward G_{apex} and the M_{apex} (Fig. 6.19). Using vector flow map information, direction and magnitude of both gravity and magnetic data can be derived from the two grids. Gravity and magnetic vectors are drawn at each resampled grid node and illustrate the gravity and magnetic distribution around salt domes. Arrow symbol points in the "downhill" direction and the length of the arrow depend on the magnitude or steepness of the slope. A vector is drawn at each grid nodes. Changes in direction and steepness can provide information about the geometry and distribution of mass and magnetic susceptibility around the salt diapirs. Dissymmetry of the gravity and magnetic slopes could indicate dissymmetry of the salt diapirs.

However, the idea initially suggested by Saad (1993) is probably more complex and should only work if the salt reaches the surface and if the surrounding sediments are relatively similar with no significant lateral susceptibility contrasts. Furthermore, the magnetic signature of the salt structures is not only influenced by the diamagnetism of the salt itself but also by the structural dip and the susceptibilities of surrounding sediments. The geometry of the sedimentary rocks overlapping the salt dome could influence the location of the centroid, which can be shifted from the real diamagnetic centroid. To get good results, the main diamagnetic source region, in this study defined as the "diamag zone" should be located above the maximum edge of the overhang and the gravity source region should be deeper and cross over the Nil zone (zone where both sedimentary rocks and salt have a similar density) (Fig. 6.17). We expect some complexities if the centroid of the diamag source region is deeper than the maximum edge of the overhang. The top of the diamag zone is obviously shallow but the meaning of its depth is not so well understood. More investigations are required to better define and understand the concept of diamag zone and its relationships with overhang structures.

Consequently, interpretation of the shifts between $G_{centroid}$ and the $M_{centroid}$ must be apprehended carefully and should be quantified in a second modelling step. At that stage, some uncertainties and open questions remain and should be better investigated to refine the level of detail. One of the major problems in this project was certainly the lack of seismic lines properly located to constrain the salt geometry. Sparse information about sediment susceptibility is also a limiting factor.

There is also some uncertainties about the $G_{centroid}$. Usually, salt dome intruding sedimentary rocks produces a gravity low. Gravity modelling performed by Prieto (1993) illustrates this effect at various depths. Prieto (1993) shows that the salt column at depth produced a broad negative anomaly, increasing in amplitude and frequency with shallower

levels (Fig. 6.20).

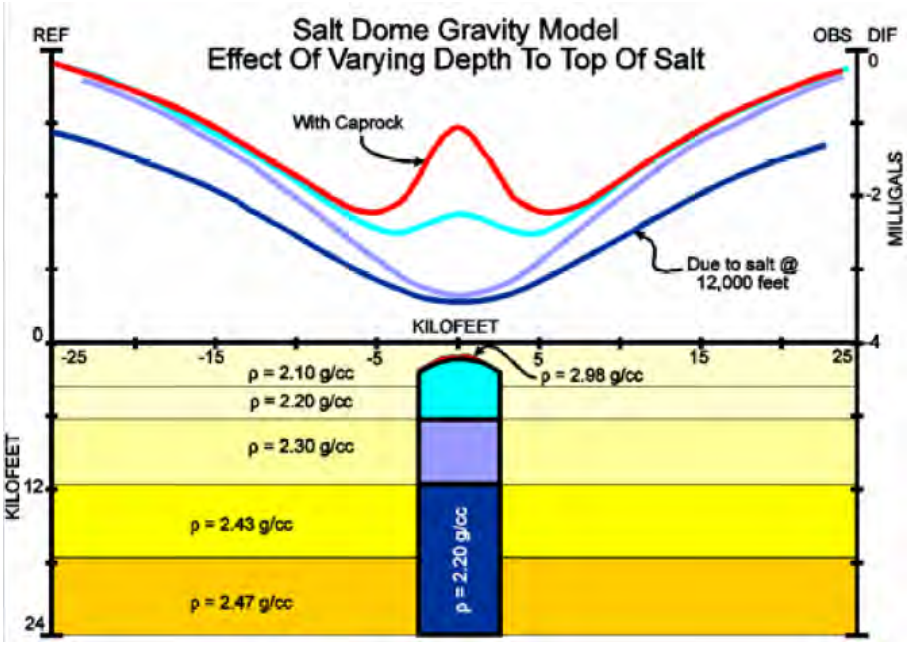

Figure 6.20 Gravity anomaly produced by a salt dome at various depths (Prieto 1993).

For most of the anomalies, the centroid of the gravity signature coincides with the apex of the salt mass. Nevertheless, complex interaction between the salt and the Nil zone can change this standart case. The Nil zone (Bain et al. 1993, Prieto 1993) is the area at depth where salt and sediments have the same density (2.16-2.2 $g.cm^{-3}$). Prieto (1993) demonstrates that if the salt moves above a shallow Nil zone, a positive gravity anomaly is generated and superimposed on the broader negative anomalies due to the deeper negative density contrast. This kind of perturbation of the gravity field can shift the location of the $G_{apex,}$ leading to misinterpretation of the salt geometry if seismics are not involved in the interpreation.

We would also point out that the $G_{centroid}$ versus $M_{centroid}$ approach should only work if vertical density variation exists beneath the maximum edge of the overhang as illustrated on Fig. 6.17. If the Nil Zone starts at that level and if the base salt does not extend to greater depths, it should be difficult to detect any overhangs using the G_{apex} versus M_{apex} technique. Fortunately, the salt diapirs and walls, observed in the Nordkapp Basin are deeply rooted and certainly cross over the Nil zone to the deeper parts of the basin.

Finally the resolution and quality of both gravity and magnetic grids are also limiting factors.

7 2¾D-GRAVITY AND MAGNETIC MODELLING ALONG TRANSECT

Laura Marello and Laurent Gernigon

7.1 Introduction: using potential field to define crustal architecture

The depth to basement along the BAS-06 is investigated in this section. The Salt imaging problem in the Nordkapp Basin does not allow to clearly identify the top basement and the potential geometry of overhang features. We used potential field data to investigate the basin geometry and the maximum depth of the crystalline basement along selected transects across the BAS-06 survey (Fig. 7.1)

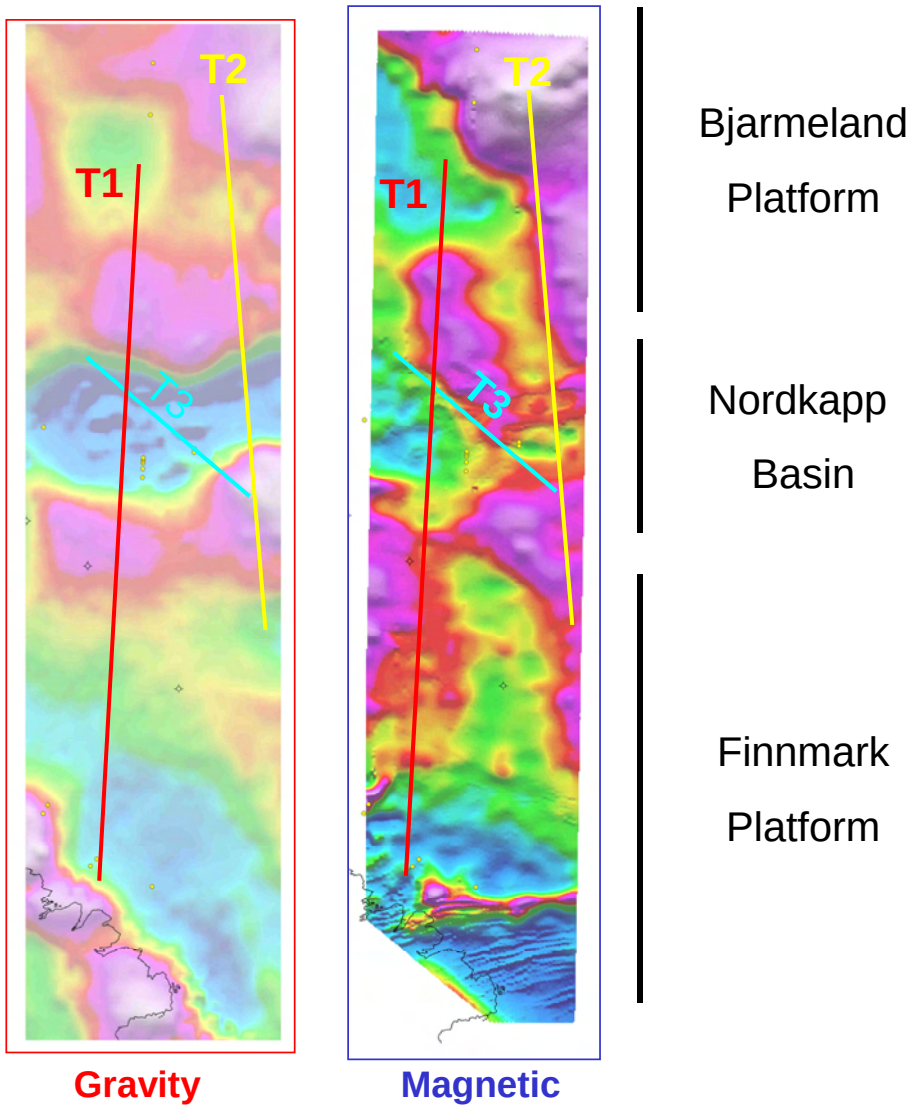

Figure 7.1 Bouguer gravity map (left) and magnetic map (right). The solid lines show three modelled transects (T1, T2, T3).

The 2¾D modelling has been carried out using the commercial software GM-SYS Montaj. GM-SYS is an interactive 2¾D gravity and magnetic modelling program using a method of summing irregular polygons modified after Talwani (1973). With the 2¾D approach, the structures (bodies) of varying and limited extent, both laterally and perpendicularly to the line, in front of and behind the plane of the profile may be defined, and their effect included in the calculated anomaly.

Seismic transects have first been depth-converted using the software Easydepth^{TM} from Beicip-franlab. Regional interval velocities have been used (Table 7.1) and interpolated with well data when possible. The depth-converted SEG-Y files have been imported as background in GM-SYS. Since no wide-angle data are currently available along the selected transects, Moho and top basement geometries have been used as initial crustal constraints derived from a pre-existing but coarse regional compilation [Barents 50 from Ritzmann et al. (2007) and former NGU top basement compilation of the Barents Sea (Skilbrei et al. 1993)]. More informations can be found at http://www.norsar.no/seismology/barents3d/. Moho and top basement grids (Geosoft format) for the BAS-06 survey area are provided on the archive DVD.

Forward modelling allowed us to refine and adjust as much as possible the initial geometry. The 2¾D gravity-magnetic modelling attempted to test the validity and uniqueness of the seismic interpretation, the latter of which more accurately locates interface depths and geometry, model layer boundaries were left unaltered.
Minor adjustments of the boundary between sedimentary strata and salt bodies were required to generate a gravity anomaly, that matched the observed data.

The model was built in different steps including. 1) the definition of the 2D crustal geometry, 2) the lateral and perpendicular extension of the main horizons to infinity in order to reduce the edge effects, 3) the definition of the appropriate density and susceptibility values and 4) the forward modelling interaction.

No direct density and susceptibility measurements were available for this study. Densities along the transects have been determined using the mean of seismic velocities used for depth conversion. We associate to every interval of velocities a density using the Nafe-Drake relation a velocity-density function (Nafe and Drake 1957, Ludwig et al. 1970) defined by a fifth-order polynomial equation:

$$\text{DENSITY}(g/cm3) = 1.6612Vp - 0.4721Vp^2 + 0.0671Vp^3 - 0.0043Vp^4 + 0.000106Vp^5.$$

This relationship for sedimentary and crystalline rocks is widely accepted as a standard for sedimentary basins (Brocher 2005). The average density for each polygon can then be calculated from the interval velocities. Top basement and Moho usually coincide with the main density contrasts in the lithosphere. We assumed a constant density for the basement, without density increment. In agreement with Martinec (1994), we chose a density of 3100 kg m^{-3} value for the mantle, which resulted in a density contrast between basement and mantle of 350 kg m^{-3}.

Gardner et al. (1974) suggest that the densities of salt vary between 2000 to 2200 kg m^{-3} while Jackson & Talbot (1986) suggest a density range between the density 2150 to 2200 kg m^{-3}. Jackson and Talbot (1986) and Bain et al. (1993) also suggest that salt tends to decrease slightly with increasing depth, as the salt volume increases faster with increasing temperature than it contracts from the increase of overburden pressure. For the modelling purpose, a constant density value has been considered for the salt diapirs.

For susceptibility parameters, we used previous compilations that define the ranges for various rock types (Dobrin & Savit 1988, Clark 1997, Musset et al. 2000). Assuming well information (e.g. 7229/11-1) and recent paleogeographic models (Larsen et al. 2005, Worsley 2006), we associate the stratigraphy with the most appropriate and representative parameters (Table 7.1). We define remanent magnetization only for the basement with an inversion routine. We consider its component along the Earth's present magnetic field since we assume a viscous remanence.

The magnetic modelling was used to investigate the lateral variation of the physical basement characteristics that produce long wavelength anomalies. Being aware of potential 3D (border) effects, we believed that using unconstrained magnetic modelling to fit the short wavelengths anomalies would be too speculative and subject to misinterpretation. Nevertheless, the sections could be updated if multi-2D interpretation of the survey area is carried out later.
The geometry of the three transects defines 13 bodies including a water layer, 9 sedimentary strata (Carboniferous to Plio-Pleistocene), salt diapirs, basement and mantle. The densities of the layers from Early Triassic to Late Jurassic were adjusted from the initial values (<200 kg m^{-3}) to generate a Bouguer gravity anomaly that matched the observed data. Table 7.1 shows the nomenclature of the modelled bodies, the adapted age the mean seismic velocity, density and susceptibility.

Layer	Time	Seismic velocity (m/stwt)	Density (Kg m^{-3})	Susceptibility (SI)	Remanence mA/m
water			2200		
Nordland	(Plio-Pleistocene)	1900	1900	0.00056	
Adventdalen	Cretaceous	2200	2050	0.00052	
Hekkingen	Latest Jurassic/Early Cretaceous	2690	2200	0.00040	
Fulgen	Late Mid. Jurassic	2600	2150-2175	0.00065	
Sassendalen	Mid Triassic	3500	2300-2550	0.00065	
Intra-Lower Trias	Base Anisian	3850	2400-2550	0.00065	
Bjarmeland	Early Trias-Early Permian	4425	2450-2575	0.00029	
Gipsdalen	Early Permian	5250	2600	0.00094	
salt	Carboniferous-Early Permian	4500	2150	-0.00001	
Carboniferous	Carboniferous- Older sediments	5750	2650	0.0001	
basement		(?)	2750	***	0.02
mantle		(?)	3100		

*Table 7.1. Summary of physical parameters used in the potential field modelling. The colors refer to the International Stratigraphic Geological Chart (http://www.stratigraphy.org/). ***: basement susceptibilities defined by inversion of the aeromagnetic data.*

7.2 T1: First transect

The first transect runs north-south from the Finnmark Platform to the Bjarmeland Platform and crosses the Nordkapp Basin (Fig. 7.2). This transect is well constrained by the well 7229/11-1 and is the longest transect that we modelled (350 km).

The long wavelengths of the gravimetric and magnetic anomaly fields show good correlations in the central area of the section. However, in the northern part of the transect,

the two curves do not fit so well. The gravity anomaly values are positive and show a maximum while the magnetic field on the other hand is dominated by high and low values. The minimum gravity anomaly is dominated by an asymmetry and a shorter wavelength variation with its minima corresponding with the salt bodies. The fields in the Finnmark Platform are dominated by both high gravity and magnetic anomalies that decrease in the southern direction. This variation is smoother for the gravity more evident for the magnetic anomaly.

Trial and error adjustments of the initial 2¾-D model have been tested. We investigate the most reliable geometry of the Nordkapp Basin and surrounding areas. When the final geometry was defined, we used the magnetic total field to investigate lateral variation of the susceptibilities.

First, we tested the Moho geometry in order to adjust the long wavelength anomalies. Our final modelled Moho differed from the Ritzmann et al. (2007) Moho but not by more than 2 km, which is in the possible range of error for the model. The model shows a deeper Moho in the Finnmark and Bjarmeland Platforms and a shallow Moho (at 25 km) below the Nordkapp Basin.

In a second step, we investigated the basement geometry; the final results suggest a half-graben architecture of the Nordkapp Basin. A quite smooth basement at a depth of about 8 km dominates the Bjarmeland Platform. The deeper basement is observed in the Nordkapp Basin. The base of the graben locally reaches 15.5 km. In the southern part, the top basement lies between 5 and 8 km below the Finnmark Platform and the basement depth is reduced to values of 500 m, close to the coastline. Along the margins of the Nordkapp Basin, major crustal faults intersect the sedimentary strata, and are continuous down to a depth of 10 km. On the Finnmark Platform, the sedimentary strata are truncated and sub-crop in the southernmost part of the transect.

In the Nordkapp Basin, we refined 3 salt bodies which coincide with short wavelengths gravity lows; the salt diapir in the northern part is the most voluminous with thickness around 11.5 km, and a width of 13 km. The other two salt bodies have the same height but are narrow with widths around 5 to 6 km.

The density contrasts of the shallows bodies influence the short wavelength anomalies. Between salt and sediments, the contrast (300 kg/m^3) in our initial model was not sufficient to reproduce the observed anomaly. To explain the short wavelengths anomalies, the density of the Early Permian to Early Cretaceous layers has been slightly increased. This

increment of density contrast produces an improved fit to the observed gravity anomaly field and is reasonable in consideration of the lithostatic effect due to a deeper burial of the sedimentary rocks.

These final models produce a good fit between the observed and calculated gravity field, with an average error of 2.91 mGal. In the northern part of the transect, the gravity field is the effect of a more shallow basement. In the Nordkapp Basin the main minimum is dominated by an asymmetry of the gravity field that is indicating an asymmetric graben structure. The minimum of the shorter wavelengths are linked with the salt bodies. In the Finnmark Platform the lower gravity is a consequence of the deepening of the Moho.

To improve the fit to the observed magnetic anomaly, the basement has been split into three parts. The inversion of the susceptibility parameter in the basement suggests higher values in the central part. The final calculated magnetic anomaly provides a reliable correlation at long wavelengths with an average error of 8.4 nT. The error represents the uncertainties of the short wavelengths, indicating larger uncertainties for the superficial bodies.

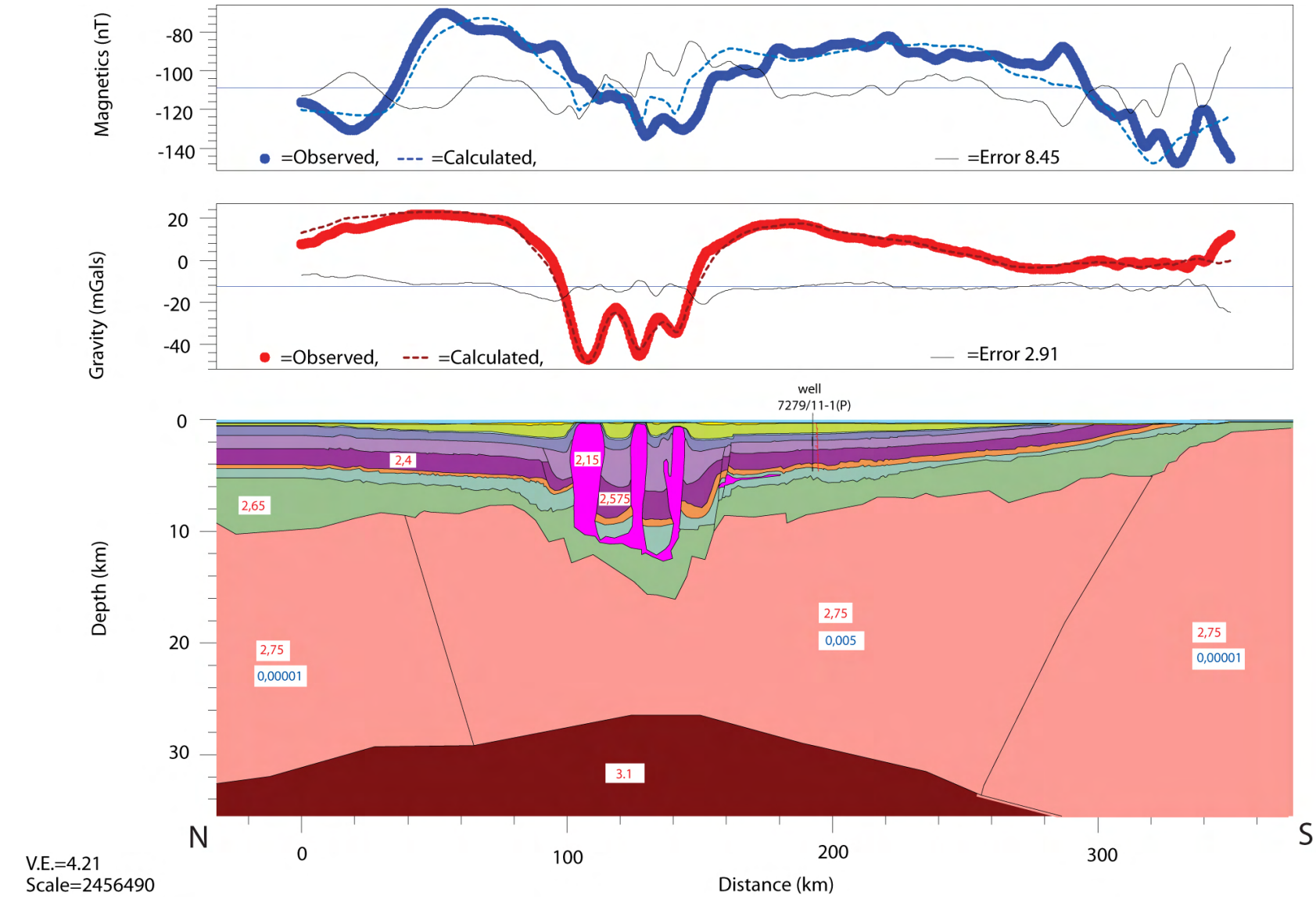

Figure 7.2. Final model along Transect 1. The values in the white small boxes indicate the petrophysical parameters. Red curve and numbers: density; blue curve and numbers: susceptibility.

7.3 T2: Second Transect

This section (Fig. 7.3) runs approximately north-south. It is about 260 km long and it is almost parallel to the T1 section but located more in the eastern segment of the Nordkapp Basin.

In contrast to the T1, the magnetic and gravimetric fields along T2 are not so similar. The gravity anomalies present a long wavelength variation that follows approximately the curve of the field observed along the T1 Transect. A maximum in the northern part (23 mGal), a minimum in the Nordkapp Basin around -34 mGal, and a relatively smooth curve with anomalies between 13 and 20 mGal in the Finnmark Platform are observed. The magnetic field is dominated by high values in the Bjarmeland Platform, with maximum values of 32 nT, and lower values, between –74 and -105 nT in the Nordkapp Basin and Finnmark Platform. There is no noticeable minimum in the central part observed in Transect T1.

In order to model this second transect we use a similar approach to the modelling of T1: first we define the initial geometry from seismic lines, fallowed by locating the preliminary basement and the Moho from Ritzmann et al. (2007). Then we only considered minor adjustment to make the modelled gravity matched the observed Bouguer gravity data. The final geometry for the deeper interfaces to fit the long wavelengths are defined first, thereafter the shallower interface are adjusted to fit the short wavelengths.

The final modelled Moho shows, like for the previous section, a smooth surface and the difference from the interpreted Moho of Ritzmann et al. (2007) is not more than 3 km. The Moho is characterised in both the north and south mostly by a similar depth of about 31 km. The Nordkapp Basin exhibits a shallow Moho at approximately 26 km.

The resulting top basement is smooth and with small vertical variation in the northern and southern parts. The basement depth in both these areas is around 7 km. The Nordkapp Basin is dominated by a graben structure, with a deepening in the central part of about 8 km, in correspondence with the uplift of the mantle and the intrusion of the salt. With the graben a simple symmetry can be delineated, and the top basement is shallower in comparison with the graben in transect T1.

The sedimentary bodies show dissimilar characteristics. We can divide the basin into three regions. In the north they are nearly horizontal with a small tilt towards the south. In the centre, they are deeper and dominated by a greater thickness. Therefore, we have increased their densities by about 150 kg/km^3. The southern part of the transect is symmetric to the

northern part; nearly horizontal layers with a small downward tilt towards the north.
In the Nordkapp Basin, there are three salt bodies; the largest being in the central part. It is around 10 km deep and around 10 km wide. The others two are about 10 km deep and 4.5 km wide. The final calculated gravity effect is close to the observed field for the long and short wavelengths. The average error is about 2.3 mGal. The maximum is correlated with the shallowest basement depth and the local minima coincide with the salt bodies.

The magnetic modelling led us to consider different values for the basement. In order to model the long wavelength field, we had to use a very high susceptibility in the northern basement block moderate to low values in the intermediate block and low values in the southern block (Fig. 7.3). The average final difference between calculated and observed field is 10.9 nT.

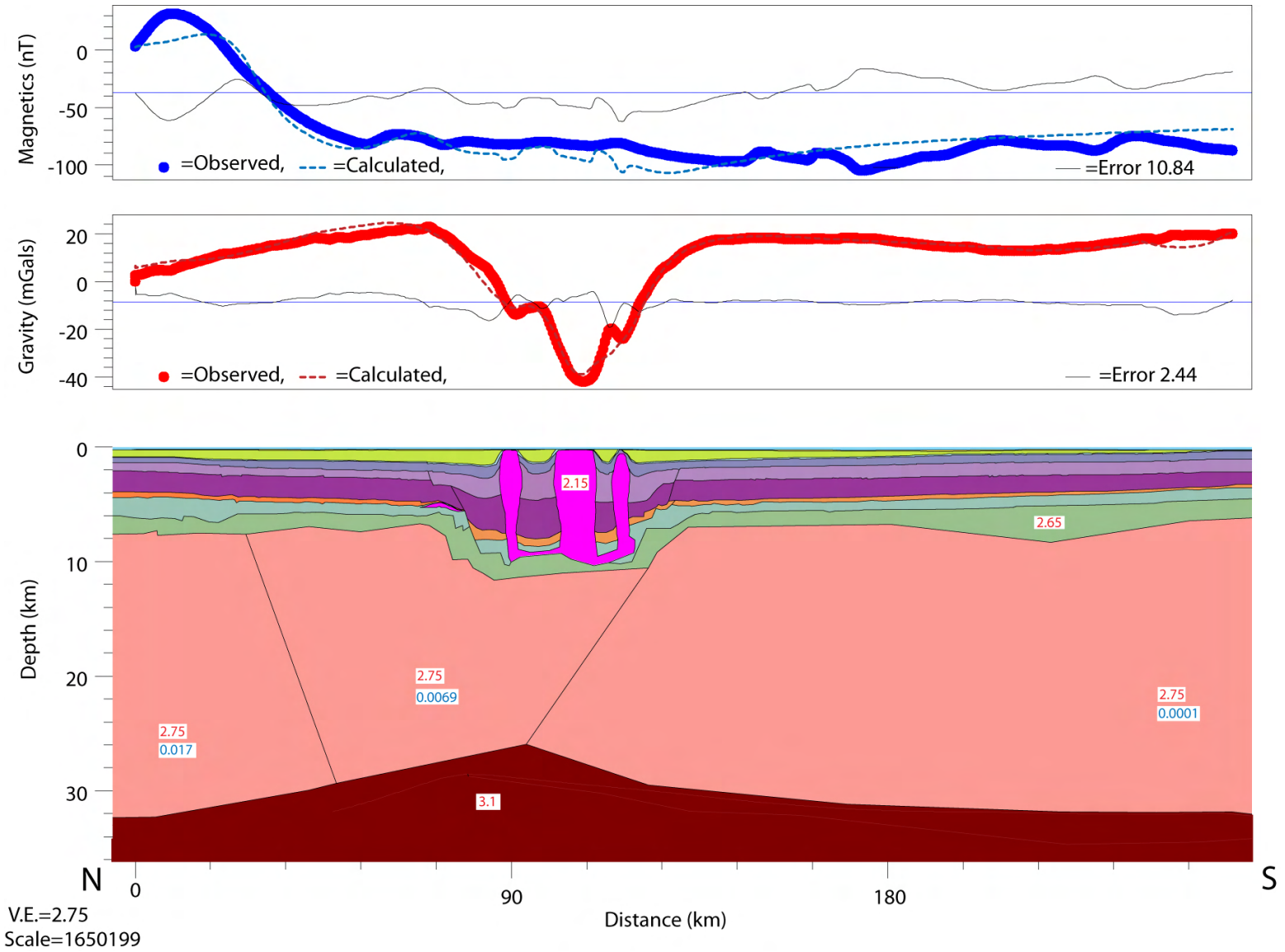

Figure 7.3 Final model along Transect T2. The values in the small boxes indicate the petrophysical parameters. Red curve and numbers: density; blue curve and numbers: susceptibility.

7.4 T3: Third transect

The third transect (Fig. 7.4) is oriented NE-SW, and is the shortest of the modelled profiles. Unfortunately, it only crosses the first transect. The effect of the most voluminous salt body on the gravity field is obvious, since the minimum of the gravity anomaly is located there. The magnetic anomalies in the central and in the southern areas can be correlated with the gravity. Discrepancies are present in the northern area.

Considering the length of the section (100 km), the Moho surface is quite flat and corresponds with the Ritzmann et al. (2007) Moho. Steps that mimic a graben structure found in Transects T1 and T2 characterize the basement. The depth of this graben varies from 10 to 14 km. The final geometry of the sedimentary layers, due to lack of good seismic data follows the structure of the other two sections. The Carboniferous is characterized by a larger thickness in the northern area. It is 2 km more than in the southern area, and 2 km more than the Carboniferous thickness in the first transect.

The seismic signal does not provide enough information about the deep salt geometry. We modelled the large salt body (23 km) and when comparing it to the initial model, we conclude that the big salt dome could be narrow at depth. Overhang geometry is suggested in our final model but is not observed in the seismic due to large covering of the top salt. However, we point out that magnetic boundary effects due to the ambiguous location of Transect T3 could influence this interpretation.

The calculation of the magnetic anomaly field follows the same approach that we used for T1 and T2. We split the basement in three parts in correlation with the graben geometry and main anomaly variations. We looked for the physical parameters that provide the best fit. We found that the difference between the three blocks is not as significant as they are in the other two sections, but higher values are suggested for the central block. The resulting calculated anomaly field fits well for the long wavelengths and the difference from the calculated anomaly is about 4.5 nT.

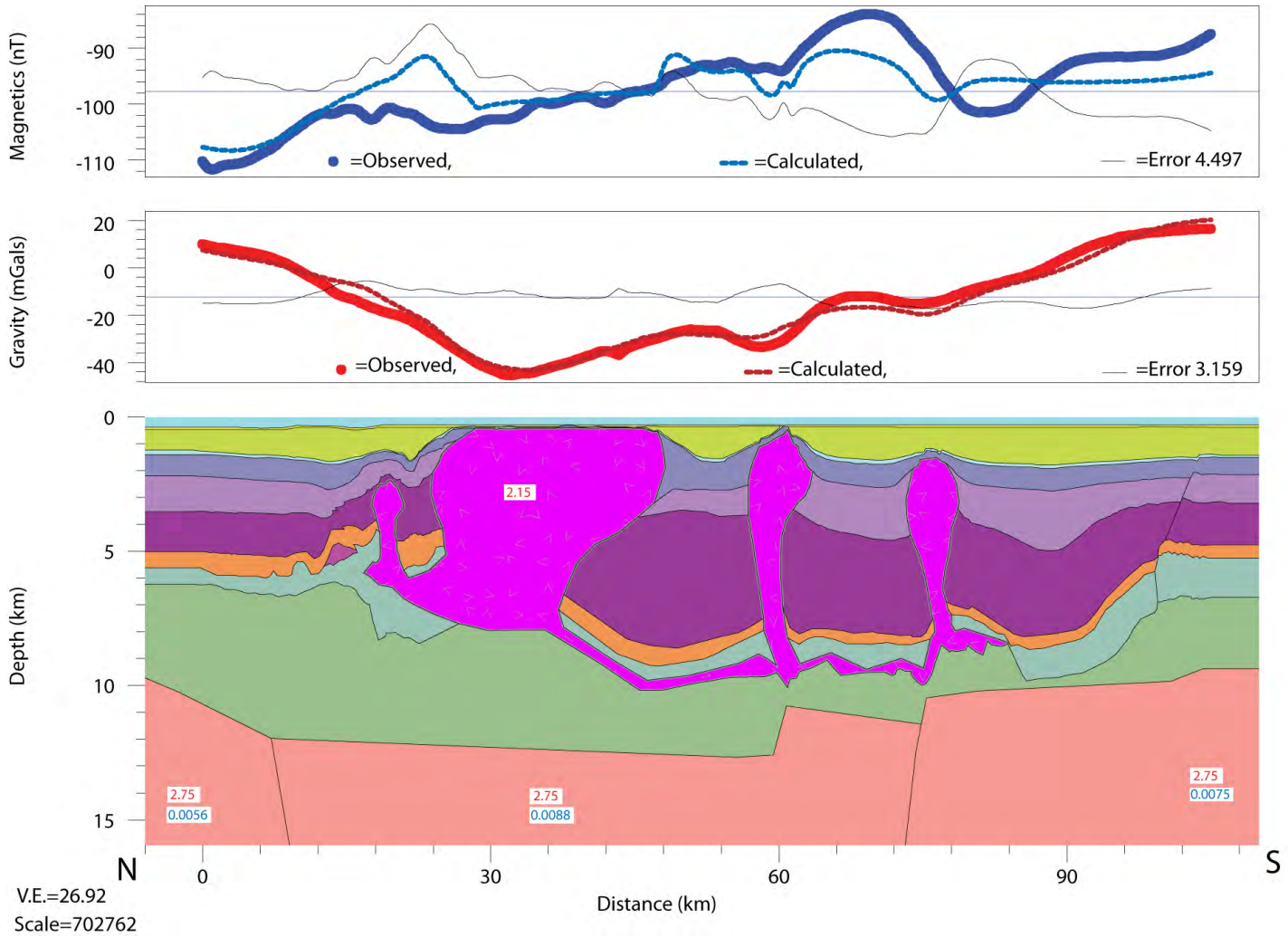

Figure 7.4 Final model along Transect 3. The values in the small boxes indicate the petrophysical parameters. Red curve and numbers: density; blue curve and numbers: susceptibility.

7.5 Conclusion

We have interpreted possible structures along the BAS-06 survey using 2¾-D gravity and magnetic modelling along three transects. These are preliminary models but they provide some important information about sub-salt basement geometry, basin segmentation as well as Moho topography. We have also tested and refined the salt geometry using potential field data. We found that segmentation in the Nordkapp Basin is plausible as suggested by the shallowing of the top basement to the east.

We reported the minimum, the maximum and the mean depth values for these two surfaces in the table below.

	Max (m)	**Mean (m)**	**Min (m)**
Top Basement			
Transect 1	497.6	16066.7	10391
Transect 2	6188.8	11622.5	8484.6
Transect 3	9384.6	12945.5	10821.1
Moho			
Transect 1	26456.2	443940.7	33219.5
Transect 2	25855.6	35222.7	31182.1
Transect 3	28949	30048.9	29421.8

Table 7.2 *Minimum, maximum and mean depth-values for the basement and for the mantle along three modelled sections.*

For more clear and detailed definition of the crustal magnetic domains we need more constrain. Especially more recent NGU susceptibility measurements from the OSRAM II Project (Lauritsen et al., 2007) should be used for a more realistic magnetic modelling.
More advanced 3D modelling ought to be carried out in the future to refine the preliminary results, and several modelling should be combined (seismic tomography, 3D isostasy and gravimetric regional modelling).

8 THE MJØLNIR IMPACT STRUCTURE

S. C. Werner

On Earth, currently 174 impact structures are confirmed, although many more structures are listed as possible impact craters. The majority of the recognized impact sites are found on land, because they are easier to detect (visible circular depressions) and commonly continental crust as well as shelf regions are older. Impact cratering is a random geological process, and the spatial crater distribution is depending only on the surface age (and evidently on the resurfacing-state of the surface unit). Nevertheless, Dypvik and Jansa (2003) recognized 27 marine impact structures, of which 7 are still situated in marine environment.

The Mjølnir crater is one of the few marine impact craters, and located at 73˚ 48' N and 29˚ 40' E. It was first interpreted as impact crater by Gudlaugsson (1993). Later, Dypvik et al. (1996) could confirm the impact origin of the structure by indicators such as impact ejecta, iridium enrichment and shocked quartz in drill core 7430/10–U-01. The impact crater formed on the north-eastern Bjarmeland Platform area. Its formation age has been derived from biostratigraphic relations of the successive infill, and it took place close to the Volgian-Ryazanian boundary, implying 142±6 Ma ago. The diameter of the structure is 40 km. The crater is well-preserved under a sedimentary layer of about 500 m thickness, and covered by shallow water (about 360 m). Tsikalas et al. (1998 a, b, c) utilized seismic reflection lines and well data to derive detailed sub-sedimentary morphology of the crater as well as the deeper structural extent. They found that the crater includes an 8-km wide central uplift, surrounded by a 4-km wide trough and further by a 12-km wide outer zone. The crater diameter is expressed in seismic as disturbance and in the gravity as an1-2 mGal relative minimum with a central broad maximum of 2-3 mGal, which is correlated with the central uplifted "basement" part. The apparent depth of the crater ranges between 30-70 m, and is very shallow compared to other terrestrial craters of this size. The impact-related disturbance influences the subsurface structure at least to a depth of about 5 km, visible in the seismic data.

Earlier (shipborne) magnetic measurements were performed together with gravity and additional seismic measurements crossing the structure diagonally. Such profile constellation represents circular structures quite well in seismic and gravity measurements, but the magnetics might suffer from it. Unlike the gravity and morphologic expression of a crater, the magnetic anomaly pattern is not straightforward for such structures. Impact-melt distributions are patchy. Naturally, the magnetic anomaly map shows a higher frequency content, therefore the interpolation between the lines overlapping only at one point, the lack of tie lines, as well as a good diurnal variation model (considering relatively low speed of the ship), might result in an artificial anomaly pattern. Considering the target material (Bjarmeland Platform) being largely non-magnetic, anomaly variations of only a few nT are expected. The depth of the magnetic basement is estimated by Johanson et al. (1993) to be at least at 6-7 km, while the impact crater related features will be found at depths less than 5 km. For Mjølnir, Tsikalas et al. (1998a) used slope and half-slope estimates of

the local anomalies to find source depths, which resulted in estimates ranging between 1.6 and 3.4 km in depth.

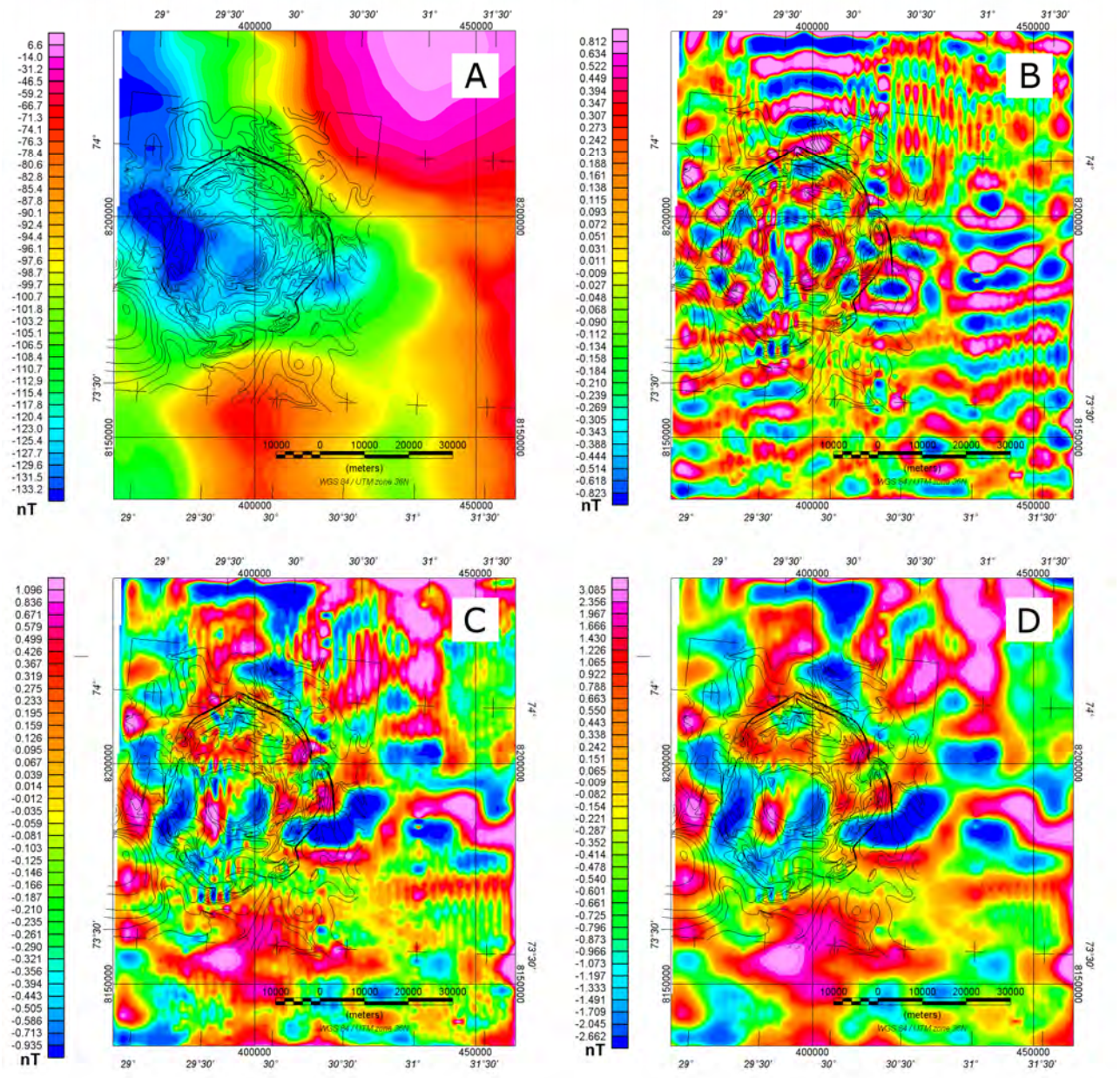

Figure 8.1 The total magnetic field anomaly map for the Mjølnir impact structure, the subsurface morphology after Tsikalas et al. (1998 a,b, c) is superimposed as black contour lines. (A) Unfiltered, (B) simple high-pass filtered with a wavelength cut-off at 10km, (C) Gaussian filtered with a cut-off wavelength at 10 km, and (D) the same as (C) with a cut-off wavelength at 20km.

The impact cratering process includes the radial distribution of impact ejecta material over far distances. In the vicinity of Mjølnir such an ejecta bed has been identified in core charts (Dypvik et al. 2004). Cratering mechanic modelling explains, that the excavated material form the impact site is deposited in reverse order of the stratigraphic column in the ejecta blanket (overturn flap), and additionally the material from deeper strata will be deposited along ballistic trajectories further away from the site than shallow-laying material. In that way an impact crater can be used as a wide-open analogy to drill core probing. When correlating various drill-core charts, the possible influence of the impact crater event (deposition of deeper strata at remote areas) and also the backwash effect of the water masses moving sediments further away from the impact side or opposite into the impact side, need to be considered.
The BAS-06 aeromagnetic survey above the Mjølnir structure, compared to previous surveys, is benefiting from dense line and tie-line spacings. Figure 8.1-A shows the total magnetic field anomaly for the Mjølnir impact site and closer surrounding. The subsurface morphology (Tsikalas (1998a, b, c) is superimposed for orientation. Figure 8.1 (B, C, and D) show filtered versions of the field anomaly. Simple high-pass filtering (cut-off at 10 km) shows an anomaly pattern strongly related to the tie-line pattern with amplitudes of less than 1 nT. Figure 8.1-C and D shows Gaussian filtered maps of the same area, for the purpose of extracting impact related signatures. Both maps show similar features, but Figure 8.1-D with a slightly higher cut-off (20 km instead of 10 km) shows that most of the features in Figure 8.1-C are reliably, but the relative noise level is lower.

Summarizing, the magnetic anomaly pattern does not match earlier measurements and need further attention for a final conclusion. Nonetheless, final processing steps have to be repeated, because the globally applied micro-levelling was not modified for higher line spacing above the crater. Line-spacing related artefacts are visible, when high-pass filters are applied (Fig. 8.1-B). Within the new source depth estimate for the entire survey, the possible occurrence of shallow magnetic sources needs to be revisited for the Mjølnir site.

For the future, reprocessing of the area is planned for the purpose of a detailed magnetic and gravity modelling in perspective of the planned ICDP drilling of the impact site.

9 CONCLUSIONS

A high sensitivity aeromagnetic survey, BAS-06 was carried out in an area of 42530 km^2 from the Finnmark Platform to the Bjarmeland Platform in the Barents Sea. Data processing comprised spike removal and data editing, systematic (IGRF and lag) corrections, statistical, median and (Geosoft) decorrugation micro levelling. The result provided a new and relevant magnetic picture for our geological understanding of the Barents Sea.

The magnetic survey, with a 2x6 km line-tie line spacing configuration, was used successfully to extract new structural and geological information generally along a large area of the Barents Sea. Trend enhancement filters and a preliminary interpretation of the BAS-06 survey have been proposed. High-pass and derivatives filters were used to enhance the structural information in specific areas like the Bjarmeland Platform, the Nordkapp Basin, the Finnmark Platform and the near-shore area of the Varanger Peninsula. Some interpreted lineaments were closely correlated to faults and salt structures shown on published maps from the area. The processed magnetic data could confirm most of the previously mapped faults but some new faults zones related lineaments appear or seem to be more complex in the Finnmark Platform and in the Nordkapp Basin. Even if the seismic database available that was available for the BAS-06 project was extremely sparse along the BAS-06 survey area, we also found good correlation with the structures observed on seismics.

Interesting onshore-offshore relationships and new trends also appeared near the Varanger Peninsula. They witness a complex tectonic setting involving the Caledonian deformation front probably streaming above NE-SW Timanian pre-existing structures, acting most likely as a free border level during the Caledonian Orogeny. Regional arch-shaped anomalies suggest that the main trend of the Caledonian Nappes probably bifurcate from NE-SW close to the Varanger Peninsula to the NW-SE near the Nordkapp Basin. This system could be part of a larger system involving several nappes and thrusts as well as major faults including the main border fault of the Loppa High.

Finally, one of the major results of this survey was the clear demonstration that modern, high-resolution aeromagnetics can provide an efficient tool for mapping salt features and mini-basins in the Barents Sea. In the Nordkapp Basin, there are regions with circular features and of high lineament density probably related to salt tectonics. Salt diapirs coincide with negative magnetic anomalies when the salt domes reach the near-surface; magnetic lineations coincide with sedimentary layers deformed by the rising salt. Consequently, it can significantly add to the qualitative mapping, on both a regional and prospect scale, offshore Norway.

An archive DVD of the survey is enclosed in the present report.

10 RECOMMENDATIONS FOR FURTHER WORK AND PERSPECTIVES

The present study clearly shows that the new survey seriously improves the geophysical picture of the study area. However, a large part of the Barents Sea area remains poorly covered by such modern aeromagnetic datasets. The BAS-06 technical configuration proves to be efficient to investigate the first order structures of the Barents Sea. However, the line-tie line configuration could be slightly modified by using a tie line spacing of 4-5 km instead of 6 km if we plan similar surveys in this part of the Barents Sea area. 6 km tie line spacing was probably not enough to remove all the E-W artificial trends, locally present after levelling in such a relative low magnetic region. A smaller tie line spacing of 4-5 km might be required to improve and facilitate the levelling of future and contiguous surveys, although increasing the budget.

Because of the small amplitudes of some magnetic anomalies due to salt diapirs (1-3 nT), processing of the survey data was a challenging task with the risk of removing significant parts of the geophysical signal during the levelling. To achieve improvements in delineating magnetic anomalies from the salt domes in the Nordkapp Basin, we propose to carry out additional aeromagnetic tie-lines within the BAS-06 survey. There is a need for an increased number of tie-lines because of the low amplitudes of the magnetic anomalies (1-3 nT). New aeromagnetic acquisition to specifically investigate the salt domes implies to decrease locally tie-line spacing from 6000 m to 3000 m by adding a new tie-line between each of the existing tie-lines. We should also use this opportunity to refly some intermediate quality profiles along specific parts of the BAS-06 (the northern part of the Bjarmeland Platform for example).

Further profiles close to the Varanger Peninsula will be interesting as well. NGU is currently processing a high resolution bathymetric survey (50x50 m) around the coastline (still confidential) and some correlation between the magnetic trends described in this report could be improved by increasing the data resolution in this area as well.

The result of this type of study might be useful to help further detailed geological mapping. Due to sparse seismic coverage available for the preliminary interpretation, a full constraint on the meaning of each magnetic anomaly and structures highlighted by the new survey was not always possible. Further studies combining seismic, gravity and the new magnetic data would be appropriate to refine the geological model in the future. NGU suggests to reinvestigate the Nordkapp Basin and specific trends in details using more confined interaction between seismic data, the new magnetic grid and the high-resolution gravity DRAGON database (available only to specific partners). Such an integrated study could be useful to update the structural map of the survey area before further aeromagnetic acquisition. 2D and /or 3D gravity modelling along the survey can be proposed to investigate structures and basement geometries with higher degree of confidence.

One of the primary difficulties in deriving accurate modelling results from magnetic data in this

study was the very low amount of sedimentary and salt susceptibility measurements that have been made (or released) in the Nordkapp Basin area. NGU has just completed a study on the present magnetic susceptibilities from the Finnmark Platform and Nordkapp Basin (OSRAM II project, Lauritsen et al. 2007). It will be useful to complete and refine the modelling later with these results.

Literature dealing with magnetic response due to salt intrusion is extremely sparse, even quasi-inexistent. Consequently, we think that the magnetic response due to salt features intruding sedimentary sequences need to be understood better. Particularly, the relationships between G_{apex} and the $M_{apex,}$ should be investigated to test the validity, sensitivity and uncertainties dealing with this approach.

Both gravity and magnetic signature characteristics of the salt intrusion are the result of one or more physical parameters such as the configuration of the anomalous zone, inclination, declination, density, model velocity, susceptibility contrasts with surrounding sediments, as well as depth and geometry of the investigated bodies. 2D and/or 3D synthetic modelling involving simple and complex salt geometries could be realised as guidelines to better understand the complex interpretation of magnetic features observed in the real case. It will be a relevant and useful exercise for magnetic pattern recognition in the Barents Sea. Interpretation of magnetic features influenced by salt tectonics in this part of the Barents Sea could also be particularly relevant and certainly strategic if one day a similar survey is purchased in underexplored saliferous areas like the disputed area between Norway and Russia.

From a petroleum perspective, new magnetic data and an updated onshore-offshore interpretation of the Finnmark Platform will also be relevant to better refine the structural setting and fault pattern of this complex area. In some cases there is usually a direct correlation between major faults and hydrocarbon occurrences while in other cases these faults may be used to bound areas that are prospective for exploration. Slopes in the basement (topography) are evident in the gravity data and their boundaries are usually detectable by magnetic edge enhancement filters. Local highs can be used to target structural traps. The present study shows that basement and intra-sediment trends can be observed in the magnetic data and that good onshore-offshore correlations can be used to constrain the meaning of the magnetics trends and basement features on a large part of the Finnmark Platform. A better geophysical and structural map of the area will certainly contribute to a better assessment of the petroleum system. In such a context, a contiguous survey with the BAS-06 (BAS-08?) will be a relevant and natural option in the near future. The new Nucula discovery closer to the BAS-06 survey also proves that a large part of the Finnmark Platform remains prospective and attractive. No details were given on the size of the discovery, but the NPD has informed that well 7125/4-1 in the Nucula prospect had confirmed the presence of both oil and gas. A press release suggests that the find could contain as much as 300-500 million? barrels of oil, enough to dwarf the nearby Goliath field, which is thought to contain 250 million barrels. In such an optimistic context, NGU proposes to extend the BAS-06 to the west, with a similar size and N-S

extent from the coastline up the Bjarmeland Platform.

ACKNOWLEGMENENT

Chevron Norge, Eni Norge, NGU, NPD, RWE Dea Norge and Statoil financed the BAS-06 Survey. Tore Høy (from NPD) provided seismic and well informations used for the report. We express our thanks to these companies, institutions and persons.

11 REFERENCES

Alsgaard, P. 1993: Eastern Barents Sea late Palaeozoic setting and potential source rocks. *In* Vorren, T.O., Bergsager, E., Dahl-Stamnes, Ø.A., Holter, E., Johansen, B., Lie, E., Lund, T.B. (eds) Arctic Geology and Petroleum Potential. *Norwegian Petroleum Society, Special Publication 2, Elsevier, Amsterdam*, 405-418.

Åm, K. 1975: Aeromagnetic basement mapping north of latitude 62°N, Norway. *Norges geologiske undersøkelse Bulletin 316*, 351-374.

Arkani, H. J. 1988: Differential reduction to the pole of regional magnetic anomalies: Geophysics, 53, 1592-1600.

Bain, J. & Weyand, J. A. 1993: Complex salt features resolved by integrating seismic, gravity and magnetics. *EAGE/EAPG Annual Meeting, Expanded abstracts.*

Bain, J., Weyand, J. & Weber, M. 1994: Resolving Complex Salt Features Using Gravity and Magnetics. *Fugro-LCT Technical Papers.*

Bainbridge, G., Musselman, C., Whitehead, N. & McDonald, N., 2002: Euler 3D Deconvolution (v5.1.5). Processing, analysis and visualization system for 3D inversion of potential field. Tutorial and User guide. *Geosoft Manual*. 66pp.

Bhattacharyya, B. 1966: Continuous spectrum of the total-magnetic field anomaly due to a rectangular prismatic body. *Geophysics 31,* 97-121.

Blakely, R. 1995: Potential Theory in Gravity and Magnetic Applications. *Cambridge University Press*, 461p.

Breivik, A. J., Gudlaugsson, S. T. & Faleide, J. I. 1995: Ottar Basin, SW Barents Sea; a major upper Paleozoic rift basin containing large volumes of deeply buried salt. *Basin Research 7*, 299-312.

Breivik, A. J., Mjelde, R., Grogan, P., Shimamura, H., Murai, Y. & Nishimura, Y. 2005: Caledonide development offshore-onshore Svalbard based on ocean bottom seismometer, conventional seismic, and potential field data. *Tectonophysics 401*, 79-117.

Brocher, T. M. 2005: Compressional and Shear Wave Velocity Versus Depth in the San Fransisco Bay Area, California. Rules for USGS Bay Area Velocity Model 05.0.0. *U.S.G.S open-File Report* 05-1317, 0-58.

Bugge, T., Elvebakk G., Fanavoll, S., Mangerud, G., Smelror, M., Weiss, H. M., Gjelberg J., Kristensen, S. E. & Nilsen, K. 2002: Shallow stratigraphic drilling applied in hydrocarbon exploration of the Nordkapp Basin, Barents Sea. *Marine and Petroleum Geology* 19, 13-37.

Bugge, T., Mangerud, G., Elvebakk, G., Mork, A., Nilsson, I., Fanavoll, S. & Vigran, J. O. 1995: The upper Palaeozoic succession on the Finnmark Platform, Barents Sea. *Norsk Geologisk Tidsskrift* 75, 3-30.

Chroston, P. N. 1986: Gravity anomalies on Varangerhalvøya, Finnmark. *Norges Geologiske Undersøkelse Bulletin 404*, 45-56.

Clark, D. 1997: Magnetic petrophysics and magnetic pretrology aids to geological interpretation of magnetic surveys. *AGSO Journal of Australian Geology and Geophysics* 17, 83-103.

Dengo, C. & Røssland, K. 1992: Extensional tectonic history of the western Barents Sea. *In* Larsen, R.M. (ed), Structural and tectonic modelling and its application to petroleum geology: Norwegian Petroleum Society Special Publication, 91-107.

Dobrin, M. & Savit, C. 1988: *Introduction to geophysical prospecting. 4th edition*. McGraw-Hill, 867 p.

Doré, A. 1995: Barents Sea geology, petroleum resources and commercial potential. *Arctic 48*, 207-221.

Doré, A. G., Lundin, E. R., Fichler, C. & Olesen, O. 1997: Patterns of basement structure and reactivation along the NE Atlantic margin. The role of basement reactivation in continental deformation. *Journal of the Geological Society of London 1*, p. 85-92.

Dypvik, H. & Jansa, L. F. 2003: Sedimentary signatures and processes during marine bolide impacts; a review. *Sedimentary Geology 161*, 309-337.

Dypvik, H., Gudlaugsson, S. T., Tsikalas, F., Attrep, M. J., Ferrell, R. E. J., Krinsley, D. H., Mørk, A., Faleide J. I. & Nagy J. 1996: Mjolnir Structure; an impact crater in the Barents Sea. *Geology (Boulder) 24*, 779-782.

Dypvik, H. & Jansa, L. F., 2003: Sedimentary signatures and processes during marine bolide impacts. a review. *Sedimentary Geology 161*, 309-337.

Dypvik, H., Gudlaugsson, S.T., Tsikalas, F., Attrep, M. Jr., Ferrell, R.E. Jr., Krinsley, D.H., Mørk, A., Faleide, J.I., & Nagy, J. 1996: Mjølnir Structure. An impact crater in the Barents Sea. *Geology 24*, 779-882.

Dypvik, H., Mørk, A., Smelror, M., Sandbakken,T., Tsikalas, F., Vigran, J.O., Bremer, M., Nagy, J., Gabrielsen, R.H., Faleide, J.I., Bahiru, G.M., & Weiss, H.M. 2004: The Ragnarok Formation and Sindre Bed. impact and ejecta material from the Mjølnir Crater in the Barents Sea. *Norwegian Journal of Geology 84*, 143-167.

Faleide, J. I., Gudlaugsson, S. T. & Jacquart, G. 1984: Evolution of the western Barents Sea. *Marine and Petroleum Geology 1*, 123-150.

Faleide, J. I., Solheim, A., Fiedler, A., Hjelstuen, B. O., Andersen, E. S. & Vanneste, K. 1996: Late Cenozoic evolution of the western Barents Sea-Svalbard continental margin. Impact of glaciations on basin evolution; data and models from the Norwegian margin and adjacent areas. *Global and Planetary Change 12*, 53-74.

Faleide, J. I., Vågnes, E. & Gudlaugsson, S. T. 1993: Late Mesozoic-Cenozoic evolution of the south-western Barents Sea in a regional rift-shear tectonic setting. *Marine and Petroleum Geology 10*, 186-214.

Fichler, C., Rueslåtten, H., Gram, C., Ingebrigtsen, A. & Olesen, O. 2007: Salt interpretation with special focus on magnetic data, Nordkapp Basin, Barents Sea. EGM 2007 International Workshop Innovation in EM, Grav and Mag Methods. a new Perspective for Exploration. Capri, Italy, 16-18 April 2007 .

Fichler, C., Rundovde, E., Johansen, S. & Sæher, B. M. 1997: Barents Sea tectonic structures

visualized by ERS1 satellite gravity with indications of an offshore Baikalian trend. *First Break 15*, 355-363.

Flanagan G., Davis S., Campbell, C. & Doughtie, J. 1988: Integration of high sensitivity aeromagnetics and seismic to define salt and sediment structures in the Gulf of Mexico. 5*8th Annual International Meeting, Society of Exploration Geophysics, Expanded Abstracts*, 582-585.

Gabrielsen, R. & Færseth, R. 1989: The inner shelf or North Cape, Norway, and its implications for the Barents Shelf-Finnmark Caledonide boundary. *Norsk Geologisk Tidsskrift 69*, 57-62.

Gabrielsen, R. 1984: Long-lived fault zones and their influence on the tectonic development of the southwestern Barents Sea. *Journal of the Geological Society, London 141*, 651-662.

Gabrielsen R., Færseth, R., Jensen, L., Kalheim, J. & Riis, F. 1990: Structural elements of the Norwegian Continental Shelf. Part 1.The Barents Sea region. *Norwegian Petroleum Directorate Bulletin 6*, 0-33.

Gabrielsen, R. H., Klovjan, O. S., Rasmussen, A. & Stolan, T., 1992: Interaction between halokinesis and faulting; structuring of the margins of the Nordkapp Basin, Barents Sea region, *In* Larsen, R.M. et al., (eds.) Structural and tectonic modelling and its application to petroleum geology; proceedings. *Norwegian Petroleum Society (NPF) Special Publication 1*, 121-131.

Gardner G., Gardner, L. & Gregory, A. 1974: Formation velocity and density-the diagnostic basics for stratigraphic traps. *Geophysics 39*, 770-780.

Gee, D. G. & Pease, V., 2004: The Neoproterozoic Timanide orogen of eastern Baltica; introduction. The Neoproterozoic Timanide Orogen of eastern Baltica. *Memoirs of the Geological Society of London 30*, 1-3.

Gee, D. G. & Teben'kov, A., 2004: Svalbard; a fragment of the Laurentian margin; The Neoproterozoic Timanide Orogen of eastern Baltica. *Memoirs of the Geological Society of London 30*, 191-206.

Gee, D. G., Bogoledpova, K. & Lorenz, H., 2006: The Timanide, Caledonide and Uralide orogens in the Eurasian high Arctic, and relationships to the palaeo-continents Laurentia, Baltica and Siberia. In. Gee, D.G and Stephenson, R.A. European Lithosphere Dynamics. *Geological Society, London, Memoirs 32*, 507-520.

Geosoft, 2004: OASIS Montaj v 6.0 Mapping and processing system, The core software platform for working with large volume spatial data. Quick start tutorials. *Geosoft Incorporated*, 258p.

Geosoft, 2005a: OASIS Montaj MAGMAP Filtering. 2D frequency domain processing of potential Field Data tutorial. *Geosoft Incorporated*, 66pp.

Geosoft, 2005b: Montaj Geophysics Levelling System, Processing and Enhancing Geophysicsl Data Extension for Oasis montja v6.2. Tutorial and user guide. *Geosoft Incorporated*, 68pp.

Gibson, R. I. & Millegan, P. 1998: Geologic applications of gravity and magnetics; case histories. *AAPG Studies in Geology 43*.

Grogan, P., Nyberg, K., Fotland, B., Myklebust, R., Dahlgren, S. & Riis, F. 1998: Cretaceous

Magmatism South and East of Svalbard. Evidence from Seismic Reflection and Magnetic Data. *Polarforschung 68*, 25-34.

Gudlaugsson, S. T. 1993: Large impact crater in the Barents Sea. *Geology (Boulder) 21*, 291-294.

Gudlaugsson, S. T., Faleide, J., Johansen, S. & Breivik, A. 1998: Late Palaeozoic structural development of the southwestern Barents Sea. *Marine and Petroleum Geology 15*, 73-102.

Hrouda, F., Smid, J. & Schulmann, K. 2001: Anisotropy of magnetic susceptibility and its carriers in salt domes of the SW Zagros Mts., Iran. *American Geophysical Union, Fall Meeting* 2001, abstract #GP41A-0247.

Hsu, S. -K. 2002: Imaging magnetic sources using Euler's equation. *Geophysical Prospecting 50*, 15-25.

Hsu, S. K., Sibuet, J. C. & Shyu, C. T. 1996: High-resolution detection of geologic boundaries from potential-field anomalies: An enhanced analytical signal technique. *Geophysics* 61, 373-386.

Ivanova, N. M. 2001: The geological structure and petroleum potential of the Kola-Kanin Monocline, Russian Barents Sea. *Petroleum Geoscience 7*, 343-350.

Ivanova, N. M., Sakoulina, T. S. & Roslov, Y. V. 2006: Deep seismic investigation across the Barents-Kara region and Novozemelskiy fold belt (Arctic shelf). Seismic probing of continents and their margins. *Tectonophysics 420*, 123-140.

Jackson, M. P. & Talbot, C. J. 1986, External shapes, strain rates, and dynamics of salt structures. *Geological Society of America Bulletin 97*, 305-323.

Jensen, L. N. & Sørensen, K. 1992: Tectonic framework and halokinesis of the Nordkapp Basin, Barents Sea. Structural and tectonic modeling and its application to petroleum geology; proceedings. *Norwegian Petroleum Society (NPF) Special Publication 1*, 109-120.

Johansen, S., Ostisty, B., Birkeland, Ø., Fedorovski, Y., Martirosjan, V., Christensen, O., Cheredeev, S., Ignatenko, E.A. & Margulis, L. 1993: Hydrocarbon potential in the Barents Sea region. play distribution and potential. *In* Vorren, T.O., Bergsager, E., Dahl-Stamnes, Ø.A., Holter, E., Johansen, B., Lie, E., Lund, T.B. (eds.). Arctic Geology and Petroleum Potential. *Norwegian Petroelum Society, Special Publication 2*, Elsevier, Amsterdam, 273-320.

Karpuz, M. R., Roberts, D., Moralev, V. & Terekhov, E. 1993: Regional lineament framework of eastern Finnmark, Norway, western Kola Peninsula, Russia, and southern Barents Sea.; Proceedings of the Ninth thematic conference on Geologic remote sensing; exploration, environment, and engineering. *Proceedings of the Thematic Conference on Remote Sensing for Exploration Geology 9*, 733-750.

Karpuz, M. R., Roberts, D., Moralev, V. M. & Terekhov, E. 1995: Regional lineaments of eastern Finnmark, Norway, and the western Kola Peninsula, Russia. Geology of the eastern Finmark-western Kola Peninsula region; proceedings of the International Barents symposium on "Geology and minerals in the Barents region". *Special Publication - Norges geologiske undersøkelse 7*, 121-135.

Keating, P. 1998: Weighted Euler deconvolution of gravity data. *Geophysics 63*, 1595-1603.

Koyi, H., Talbot, C. J. & Torudbakken, B. O. 1993: Salt diapirs of the Southwest Nordkapp Basin;

analogue modelling. New insights into salt tectonics; collection of invited papers reflecting the recent developments in the field of salt tectonics. *Tectonophysics 228*, 167-187.

Larssen, G. B., Elvebakk, G., Henriksen, L., Kristensen, S. E., Nilsson, I., Samuelsberg, T., Svånå, T., Stemmerik, L. & Worsley, D. 2005: Upper Palaeozoic lithostratigraphy of the southern part of the Norwegian Barents Sea. *NGU- Norge Geologiske Undersøkelse Bulletin 444*, 3-443.

Lauritsen, T., Blomstrand, L.B., Olesen, O. & Mørk, A. 2007: OSRAM II-Origin of sediment-Related AeroMagnetic II. Magnetic Susceptibility Measurements on Shallow Stratigraphic Cores from Finmark Platform, Nordkapp Basin and Svalis Dome. *Geological Survey of Norway (NGU) Report 2007.028*. 99p.

Lippard, S. & Roberts, D.G. 1987: Faults systems in Caledonian Finnmark and the southern Barents Sea. *Norges Geologiske Undersøkelse Bulletin 410*, p. 55-64.

Løvaås, L., Mogaard, J., Olesen, O., Koziel, J. & Lynum, R. 2006: Southern Nordkapp Basin Aeromagnetic Survey 2006 (SNAS-06). Data acquisition and processing report. *Geological Survey of Norway (NGU) Report 2006.089*. 51pp.

Ludwig, W., Nafe, J. & Drake, C. 1970: Seismic refraction. *In* Maxwell, A.E. (ed) The Sea, Volume 4. *Wiley-interscience, New York*, 53-84.

Maher, H. D. J. 2001: Manifestations of Cretaceous High Arctic large igneous province in Svalbard. *Journal of Geology 109*, 91-104.

Marson, I. & Klingele, E. E. 1993: Advantages of using the vertical gradient of gravity for 3-D interpretation. *Geophysics 58*, 1588-1595.

Martinec, Z. 1994: The density contrast at the Mohorevicic discontinuity. *Geophysical Journal International 177*, 539-544.

Mathisen, O. 1976: A method for Bouguer reduction with rapid calculation of terrain corrections *Geographical Survey of Norway geodetic publications 18*, 40 p.

Mauring, E. & Kihle, O. 2006: Leveling aerogeophysical data using a moving differential median filter. *Geophysics 71*, L5-L11.

Mauring, E., Beard, L. P., Kihle, O. & Smethurst, M. A. 2002: A comparison of aeromagnetic levelling techniques with an introduction to median levelling. *Geophysical Prospecting 50*, 43-54.

McDonald, A. J., Fletcher, C. J., Carruthers, R. M., Wilson, D. & Evans, R. B. 1992: Interpretation of regional gravity and magnetic surveys of Wales, using shaded relief and Euler deconvolution techniques. *Geological Magazine 5*, 532-531.

Mudge, S. 1991: New developments in resolving detail in aeromagnetic data. *Exploration Geophysics 22*, 277-284.

Murphy, C. 2007. Interpreting FTG Gravity Data using Horizontal Tensor Components. EGM 2007 International Worshop. Innovation in EM, Grav and Mag Methods:a new Perspective for Exploration, Capri, Italy, April 15-18. Extended Abstract.

Musset, A. & Khan, M. 2000: Looking into the Earth. Cambridge University Press.

Nabighian, M. N. 1974: Additional comments on the analytic signal of two-dimensional magnetic

bodies with polygonal cross-section. *Geophysics 39*, 85-92.

Nabighian, M. N. 1984: Toward a three-dimensional automatic interpretation of potential field data via generalized Hilbert transforms; fundamental relations. *Geophysics 49*, 780-786.

Nabighian, M. N. 1972: The Analytic Signal of Two-Dimensional Magnetic Bodies with Polynomial Cross-Sections; Its Properties and Use for Automated Anomaly Interpretation. *Geophysics 37*, 505-517.

Nafe, J. E. & Drake C. 1957: Variation with depth in shallow and deep water marine sediments of porosity, density and the velocities of compressional and shear waves. *Geophysics 22*, 523-552.

Naidu, P. S. & Mathew, M. P. 1998: Analysis of geophysical potential fields. a digital signal processing approach. *In* Berkout, A.J. (ed). *Advances in Exploration Geophysics series, Elevier, Amsterdam 5*, 0-295.

Nettleton, L. L. 1976: Gravity and Magnetics in Oil prospecting. *McGraw-Hill, New York*, 462p.

Nilsen, K. T., Vendeville, B. C. & Johansen, J. T. 1995: Influence of regional tectonics on halokinesis in the Nordkapp Basin, Barents Sea, *In* Jackson, M.P., Roberts, D.G. and Snelson, S. (eds), Salt tectonics: a global perspective. *AAPG Memoir 65*, 413-436.

Nilsen, K. T., Vendeville B. C., Johansen J. T. & A.. 1994: An example of salt tectonics controlled by regional tectonics; the Nordkapp Basin, Norway. AAPG annual convention. *Annual Meeting Abstracts - American Association of Petroleum Geologists and Society of Economic Pale*, 1994, 225.

Nyland, B., Jensen, L.N., Skagen, J., Skarpnes, O. & Vorren, T.O. 1992. Tertiary uplift and erosion in the Barents Sea: magnitude, timing and consequences. In Larsen, R.M., Brekke, H., Larsen, B.T. and Tallerås, E. (eds). Structural and tectonic modeling and its apllication to petroleum geology. *Norwegian Petroleum Society Special Publication 1*, Elsevier, Amsterdam, 153-162.

Ritzmann, O., Maercklin, N., Faleide, J., Bungum, H., Mooney, W. & Detweiler, S. 2007: A 3D geophysical model for the crust in the greater Barents Sea region. Model construction and basement characterization. *Geophysical Journal International*, in press.

Olesen, O., Håbrekke, H., Kihle, O. & Smethurst, M. 1992: Finnmark fykke, aeromagnetisk anomalikart, M. 1:500.000. *Norges Geologiske Undersøkelse (NGU)* .

Olesen O., Gernigon L., Ebbing, J., Mogaard, J., Pascal, C. and Wienecke, S., 2006: Interpretation of aeromagnetic data along the Jan Mayen Fracture Zone, JAS-05. *Geological Survey of Norway (NGU)* Report 2006.018. 162p.

Pilkington, M., Miles, W. F., Ross, G. M. & Roest, W. R. 2000: Potential-field signatures of buried Precambrian basement in the Western Canada Sedimentary Basin: The Lithoprobe-Alberta basement transect-Le transect Lithoprobe du socle Albertain. *Canadian Journal of Earth Sciences = Revue Canadienne des Sciences de la Terre 37*, 1453-1471.

Pilkington, M., Jansa, J. F. & Grieve, R. A. F. 1995: Geophysical studies of the Montagnais impact crater, Canada. *Meteoritics 30*, 446-450.

Press, W.H., Teukolsky, S.A., Vetterling, W.T. & Flannery, B.P. 2002: Numerical Recipes in C++.

The art of Scientific Computing Second Edition. Cambridge University Press. 972p.

Prieto, C. 1993: Gulf of Mexico-understanding the magnetic response due to salt intrusion. International Geophysical Corporation Footnote Series.

Ravat, D. 1996: Analysis of the Euler method and its applicability in environmental magnetic investigations. *Journal of Environmental and Engineering Geophysics 1*, 229-238.

Ravat, D., Wang, B., Wildermuth, E. & Taylor, P. T. 2002: Gradients in the interpretation of satellite-altitude magnetic data; an example from central Africa. Earth's gravity and magnetic fields from space. *Journal of Geodynamics 33*, 131-142.

Reid, A., Allsop, J., Granser, H., Millet, A. & Somerton, I. 1990: Magnetic interpretation in three dimensions using Euler deconvolution. *Geophysics 55*, 80-91.

Rice, A. H., Gayer, R. A., Robinson, D. & Bevins, R. E. 1989: Strike-slip restoration of the Barents Sea Caledonides terrane, Finnmark, North Norway. *Tectonics 8*, 247-264.

Ritzmann, O., Hinz, K., Jokat, W., Reichert, C., Coffin, M. F., Duncan, R. A., Erzinger, J., Hinz, K. & Talwani, M. 1997: Crustal structure of the East Antarctic passive margin at 6 degrees E.; Abstracts of the International Lithosphere program workshop on Volcanic margins. p. 34-35.

Roberts, D. 1972: Tectonic Deformation in the Barents Sea Region of Varanger Peninsula, Finnmark. *Norges Geologiske Undersøkelse (NGU), Trondheim 282*, 1-39.

Roberts, D. 2003: The Scandinavian Caledonides; event chronology, palaeogeographic settings and likely modern analogues; Collisional orogenesis in the geological record and modern analogues. *Tectonophysics 365*, 283-299.

Roberts, D.G. & Lippard, S. 2005: Inferred Mesozoic faulting in Finnmark. current status and offshore links. *Norges Geologiske Undersøkelse Bulletin 443*, 55-60.

Rønnevik, H. C., Illing, L. V. & Hobson, G. D. 1981: Geology of the Barents Sea. *In* Illing, L.V. and Hobson, G.D. (eds), Petroleum geology of the continental shelf of North-West Europe. *Proceedings of the second conference*, 395-406.

Rønnevik, H.C. & Jacobsen, H.P. 1984. Structural highs and basins in the western Barents Sea, In Spence A.M. (ed), Petroleum Geology of the north European margin. *Norsk Petroleum Forening, London*, Graham and Trotman, 19-32.

Roest, W. R., Verhoef, J. & Pilkington, M. 1992: Magnetic interpretation using the 3-D analytic signal. *Geophysics 57*, 116-125.

Saad, A. 1993: Interactive integrated interpretation of gravity, magnetic and seismic data-tools and examples. *Offshore Technology Conference abstract*, OTC#7079

Shuvalov, V., Dypvik, H., & Tsikalas, F. 2002: Numerical simulations of the Mjølnir marine impact crater. *Journal of Geophysical Research* 107 (E7), 1/1-13 (doi. 10.1029/2001JE001698).

Siedlecka, A. & Roberts, D. 1992: The bedrock geology of Varanger Peninsula, Finmark, North Norway; an excursion guide. *Special Publication - Norges Geologiske Undersokelse 5*, 0-45.

Siedlecka, A. & Roberts, D. 1996: Finnmark Fylke. Berggrunnsgeologi M1:500 000. *Norges Geologiske Undersøkelse (NGU), Trondheim.*

Siedlecki, S. 1980. Geologisk kart over Norge, berggrunnskart VADSØ-M. 1. 250.000. Norges geologiske undersøkelse (NGU).

Simonov, A. G., M. & Yakovlev, Y. 1998: The Riphean oil of the Rybachiy Peninsula. Myth or key to a major direction for oil and gaz prospecting within the Barents Sea (in Russian). Bulletin of Murmansk´sState technical University, 1.

Skilbrei, J.R., Habrekke, H., Christoffersen, T. & Myklebust, R.A. 1990: Aeromagnetic surveying at high latitudes, a case history from the northern Barents Sea. *First Break 8*, 2, 46-50.

Skilbrei, J.R. 1991: Interpretation of depth to the magnetic basement in the northern Barents Sea (south of Svalbard). *Tectonophysics 200*, 127-141.

Skilbrei, J.R. 1992: Preliminary interpretation of aeromagnetic data from Spitsbergen, Svalbard Archipelago (76°-79°N): Implications for structure of the basement. *Marine Geology 106*, 53-68.

Skilbrei, J. R. 1993: An evaluation of magnetic top basement depth determinations from the southwestern Barents Sea. *Doktor ingenøravhandling 1993:68*. Norges tekniske høgskole, Trondheim.

Skilbrei, J. R., Kihle, O., Olesen, O., Gellein, J., Sindre, A., Solheim, D. & Nyland, B. 2000: Gravity anomaly map of Norway and adjacent ocean areas, scale 1: 3 Million: Geological Survey of Norway (NGU), Trondheim.

Spector, A. & Grant, F. S. 1970: Statistical models for interpreting aeromagnetic data. *Geophysics*, *35*, 293-302.

Stemmerik, L. & Worsley, D. 1989: Late Palaeozoic sequence correlations, North Greenland, Svalbard and the Barents Shelf. *In* Collison, J.D. (ed.), Correlation in hydrocarbon exploration. *Norwegian Petroleum Society, Graham and Trotman, London*, 99-111.

Talwani, M. 1973. Computer Usage in the Computation of Gravity Anomalies. *Methods in Computational Physics 13*, 343-389.

Thompson, D. 1982: EULDPH. A new technique for making computer-assisted depth estimates from magnetic data. *Geophysics 47*, 31-37.

Thurston, J. & Brown, R. 1994: Automated source-edge location with a new variable pass-band horizontal-gradient operator. *Geophysics* 59, 546-554.

Tsikalas, F., Gudlaugsson, S.T., Eldholm, O., & Faleide, J.I. 1998a: Integrated geophysical analysis supporting the impact origin of the Mjølnir Structure, Barents Sea. *Tectonophysics* 289, 257-280.

Tsikalas, F., Gudlaugsson, S.T. & Faleide, J.I. 1998b: The anatomy of a buried complex impact structure: the Mjølnir Structure, Barents Sea. *Journal of Geophysical Research 103*, 30,469-30,484.

Tsikalas, F., Gudlaugsson, S.T., & Faleide, J.I. 1998c: Collapse, infilling, and post-impact deformation at the Mjølnir impact structure, Barents Sea. *Geological Society of America Bulletin 110*, 537-552.

Vendeville, B. & Jackson, M. P.1992. The rise of diapirs during thin-skinned extension. *Marine and Petroleum Geology 9*, 331-353.

Verduzco, B., Fairhead, J. D., Green, C. M. & MacKenzie, C. 2004: New insights into magnetic derivatives for structural mapping. *The Leading Edge (Tulsa, OK) 23*, 116-119.

Worsley, D. 2006: The post-Caledonian geological development of Svalbard and the Barents Sea. The Boreal Triassic conference, Longyearbyen, Svalbard, *NGF extended Abstract and Proceedings*.

12 FIGURES

Figure 3.6 Total magnetic field grid and superimposed magnetic contours after reduction to the pole. The final result can be compared with the previous magnetic compilation (Right). Better resolution and higher frequency anomalies are observed on the new survey.

Figure 3.7 Merge of the BAS-06 with the previous regional NGU magnetic grid (Åm 1975, Skilbrei, 1991, 1992, 1993 ,Skilbrei et al. 1990, Olesen et al. 2006).

Figure 3.8 Other datasets available for the BAS-06 study. NGU bathymetric compilation (left), NGU Bouguer gravity compilation (centre) and 2D seismic lines provided by the Norwegian Petroleum Directorate draped above the BAS-06 magnetic total field, reduced to the pole (right). Yellow circles represent the IKU shallow well location, Black symbols represent exploration wells. The fault pattern (Gabrielsen et al. 1990) and cultural information have been downloaded from the NPD web site. T1, T2 and T3 represent the three transects modelled in the present study (cf. Chapter 7).

Figure 4.1 Magnetic total field of the BAS-06 (left) and 30km and 15km of high-pass filtering of this grid respectively (right). Medium to high frequency anomalies are mostly observed around the Nordkapp Basin and in the southern part of the Finnmark Platform, south of 71°40´. Along the Nordkapp Basin, E-W to NW-SE elongated anomalies and round-shaped magnetic pattern are observed. High-pass filtering with 15 km cut off wavelength highlights better N70° to N80° high frequency linear features in the southern part of the survey area. They progressively disappear to the north on the Finnmark Platform.

Figure 4.2 15 km low pass filtering of the magnetic total field and upward continuation of the total field to 2 and 4 km. These filters smooth the magnetic signal and underline the distribution of the main magnetic units. A prominent N°70 oriented anomaly divides the regional magnetic low observed in the southern part of the survey. Broad and high amplitude anomalies are mostly observed in the northeastern part of the Bjarmeland Platform and south of the Nordkapp Basin, where a prominent arc-shaped positive magnetic unit is observed west of 30°25'. A distinct N135° to N140°- trending elongated anomaly is continuous from the central part of the Nordkapp Basin to the southern part of the Bjarmeland Platform. It seems to be linked with a similar N130° bending anomaly south of the saliferous basin.

Figure 4.3 Directional horizontal derivatives of the BAS-06 dataset. The filters enhance the high frequencies along the N-S trend (left) and the E-W trend (right).

Figure 4.4 Directional horizontal derivatives along the BAS-06 area. The filters enhance the high frequencies along the NE-SW direction (left) and the NW-SE direction (right).

Figure 4.5 Analytic signal (left), first vertical derivative (centre) and AGC (automatic gain control) signal filters applied to the magnetic total field reduced to the pole.

13 ANNEXES

13.1 CD short description

13.1.1 Folders:

1. DATABASE_PROCESSING_BAS06. database folder
2. MICROLEVELLING_IN_OUT_FILES
3. GRIDS_GEOSOFT_BAS06_FOR_PARTNERS
4. MAPS_BAS06_GEOSOFT
5. MAPS_BAS06_pdf
6. GMSYS_MODELS
7. BAS-06_REPORT
8. PRESENTATION_29Mars
9. LITERATURE: selected .pdf about the Barents Sea

13.1.2 DATABASE_PROCESSING_BAS06. database folder

Rawdata_and_Montajlevel_BAS06_2.gdb.
Geosoft with channels from Raw data up to Geosoft full-levelling and Geosoft FFT decorrugation microlevelling

microlevelling_database07_2.gdb.
Database with different channels describing the microlevelling done using Mauring´s software (Mauring and Kihle, 2004)

Rawdata_and_Montajlevel_BAS06_2.gdb (in Database folder)

LAT: latitude geographic
LONG: longitude geographic
XUTM36_ED50:X UTM coordinates in UTM 36-ED 1950
YUTM36_ED50:Y UTM coordinates in UTM 36-ED 1950
XUTM36_WGS84:X UTM coordinates in UTM 36- WGS84
YUTM36_ WGS84:Y UTM coordinates in UTM 36- WGS84
TIME. GPS time
GPS_ALTITUDE: GPS altitude
Radar_ALTITUDE: Plane radar altitude (in feet)

Diurnal_land station: Diurnal magnetic field at land station (Leknes)
MAG_RAW: raw data magnetic recording
Mag_spike and mag_filt: preliminary noise filtering
Mag_lag: lag correction of the filtered magnetic raw data (mag_filt)
Mag_lag_head: head correction
IGRF: IGRF field
TFIELD: non-levelled magnetic total field (IGRF corrected)
Tie_levelling: magnetic levelling of the Tie line only
full_levelling: Geosoft statistical full levelling of the lines
full_leveling_AKIMA: Geosoft statistical full leveling of the lines+Akima filter
geosoft_microlevelingFFT: microleveling of full_leveling_AKIMA using the Geosoft FFT decorugation technique.

microlevelling_database07_2.gdb (in Database folder)
XUTM36_ED50: X UTM coordinates in UTM 36-ED 1950
YUTM36_ED50: Y UTM coordinates in UTM 36-ED 1950
XUTM36_WGS84: X UTM coordinates in UTM 36- WGS84
YUTM36_ WGS84: Y UTM coordinates in UTM 36- WGS84

Mauring_3000_6000_microlevel: microlevelling of full_leveling_AKIMA using the NGU moving differential median microleveling filter described in Mauring and Kihle, 2004. 3000 is the distance used for the 1D median filter, 6000 is the distance used for the 2D median filter.

Mauring_5000_8000_microlevel: microlevelling of full_leveling_AKIMA using the NGU moving differential median microleveling filter described in Mauring and Kihle, 2004. 5000 is the distance used for the 1D median filter, 8000 is the distance used for the 2D median filter.

Mauring_6000_6000_microlevel: microleveling of full_levelling_AKIMA using the NGU moving differential median microleveling filter described in Mauring and Kihle, 2004. 6000 (the first) is the distance used for the 1D median filter, 6000 is the distance used for the 2D median filter.

Mauring_1000_5000_microlevel: microlevelling of full_leveling_AKIMA using the NGU moving differential median microleveling filter described in Mauring and Kihle, 2004. 1000 is the distance used for the 1D median filter, 5000 is the distance used for the 2D median filter.

Mauring_2000_6000_microlevel_BEST_VERSION: microleveling of full_levelling_AKIMA using the NGU moving differential median microleveling filter described in Mauring and Kihle, 2004. 2000 is the distance used for the 1D median filter, 4000 is the distance used for the 2D median filter.

I obtained the best result with these 2 parameters (see other grids and Geosoft FFT microlevelling grid for comparison).

The main channels have been gridded (minimum curvature only!, grid cell 500m) and the grids names refer to the channels names (GRIDS_UTM_WGS84 folder). The file maps_and_interpretations.map and the BAS_06_geosoft_project.gpf in folder MAPS_BAS06_GEOSOFT displays all these Geosoft grids.

13.1.3 MICROLEVELLING_IN_OUT_FILES

Microlevelling data (.xyz) (aslo in the Geosoft database). I also provide a .pdf of the Mauring and Kihle paper describing the microlevelling technique developed by NGU.

13.1.4 GRIDS_GEOSOFT_BAS06_FOR_PARTNERS

Released Geosoft grids used in that project. The grids are all in UTM36 WGS 84.
Description of the grids by alphabetic order

- AGC_magRTP.grd: AGC filter of the magnetic total field reduced to the pole
- Analy_Signal_RTP_mag.grd: Analytic signal of the magnetic total field reduced to the pole
- directionalGradientmagRTP_0.grd: N-S directional filter of the magnetic total Field reduced to the pole
- directionalGradientmagRTP_45.grd: NE-SW directional filter of the magnetic total field reduced to the pole
- directionalGradientmagRTP_90.grd: E-W directional filter of the magnetic Total field reduced to the pole
- directionalGradientmagRTP_135.grd: NW-SE directional filter of the magnetic total Field reduced to the pole
- directionalGradientmagRTP_145.grd: NW-SE directional filter of the magnetic total field reduced to the pole
- full_levelling_AKIMA_end.grd: full statistical modelling of the magnetic total field

- Geosoft_microlevellingFFT.grd: microlevelling grid using the Geosoft FFT decorrugation technique

- HD_TRD_magTF_RTP.grd: horizontal derivative of the magnetic total Field reduced to the pole

- HP_magTF_15km_UTM36_WGS84.grd: high-pass filter 15 km of the magnetic total field

- HR_TOPO_FINNMARK_25m_UTM36WGS84.grd: high resolution topographic grid 25

- IGRF.grd. IGRF grid along the BAS-06 survey

- LP30kmmagTF_RTP_magTF.grd: low-pass filter 30 km of the magnetic total field

- MAG_RAW.grd: raw magnetic field

- magnetometer_altitude.grd: sensor elevation altitude

- magRTP_UC_2000m.grd: 2 km upward continuation of the magnetic total field reduced to the pole

- magRTP_UC_4000m.grd: 4 km upward continuation of the magnetic total field reduced to the pole

- magTF_RTP_Geosoft_vert_derivative.grd: Vertical derivative of he magnetic total Field reduced to the pole
- magTF_RTP_HP30km.grd: high-pass filter 30 km of the magnetic total field reduced to the pole

- mauring_2000_6000_microlevel.grd: magnetic total field after microlevelling using the NGU median filter technique

- mauring_2000_6000_microlevel_Reduce_to_pole.grd: magnetic total field after microlevelling using the NGU median filter technique and reduction to the pole

- mauring_2000_6000_microlevel_slope_SURFER.grd: Terrain slope of the magnetic total field (Surfer algorithm)

- Moho_BAS-06_extra.grd: Moho compilation from the Barents Sea 3D crustal model.

http://www.norsar.no/seismology/barents3d/. See also press released in the folder PUBLICATION (Bungum et al., 2005)

- NGU_Basement_BAS-06_extra.grd: NGU top magnetic basement compilation around the Nordkapp Basin (based on the original magnetic grid)

- NGU_BATHY_BAS-06_extra.grd: NGU bathymetric compilation along the BAS-06 survey area.

- NGU_Bouguer_BAS-06_extra.grd: NGU Bouguer anomlies compilation along the BAS-06 survey area.

- Old_mag_alongBAS06.grd: former magnetic grid along the BAS-06 survey

- Ritzmann_upper_Basement_BAS-06_extra.grd: Upper Basement compilation from the Barents Sea 3D crustal model. http://www.norsar.no/seismology/barents3d/. See also press released in the folder PUBLICATION (Bungum et al., 2005)

- TFIELD_no_levelling.grd: magnetic total field before levelling and microlevelling

- tie_levelling.grd: Tie levelling

- tilt_derivative_magTF_RTP.grd: Tilt derivative of the magnetic total field reduced to the pole

- TDR_RTP_negatif.grd: Tilt derivative of the magnetic total field reduced to the pole x-1

13.1.5 MAPS_BAS06_GEOSOFT

Geosoft project and maps with shapefiles and interpretation of the potential field grids.

13.1.6 MAPS_BAS06_pdf

Selected maps in .pdf formats. Projection UTM36 WGS 84. scale M. 1/1.000.000

13.1.7 GMSYS_MODELS

The 3 GMSYS models in GMSYS format, ready to be updated

13.1.8 BAS-06_REPORT

NGU BAS-06 report (word and .pdf formats) and annexes

13.1.9 PRESENTATION_29Mars

PowerPoint presentations showed to our partners (meeting 29 Mars)

13.1.10 LITERATURE

Selected papers about the Barents Sea and microlevelling technique